JOURNAL OF THE
Electrochemical
Society

ol. 103, No. 2) February 1956

March 1956 Number:
San Francisco Meeting Program Issue

AS PARTNERS IN
YOUR PROGRESS . . .

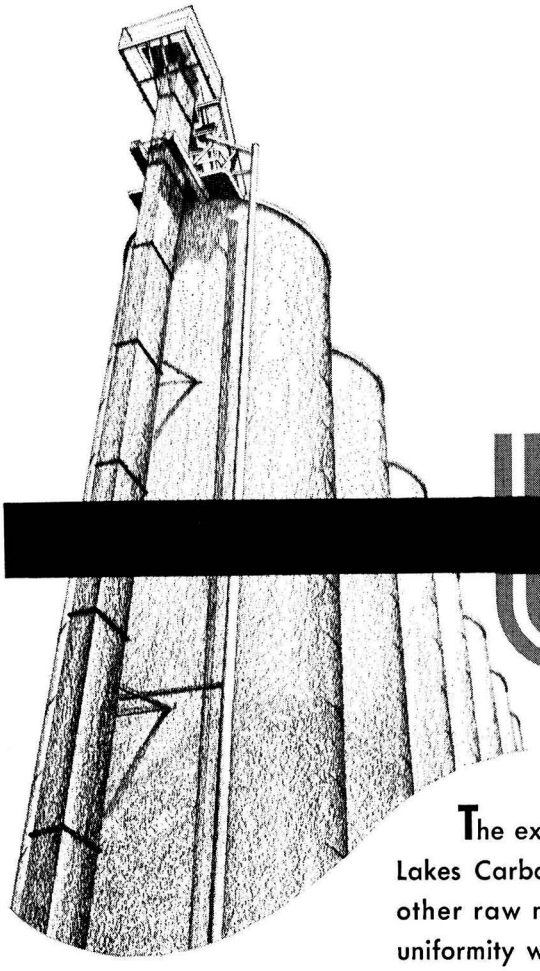

ENCLOSED STORAGE SILOS
MORGANTON, N. C., PLANT

UNIFORMITY – is a *plus* factor!

The extensive background of experience of Great Lakes Carbon Corporation in industrial carbons and other raw materials is an unique *plus* factor in the uniformity which distinguishes GLC electrodes, anodes, carbon brick and mold stock.

The high degree of integration between discoveries in our research laboratories, refinements in processing raw materials, and improved manufacturing techniques is further assurance of excellent product performance.

ELECTRODE
GLC®
DIVISION

Great Lakes Carbon Corporation

ADMINISTRATIVE OFFICE: 18 East 48th Street, New York 17, N. Y. PLANTS: Niagara Falls, N. Y., Morganton, N. C. OTHER OFFICES: Niagara Falls, N. Y., Oak Park, Ill., Pittsburgh, Pa. SALES AGENTS: J. B. Hayes Company, Birmingham, Ala., George O. O'Hara, Wilmington, Cal. SALES AGENTS IN OTHER COUNTRIES: Great Northern Carbon & Chemical Co., Ltd., Montreal, Canada; Great Eastern Carbon & Chemical Co., Inc., Chiyoda-Ku, Tokyo, Japan

Journal of the
Electrochemical Society

FEBRUARY 1956 **VOL. 103 • NO. 2**

CONTENTS

Editorial

Technical Papers

Current Affairs

Published monthly by The Electrochemical Society, Inc., Mount Royal and Guilford Aves., Baltimore 2, Md., combining the JOURNAL and TRANSACTIONS OF THE ELECTROCHEMICAL SOCIETY. Editorial offices: 216 West 102nd Street, New York 25, N. Y Statements and opinions given in articles and papers in the JOURNAL OF THE ELECTROCHEMICAL SOCIETY are those of the contributors, and The Electrochemical Society assumes no responsibility for them. Nondeductible subscription to members $5.00; subscription to nonmembers $18.00. Single copies $1.25 to members, $1.75 to nonmembers. Entered as second-class matter November 5, 1947, at the Post Office at Baltimore, Md., under the act of August 24, 1912.

SARGENT-SLOMIN ANALYZERS
are standard equipment in prominent laboratories

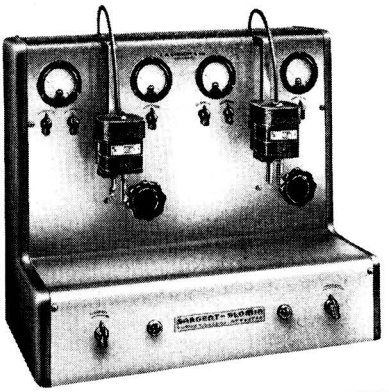

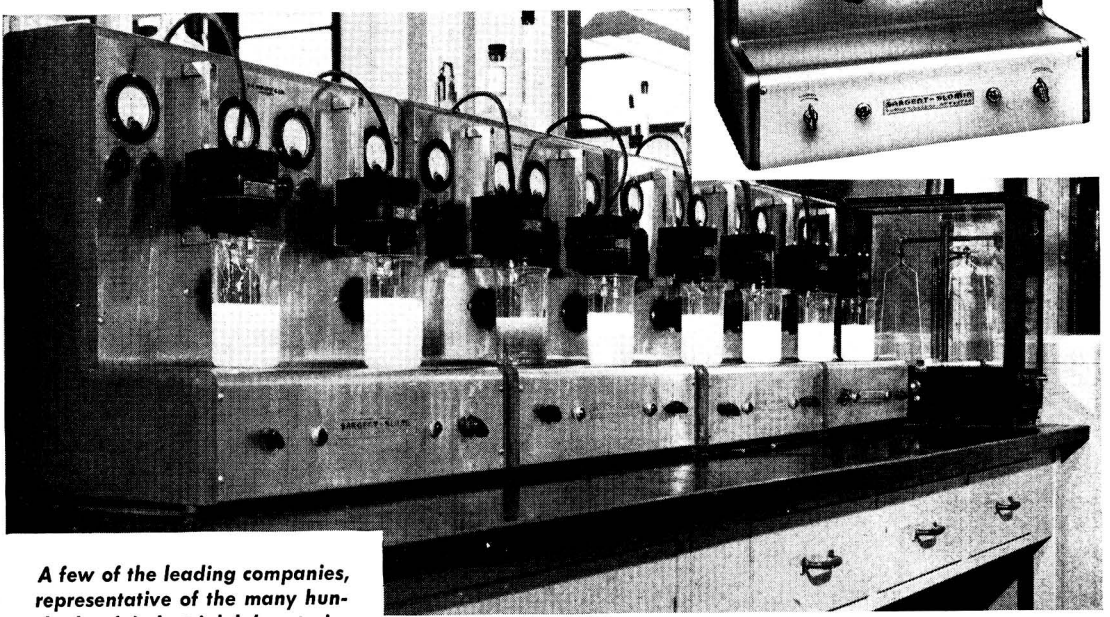

Photo Courtesy INTERNATIONAL HARVESTER COMPANY, Melrose Park, Illinois

A few of the leading companies, representative of the many hundreds of industrial laboratories using the Sargent - Slomin and Heavy Duty Analyzers for control analyses . . .

AMPCO METAL, Inc.
ANDERSON LABORATORIES
CALERA MINING COMPANY
EUREKA WILLIAMS COMPANY
THE FEDERAL METAL CO.
FORD MOTOR COMPANY
THE GLIDDEN COMPANY—Chemical, Metal and Pigment Division
HOT POINT CO.
HOWARD FOUNDRY COMPANY
INTERNATIONAL HARVESTER COMPANY
KENNAMETAL Inc.
McQUAY - NORRIS MANUFACTURING CO.
NATIONAL LEAD COMPANY, Fredericktown, Missouri
PIASECKI HELICOPTER CORPORATION
REVERE COPPER & BRASS INCORPORATED
THE RIVER SMELTING & REFINING COMPANY
SILAS MASON COMPANY
THE STUDEBAKER CORPORATION
THOMPSON PRODUCTS, INC.

Sargent-Slomin Electrolytic Analyzers are recommended for such electro analytical determinations as: Copper in—ores, brass, iron, aluminum and its alloys, magnesium and its alloys, bronze, white metals, silver solders, nickel and zinc die castings. Lead in—brass, aluminum and its alloys, bronze, zinc and zinc die castings. Assay of electrolytical copper, nickel and other metals.

Sargent analyzers are completely line operated, employing self-contained rectifying and filter circuits. Deposition voltage is adjusted by means of autotransformers, with meters indicating volts and amperes and controls on the panel. An easily replaceable fuse guards against circuit overload. Maximum D.C. current capacity is 5 to 15 amperes; maximum D.C. voltage available, 10 volts.

Sargent-Slomin Analyzers stir through a rotating chuck operated from a capacitor type induction motor, having a fixed speed of 550 r.p.m. with 60 cycle A.C. current or 460 r.p.m. with 50 cycle A.C. current. Motors are sealed against corrosive fumes and are mounted on cast metal brackets, sliding on ½" square stainless steel rods, permitting vertical adjustment of electrode position over a distance of 4". Pre-lubricated ball-bearings support the rotating shaft. All analyzers accommodate electrodes having shaft diameters no greater than 0.059 inch. Stainless steel spring tension chucks permit quick, easy insertion of electrodes and maintain proper electrical contact. Special Sargent high efficiency electrodes are available for these analyzers. Illustrated above is one model of the five types of Sargent-Slomin and Heavy Duty Analyzers.

S-29465 ELECTROLYTIC ANALYZER—Motor stirred, Two Position, 5 Ampere. With two adjustable heaters, pilot lights and control knobs. For operation from 115 volt, 50 or 60 cycle A.C. circuits.....**$475.00**

SARGENT

SCIENTIFIC LABORATORY INSTRUMENTS • APPARATUS • SUPPLIES • CHEMICALS

Catalog No. 100 Now Available

E. H. SARGENT & COMPANY, 4647 W. FOSTER AVE., CHICAGO 30, ILLINOIS
MICHIGAN DIVISION, 8560 WEST CHICAGO AVENUE, DETROIT 4, MICHIGAN
SOUTHWESTERN DIVISION, 5915 PEELER STREET, DALLAS 19, TEXAS
SOUTHEASTERN DIVISION, 3125 SEVENTH AVE., N., BIRMINGHAM 4, ALA.

The International Geophysical Year

THE INTERNATIONAL GEOPHYSICAL YEAR (IGY) is actually an 18 month period, from July 1, 1957 through 1958, during which scientists the world over have agreed to make a well-coordinated series of measurements in addition to their normal work, in order to study many natural phenomena. This IGY follows, with a gap of 25 years, the International Polar Year of the early 30's. It has been expanded to cover the entire world, and represents the first world-wide coordinated attack on the fundamental problems of the physics of our environment. It is altogether a much larger operation than the previous one and represents an effort in which perhaps a total of one hundred million dollars will be spent for research the world over.

A total of 14 different disciplines are involved at present. All these are fields in which a complete understanding necessitates a world study, for natural phenomena are no respecters of political boundaries. Such fields include meteorology, aurora and airglow, oceanography, seismology, cosmic rays, ionospheric physics, solar physics, geomagnetism, glaciology, and gravity measurements. To understand these phenomena and their complex interrelations, data must be gathered from all over the world. For example, in meteorology we do not know today whether there is a substantial and massive movement of air across the equator. We do not know much about the nature of the additional radiation that reaches us from the sun at the times of disturbances on the solar surface. We suspect that this is a charged particle radiation, and we know qualitatively that it produces many important effects. It ionizes the air through which it passes, producing important changes in the ionosphere and hence in usable radio communications frequencies. It produces auroras. It produces cosmic ray effects observable at sea level. We know very little about how, for example, it affects the heat balance of the atmosphere, how it may affect ozone distribution, and whether it has any effects in meteorology of importance to synoptic forecasting. We know it produces magnetic storms, in which the compass may suddenly point many degrees away from the usual magnetic meridian and high voltages may be induced on long overhead lines. But the details of these mechanisms and the many complex interrelations have not yet been made clear. To gain an understanding we must study the phenomena as individual subjects and also as interconnected occurrences. To get an adequate picture we must make these studies on a world-wide scale, for the fragmentary knowledge, if we must confine ourselves to any one nation, may prove of little value or even misleading.

(Continued on next page)

Editorial (continued)

Some 35 nations already have signified their interest in taking part in this work. Naturally, the contributions of the nations will not be equal, for some nations are favorably situated to study certain phenomena. For example, the zone of maximum auroral frequency passes through Alaska, Canada, and Greenland, but is too far north to be well studied in Germany, France, or Russia. In other countries with quite small populations such as Norway and Sweden, there happen to be specialists in certain branches who enjoy world fame as the leading persons in their fields. In still other countries there are very few qualified persons in any field, or at the most only in a small fraction of the fields. Consequently the organization has had to be flexible, and each nation will not be expected to contribute in every sphere. While in general it is hoped that the work in any one nation will be primarily carried out by the nationals of that country, some expeditions are contemplated to cover otherwise understaffed regions. Important assistance from England is going to the Cosmic Ray laboratory at University College in Uganda, and expeditions from France will make observations in Bangui, Equatorial Africa, and Kergulen Island in the south Indian ocean.

A major effort will also be made in the Antarctic. In this little-known area there will be at least five major expeditions, including an Australian base at Mac Robertson Land, a French expedition basing at Adelie Land, a British traverse from the Wedell Sea to the pole, a Russian expedition, and a U. S. complex consisting of a main base near the old site of Little America and at least three satellite bases, one at the South Geographic Pole itself. The total exploratory effort in this region will be enormous, and, considering that some two-thirds of the entire continent has never been seen by man, the importance of this work is obvious.

The ultimate practical value of the work and of the uses that can be made of the new knowledge gained promises to be enormous. It will be recalled that the last Polar Year work resulted in the discovery of the ionized layers in the upper atmosphere in the zone of the arctic night. The presence of these layers has made possible new communications channels. The monetary value of this discovery to the communications companies alone has been estimated as many times greater than the entire cost of all scientific work done during that year. Thus it appears that, as is so often the case with scientific work, the ultimate value far exceeds the cost and often turns up in the most unexpected fields. This major and well-coordinated attack on the basic problems of our environment promises to yield many important new facts to advancing technology, and will greatly increase our understanding of the workings of the physical world we live in.

—SERGE A. KORFF[1]

[1] Dr. Korff is with the Department of Physics, New York University, New York, N. Y.—*Ed.*

Improved Plating Techniques by Baker & Adamson

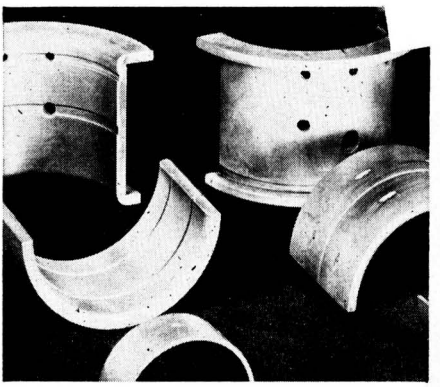

Vital Engine Parts Protected!

A harder coating, with better corrosion and wear resistance, is produced with a low tin-content B&A fluoborate bath for protecting bearings and other engine parts. Additional uses include depositing coatings on pistons and similar parts to provide marginal lubrication during break-in periods, electro-cladding wire and plating threaded parts for needed lubrication properties.

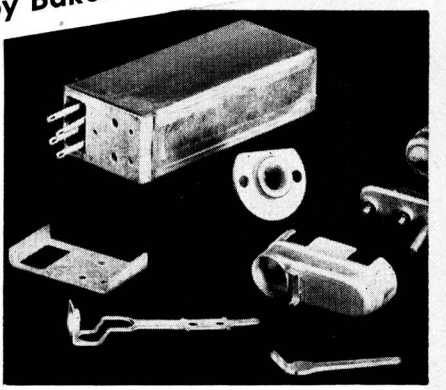

Soldering Made Easy!

A high-tin-content fluoborate bath produces coatings of excellent solderability on electronic or electrical parts where the use of a non-corrosive flux is desired. It also gives a uniform coating that expedites assembly, and where the parts can be fused, the B&A Fluoborate alloy bath can be used to deposit the solder, eliminating costly hand soldering.

NOW...You Can Plate CUSTOM-MADE Alloy Coatings with B&A Lead and Tin Fluoborates!

These are high-speed, low-cost operations . . . short-cuts to producing better, more economical products.

The plated coatings shown are actually tailor-made to specific requirements with Baker & Adamson Lead and Tin Fluoborate Solutions. When protective and lubricating coatings are required, as in bearings, lead-tin alloys of low tin content are readily plated. Where a deposit of good solderability is desired, as in electronic parts, alloys with 40-60% tin content can be produced. B&A Lead and Tin Fluoborate Solutions, combined in a bath using alloy anodes, produce dense, fine-grained, uniform deposits with pre-determined characteristics. Send the coupon for detailed technical bulletins.

B&A Fluoborate Plating Chemicals Include:

Lead • Tin • Iron • Copper • Nickel • Cadmium
Indium • Antimony* • Chromium* • Cobalt*
Fluoboric Acid

*Experimental quantities only

FINE CHEMICALS

B&A STANDARD OF PURITY

REAGENTS

Clip to your letterhead and mail today!

GC Allied Chemical

BAKER & ADAMSON® PRODUCTS
GENERAL CHEMICAL DIVISION
ALLIED CHEMICAL & DYE CORPORATION
40 Rector Street, New York 6, N. Y.

Please send, without obligation:—

☐ Your Technical Bulletins No. TC38351, RA38351, and RB38351 on applications and techniques for plating lead and tin alloy coatings.

☐ Information on applications of other B&A Metal Fluoborates. Specify type_____

Name_____

Position_____

Company_____

City_____ Zone____ State_____

IE-2

to regulate and record—

TEMPERATURE.. PRESSURE.. VACUUM..TIME

mechanical instruments by

WESTON

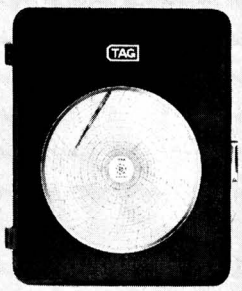

RECORDING INSTRUMENTS . . . in 9″, 10″ and 12″ chart sizes — single and multipen — for all requirements.

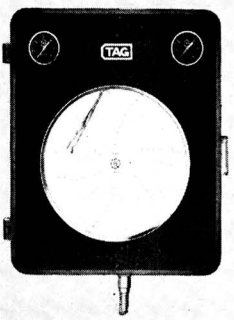

RECORDING CONTROLLERS . . . handle temperatures from —325°F to 1000°F—vacuum to 30″ mercury — pressures to 7500 psi or higher.

TIME CONTROLLERS . . . make any semiautomatic retort control system fully automatic. Available in both standard and special forms.

INDICATING CONTROLLERS . . . accurately regulate temperature, vacuum, pressure and indicate on direct-reading scale.

Just Published!

Just published . . . the new catalog M2A which fully illustrates and describes the comprehensive line of WESTON mechanical instruments, noted for their long-time accuracy and dependability. Send for your copy today; or ask your local Weston representative for help on any measurement or control problem involving temperature, vacuum, pressure. Weston Electrical Instrument Corporation, 614 Frelinghuysen Avenue, Newark 5, New Jersey, *a subsidiary of Daystrom Incorporated.*

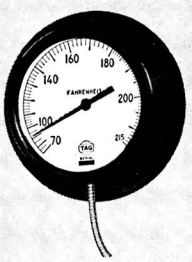

DIAL THERMOMETERS (remote reading) . . . furnished with mercury, gas, or vapor pressure actuations. Flush or wall mounting. Indicate low as —325°F., high as 1000°F.

WESTON *Instruments*

Anodization of Lead in Sulfuric Acid

JEANNE BURBANK

U. S. Naval Research Laboratory, Washington, D. C.

ABSTRACT

The anodic corrosion product formed on lead in sulfuric acid solutions depends on the potential of the metal surface.

In the potential range between lead-lead sulfate and lead sulfate-lead dioxide, the following compounds were identified by electron diffraction: monobasic lead sulfate, lead hydroxide, and lead monoxide. In addition, the diffraction pattern for an unidentified material was observed. Coordinated potential-time curves show arrests corresponding to the appearance of these compounds. The physical nature of these corrosion films is discussed.

INTRODUCTION

A study of positive grid corrosion in the lead acid storage battery led to a detailed investigation of the electrochemical and physical processes associated with anodizing lead in sulfuric acid solutions (1–3). Rate of attack and composition of the corrosion product vary with potential.

Pseudomorphic, epitaxial, and oriented overgrowths have been postulated for many systems where oxide films are formed electrochemically. Lead monoxide and lead dioxide were identified as products of anodic attack on lead. Lead monoxide was shown by Lander (1) to be the tetragonal form which is a layered structure parallel to the (001) planes described by other workers (4, 5). Wyckoff (6) gave a description of lead dioxide. Their structures indicate that these compounds may grow epitaxially on the lead lattice.

In addition to a diffraction study of the anodic products formed on lead in sulfuric acid, this investigation was concerned with discharge curves of a lead electrode coated with lead dioxide. In the discharge of such a surface, the potential remains constant under a given set of conditions, and, when a new process becomes dominant, the surface potential will change and level off again at some new value characteristic of the new set of conditions. These "plateaus" may represent distinct electrode processes, each producing characteristic compounds as corrosion products. This study was undertaken (*a*) to determine where such arrests occur on the discharge of a lead dioxide electrode in sulfuric acid, and (*b*) to identify and characterize by electron diffraction the anodic products formed at various potentials.

EXPERIMENTAL

Although most of the pure lead used for this study was manufactured by the National Lead Company, a few castings made of very pure (99.9998%) lead were used in checking runs to eliminate the possibility that some electrochemical effects were caused by impurities.

The cast specimens were milled flat, polished, and etched. The etch was followed by a rinse in saturated ammonium acetate solution and a thorough rinsing in city water, then in distilled water. For polarization studies, the specimen was inserted in the cell while still wet from the final rinse. For electron diffraction study, the specimen was cleaned in the same way, but it was also rinsed in boiling distilled water, blown dry, then mounted in the camera. In this process, less than 2 min elapsed between the final rinse and attainment of essentially full vacuum. About one out of five preparations resulted in a film-free surface despite the short time exposed to the air.

Single grains cut from polycrystalline castings were used in orientation studies. Grains having the desired orientations were selected with an optical goniometer.

After anodizing, the electrodes to be examined by electron diffraction were usually rinsed in boiled distilled water; however, in some instances no water rinse was used, and the electrodes were blotted dry with tissue or rinsed in acetone and blown dry.

The electrolyte, 1.210 specific gravity sulfuric acid, was prepared from Baker's C.P. acid and distilled water. Etchants were made from Baker's C.P. acetic and nitric acids, Merck's C.P. ammonium acetate, and Superoxol.[1]

Polarization studies were carried out in a methyl methacrylate cylinder that was threaded to receive the specimen mount described earlier (3). Specimens for electron diffraction examination were anodized by submerging a cleaned lead surface in the electrolyte in a glass beaker. By rapid manipulation of the specimens, formation of chemical reaction products could be minimized in the rinsing and drying process. Diffraction specimens were held at the desired potentials for various periods of time in order to develop coatings suitable for electron diffraction study. The time varied from 10 min to 24 hr. A sheet of pure lead was used as a cathode; its area was ten or more times the area of the anode.

Potential of the anodizing specimen was measured with a mercury, mercurous sulfate reference electrode, a high impedance bridge, and recording potentiometer. In this paper, potentials are given in reference to the electrode that is 0.68 volt positive to the normal hydrogen electrode in 1.210 specific gravity sulfuric acid. Several potentials of interest are given by Lander (1).

Polarization studies were made by applying the potential to the cell before introduction of the electrolyte or before insertion of the electrode into the solution. In this

[1] 30% H_2O_2 manufactured by Merck and Co., Inc., Rahway, N. J.

way only a short time is required for the specimen to reach the potential selected for anodization. The discharge of lead dioxide films was studied by time potential records. To obtain reproducible curves, the clean specimen, still wet with the final rinse, was polarized above the lead dioxide, lead sulfate potential as rapidly as possible, and this potential was held for specific periods of time. Potential changes and arrests displayed by lead surfaces were followed with the reference electrode (*a*) during anodization, (*b*) on open circuit stand or "self discharge," (*c*) on closed circuit discharge through a resistance, and (*d*) with discharging current applied.

In one instance the specimen was made by withdrawing an iron wire loop from molten lead to form a thin foil that could be totally anodized. The foil was anodized to translucency at a potential of −0.60 v. It was blotted dry and the diffraction pattern recorded by transmission. Other foils made by rolling or etching were anodized above the lead dioxide, lead sulfate potential.

Electron diffraction patterns were recorded with the diffraction attachment of an RCA EMU electron microscope. Patterns were taken mostly by reflection, but a few were made by transmission, and several patterns of scrapings from anodic coatings were obtained with an extended field attachment. Many attempts were made to strip the oxide films, but none proved wholly satisfactory. The usual mercury treatment (7) was not successful, but several sulfate films were stripped in glacial acetic acid. Film fragments were washed in distilled water and studied by transmission diffraction.

Several x-ray diffraction patterns were recorded with a North American Phillips geiger counter spectrometer from lead sheet specimens that were anodized in 0.0005 and 0.1M sulfuric acid.

Results and Discussion

Reproducibility of the electrochemical measurements was affected by preparation and pretreatment of the metal surface. After drying, a polished and etched lead surface became covered with an air-formed film. This deposit resulted in an open-circuit potential of approximately −0.6 v with respect to the mercury, mercurous sulfate electrode when the specimen was first introduced into the electrolyte. This film was identified as lead hydroxide by electron diffraction (8). When allowed to stand in acid, a lead surface with such a coating gradually assumed the lead, lead sulfate potential of −0.93 v if the air-formed film was thin enough. Such films present on the surface prior to anodizing interfered with prompt development of a uniform lead dioxide coating.

When first introduced into the electrolyte, a lead surface free of oxide or hydroxide films displayed an open-circuit potential of −1.1 v to the reference. After a while this potential rose to the lead, lead sulfate potential. A specimen prepared as described and introduced into the electrolyte while still wet from the final rinse consistently showed the −1.1 v potential that is attributable to the low concentration of lead ion in the acid.

Because the amount and nature of the material present on the metal surface affected electrochemical results in short term experiments such as the present ones, specimens were kept wet with distilled water after preparation and anodized immediately.

The commonly used acetic acid-Superoxol and nitric acid etches (9) formed an oriented film of $3PbO \cdot 2Pb(OH)_2$ on the surface of pure lead (10), as shown by electron diffraction examination of the etched surface. This coating could be removed by rinsing the specimen in saturated ammonium acetate solution or in nonoxidizing acids such as acetic or hydrochloric.

Satisfactory electron diffraction patterns of lead could be obtained from specimens that were dried after final rinsing if these were used within a reasonable time after preparation. In no instance was it possible to obtain the open-circuit potential of lead, Pb^{++}, or lead, lead sulfate from specimens that were dried before use. This indicated that the electrochemical measurements were sensitive to films less than 10 Å thick, which is the approximate limit registered by electron diffraction (11).

In using an optical goniometer for orientation determinations, it was found that the faces developed by the acetic acid-Superoxol etchant depended on concentration of the solution. Barrett and Levensen (12) gave the etch mixture for developing the cube planes, i.e., 2 volumes water, 2 volumes acetic acid, and 3 volumes hydrogen peroxide. The concentration of hydrogen peroxide was not stated. The relation between the etch composition and the planes developed on specimens of pure lead was determined by optical goniometer measurements (Table I).

The discharge of lead dioxide coatings formed on pure lead were recorded in time-potential curves, and the one shown in Fig. 1 is typical. For pure lead, the length of each

TABLE I. *Etch composition and planes developed on pure lead*

Volume of water	Volume of glacial acetic acid	Volume of Superoxol	Planes developed
0	95–99	5–1	(111) Octahedral
2	2	3	(100) (110) Decahedral
20	20	3	(100) Cubic

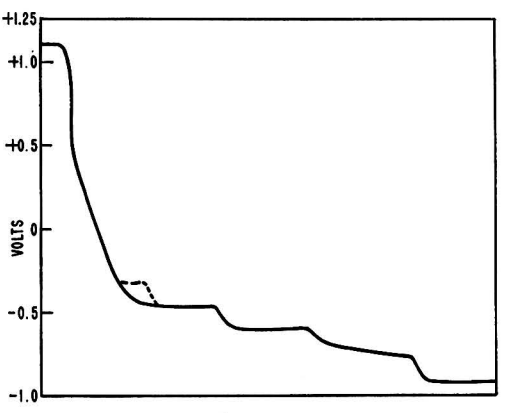

FIG. 1. Discharge of PbO_2 coating on pure Pb in 1.210 sp. gr. H_2SO_4. Potentials are shown vs. the Hg, Hg_2SO_4 electrode.

plateau varied with pretreatment of the specimen. Thus, a slow polarization up to the lead dioxide, lead sulfate potential resulted in a short arrest at this potential upon discharge, and in prolonged arrests at the intermediate plateaus. The most reproducible results were obtained by polarizing to lead dioxide as rapidly as possible. With the exception of the short arrest at −0.32 v, the discharge curves were similar in form whether taken on open circuit self-discharge, with current drain, or with discharging current applied.

As indicated in Fig. 1, arrests occurred at −0.93, −0.73, −0.61, −0.48, −0.32, and 1.1 v vs. the mercury, mercurous sulfate electrode. Compounds appearing on the surface at −0.93, −0.48, and 1.1 v were reported earlier (1) and verified in the present work as lead sulfate, lead monoxide (tetragonal), and lead dioxide, respectively.

The arrest at −0.32 v was not identified as being associated with the appearance of a particular compound. This arrest was consistently of short duration on open-circuit discharge and did not appear on closed-circuit discharge. Tetragonal lead monoxide was found on specimens anodized between a potential of −0.4 and +0.9 v. It is possible that the −0.32 arrest is a polarized lead monoxide potential.

At no time in this work was a lead dioxide film observed to discharge directly to the lead, lead sulfate potential, although thin films apparently by-passed the intermediate plateaus and discharged directly to −0.73 v.

The compound identified by diffraction on the surface of specimens that were anodized at −0.73 v was monobasic lead sulfate (13, 14). Extra lines and bands appeared in many of the electron diffraction patterns of specimens that were anodized near this potential, and this plateau had a slope. It is possible that a series of basic sulfates was actually formed during anodization.

The −0.73 v arrest was stable and frequently held for several days of soaking in the acid. If a specimen showing this potential was cut or scratched, or if a sheet electrode was further lowered into the electrolyte, the potential dropped to −0.93 v but rose again to −0.73 v, presumably as the "break" in this film "healed" by sulfation. The persistence of this plateau suggested that in aqueous solutions the basic sulfate rather than the normal sulfate was the more characteristic coating at the metal-coating interface.

The plateau at −0.64 v was associated with the formation of lead hydroxide identified on the surface of specimens that were anodized at this potential. A thin foil was totally anodized at −0.6 v, and the electron diffraction pattern showed primarily lead hydroxide with a few strong lines from lead sulfate (Table II).

The occurrence of lead monoxide and lead hydroxide in sulfuric acid solution was somewhat anomalous; however, these two compounds were readily identified by their diffraction patterns. Lander (1) suggested that the water molecule is the attacking species in sulfuric acid, and identification of the monoxide and hydroxide supports this view. The sulfate film apparently acts as a barrier to sulfate ions while permitting access of water molecules to the metal surface. Displacement of the observed potentials from the thermodynamically calculated values (Table III) is caused by the fact that the surface is not at thermodynamic equilibrium. The arrest at 1.1 v corresponded to the electrode lead dioxide, lead sulfate in sulfuric acid. An electron diffraction examination of the surface of a specimen anodized at this potential showed a clear strong pattern for lead dioxide. If a single crystal of lead was anodized for 10 min above the lead dioxide, lead sulfate potential, the film was extremely thin, oriented, and showed interference colors. The (100) plane of the lead dioxide lattice was parallel to the (110) plane of the base lead, and the [001] direction was parallel to the [100] direction in lead. Fig. 2 is a drawing of the space lattices of the two crystals. The tetragonal cell in the lead lattice (Fig. 2A), which is bounded by four (110) and two (100) planes, has the dimensions: 4.94 x 3.5 x 3.5 Å. The distances between lead atoms in the oxide structure (6) are 4.97 x 3.4 x 4.97 Å. As shown in Fig. 2B, this is an exceptionally good fit in two crystallographic dimensions; the third, however, is larger by more than 21%. Since 15% is generally accepted as the maximum difference tolerated for lattice continuity, the coating would be expected to fracture away from the base after a limited number of layers form. This was substantiated by the fact that lead dioxide of random orientation was observed on surfaces of single crystals of lead after anodization. There appeared to be a thin layer of oriented lead dioxide immediately adjacent to the metal surface. The patterns showed

TABLE II. *Electron diffraction pattern of lead hydroxide*

Electron diffraction pattern from anodized* lead		Electron diffraction pattern of $Pb(OH)_2$	
d	*I*	*d*	*I*
3.62	s	3.68	ms
3.30	vs	3.33	ms
3.01†	w	—	—
2.64	vs	2.65	s
2.39	vs	—	—
2.33	s	2.27	s
2.13	s	2.16	fm
1.92	vvw	1.91	m
1.77	vvs	1.73	fm
1.69	s	—	—
1.60	w	—	—
1.52	s	1.53	f
1.42	vs	—	—
1.37	w	—	—
1.33	w	1.33	f
1.29	w‡	1.28	f

* Anodized at −0.6 v vs. the mercury, mercurous sulfate electrode in H_2SO_4.

† The extra lines in this pattern may be accounted for from the diffraction pattern of lead sulfate.

‡ There follow many more lines in the patterns for which there are no comparison data.

TABLE III. *Standard and observed electrode potentials*

Electrode	Standard in 28% H_2SO_4 (v)	Observed (v)
PbO_2, $PbSO_4$	1.097	1.1
Hg, Hg_2SO_4	0.00	0.0
Pb, PbO	−0.344	−0.48
Pb, $Pb(OH)_2$	−0.35	−0.64
Pb, $PbSO_4$	−0.971	−0.93
Pb, $PbO \cdot PbSO_4$	−0.81	−0.73
Pb, Pb^{++}, (10^{-10}M)	−1.1	−1.1

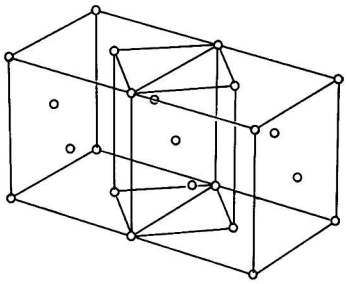

(A)

FIG. 2A. Space lattice of two face-centered cubes of Pb with the body-centered tetragonal cell indicated. (For clarity the relative atomic and ionic sizes, and the crystal structure of PbO_2 have not been indicated in these drawings. The parameters, given in Angstrom units, indicate the distances between lead atom or ion centers.)

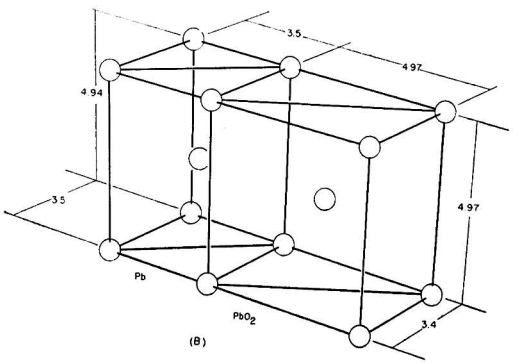

FIG. 2B. Space lattices of Pb and PbO_2 indicating the two-dimensional fit between the body-centered tetragonal cells of metallic Pb and PbO_2.

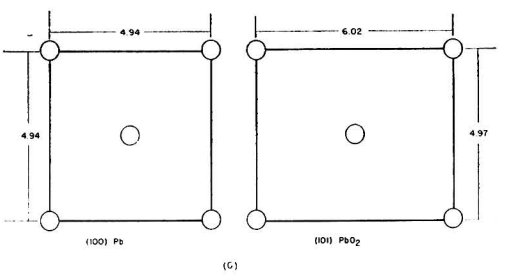

FIG. 2C. The dimensions of (100) Pb and (101) PbO_2 lattice planes.

that many small crystals developed across the surface of a single crystal of lead. The orientation was of high degree, but the spots show a divergence of 7–12°. According to the orientation shown in Fig. 2B, the (101) plane of the oxide would be expected to fall within 10° of the (100) plane of lead. Lead atoms in the (101) planes of lead dioxide have a face-centered configuration (Fig. 2C). The strain produced by such an oxide growing on a metal surface would be expected to result in distortion and possibly cause or contribute to the buckling and growth of pure lead when anodized in sulfuric acid.

TABLE IV. *Diffraction patterns of unidentified material*

Electron diffraction pattern		X-ray diffraction pattern		Calculated diffraction pattern assuming a body centered tetragonal lattice of $a_0 = 3.54$ $c_0 = 5.86$ kx	
d	*I**	*d*	*I*†	*d*	hkl
—	—	5.89	14	5.86	001
—	—	5.00	1	5.00	110
—	—	—	—	3.03	101
2.95	vs	2.93	100	2.93	002
2.53	s	2.50	14	2.50	220
—	—	1.95	13	1.95	003
—	—	—	—	1.90	112
—	—	1.83	1	—	—
1.77	m	—	—	1.77	200
—	—	1.71	8	1.71	103
—	—	1.53	1	1.53	121
1.51	m	1.52	1	1.52	202
1.45	s	1.46	20	1.46	004
—	—	1.35	1	—	—
—	—	1.29	1	—	—
1.24	w	1.24	1	1.25	440
1.16	m	1.17	2	1.17	005
1.13	w	—	—	1.13	204
1.02	vw	—	—	1.05	132
0.972	vw	—	—	0.976	303, 006
0.870	mb	—	—	0.885	400

* Intensities estimated visually.
† Intensities relative to the strongest line.

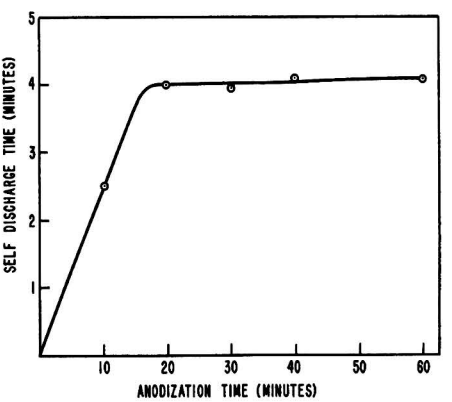

FIG. 3. Relationship of the length of the PbO_2, $PbSO_4$ plateau observed on self-discharge and the time of anodization.

This electron diffraction work showed that polycrystalline coatings of lead dioxide were not always completely converted to sulfate after discharge to the lead, lead sulfate potential. Such remaining lead dioxide was electrically isolated from the surface and contributed nothing to the discharge process.

An unidentified material believed to be a form of lead oxide was also present in some anodic coatings, and the electron diffraction pattern observed for this material is presented in Table IV. Anodized pure lead foil was examined by electron diffraction, and patterns were obtained in which the arcs of the pure lead pattern were doubled. One of the sets of spots was attributed to lead and the other to

the unidentified material. The strong orientation exhibited by this material indicated that it was formed epitaxially on the base lead. This material might have been a cause of the growth and buckling of pure lead, and it also might have contributed to the disparity in the standard and observed electrode potentials in the middle range. Unpublished work with the several lead monoxides indicates that this may be a form of lead monoxide rather than a higher oxide. Complete identification of this material and clarification of its importance to the storage battery corrosion problem rests with future investigation.

A plot of the length of the lead dioxide plateau vs. the length of anodizing time (Fig. 3) shows that anodizing above 20 min contributed little to the self-discharge time. In the first portion of the curve the relationship is essentially linear, i.e., the length of discharge time is directly proportional to the length of anodization. But, beyond 20 min, little additional discharge time is observed. The corrosion rate determined by Lander (1) showed this same configuration with time. The point of slope change in the two cases is different because of differences in experimental details. Direct proportionality at the beginning of the curves, however, suggests that this range corresponds to the lateral growth of coatings across the surface of the specimen. The leveling off may correspond to a much slower rate of film thickening. The slow rate may be even lower than indicated by the corrosion curve, since it represents an over-all corrosion process that included the increase in thickness of the coating plus the "healing" of fissures caused by discontinuities in the metal itself and fractures in the coating.

It is also notable that the leveling off of the curve occurred at about the same time that randomly oriented polycrystalline lead dioxide became the only pattern observed on the surface by electron diffraction.

Conclusions

This study showed that during discharge of a lead dioxide coating on lead, the electrode assumed a series of stable arrests believed to represent several distinct processes. The following compounds were formed upon anodizing lead in sulfuric acid: lead dioxide, lead monoxide (tetragonal), lead hydroxide, $PbO \cdot PbSO_4$, and lead sulfate. These appeared at characteristic potentials that corresponded to the arrests in the discharge process. In addition, an unidentified material believed to be a form of lead monoxide was observed.

The lead dioxide coating was oriented to a limited depth with respect to the underlying lead from which it formed. The orientation may be described:

(100) PbO_2 || (110) Pb
[001] PbO_2 || [001] Pb

The unidentified material was tentatively described as having a body-centered tetragonal space lattice of $a = 3.54$ and $c = 5.86$ kX units. If the suggested lattice is assumed, its orientation may be described:

(100) unknown || (110) Pb
[001] unknown || [001] Pb

Manuscript received July 7, 1955. This paper was prepared for delivery before the Boston Meeting, October 3 to 7, 1954.

Any discussion of this paper will appear in a Discussion Section to be published in the December 1956 Journal.

References

1. J. J. Lander, *This Journal*, **98**, 213 (1951).
2. J. J. Lander, *ibid.*, **98**, 220 (1951).
3. J. Burbank and A. C. Simon, *ibid.*, **100**, 11 (1952).
4. R. G. Dickinson and J. B. Friauf, *J. Am. Chem. Soc.*, **46**, 2457 (1924).
5. W. J. Moore, Jr., and L. Pauling, *ibid.*, **63**, 1392 (1941).
6. R. W. G. Wyckoff, "Crystal Structures," Chap. IV, Interscience Publishers, Inc., New York (1951).
7. S. Wernick, *J. Electrodepositors' Tech. Soc.*, **9**, 163 (1933/34).
8. S. Fordham and J. T. Tyson, *J. Chem. Soc.*, **1937**, 483.
9. J. R. Vilella, "Metals Handbook," p. 1558, American Society for Metals, Cleveland (1939).
10. G. L. Clark and W. P. Tyler, *J. Am. Chem. Soc.*, **61**, 58 (1939).
11. G. P. Thomson and W. Cochrane, "Theory and Practice of Electron Diffraction," p. 153, Macmillan & Co., Ltd., London (1939).
12. C. S. Barrett and L. H. Levenson, *Trans. Am. Inst. Min. and Met. Engrs.*, **137**, 76 (1940).
13. J. J. Lander, *This Journal*, **95**, 174 (1949).
14. Shell Petroleum Company, "X-Ray Diffraction Patterns of Lead Compounds," p. 48, Shell Petroleum Company, Chester, England (1954).

A Self-Discharge Reaction of Cells with Manganese Dioxide and Metal Electrodes

W. C. Vosburgh, D. R. Allenson, and Stanley Hills

Duke University, Durham, North Carolina

Introduction

Metals in water or solutions of electrolytes have been shown to reduce oxygen to hydrogen peroxide (1, 2). It has also been shown that, in ammonium chloride electrolyte, hydrogen peroxide reduces manganese dioxide instead of being entirely decomposed catalytically by it (3). It follows that a cell with manganese dioxide and metal electrodes might undergo self-discharge by this reaction in the presence of oxygen. A decrease in potential of a manganese dioxide electrode in ammonium chloride electrolyte

with a piece of zinc close to it has been observed (4). Further study has shown that this reaction is a possible source of error in experimental work, especially with silver electrodes in chloride electrolytes, if suitable precautions are not taken. It may be one of the self-discharge processes of the Leclanché cell.

Experimental

Manganese dioxide electrodes were made by electrodeposition on graphite rods (3, 4). Total manganese content was 0.2 millimole and the composition $MnO_{1.9}$. The electrodes were kept for a day after preparation in a solution 1M in ammonia and either 2M in ammonium chloride or 1M in ammonium sulfate, depending on the electrolyte in which they were to be used, or in the electrolyte itself if it was not an ammonium salt. They were then stored in water.

For use the electrodes were mounted by means of a rubber stopper in the middle of a glass vessel of about 200 ml capacity. Sheet metal electrodes of silver, zinc, or lead could be inserted into the vessels so as to line the inside wall and encircle the manganese dioxide electrode. Five different electrolytes were used: (*a*) 2M ammonium chloride with enough ammonia to give *p*H 7.3, (*b*) a similar 1M ammonium sulfate solution, (*c*) 2M ammonium chloride and 0.2M zinc chloride, *p*H 5, (*d*) like (*c*), but with enough ammonia to give *p*H 7.2, (*e*) 0.2M potassium chloride in an equimolal (0.025M) phosphate buffer, *p*H 6.7. Measurements of open-circuit potentials of the dioxide electrodes against a saturated calomel electrode were made by a recording potentiometer. The electrolytes were stirred during measurements by a magnetic stirrer.

Fig. 1, redrawn from the recorder curves, shows the behavior of manganese dioxide electrodes with and without metal electrodes present. Fig. 1A represents duplicate control experiments with ammonium chloride electrolyte and with no metal present at any time. The potential was measured for 3-hr periods on each of three successive days. The changes in potential were increases and not more than 3 mv in 3 hr. Fig. 1B shows the effect of clean silver electrodes in ammonium chloride electrolyte. The manganese dioxide electrodes in duplicate cells were affected by the silver electrodes. In a 3-hr preliminary test without the silver electrodes, one varied only a little, and the other was constant. The vertical dashed line at 3 hr indicates introduction of the silver electrode and a 24-hr period thereafter. During this time the manganese dioxide electrodes decreased in potential. The decrease continued fairly rapidly on the second day, with stirring (3–6 hr in Fig. 1) becoming slower with time. The second dashed line indicates a second 24-hr period, but without the silver electrode. A significant increase in potential took place. In the subsequent measuring period (6–9 hr without the silver electrode) one electrode was constant while the other decreased for a time and became constant. At the third dashed line the silver electrode was again inserted with only a few minutes' interruption of the measurement which continued for another 3 hr. After a period of constancy the potential decreased significantly, but less than when the electrodes had stood overnight.

The decrease in potential indicates reduction of the manganese dioxide. It may be postulated that a reducing agent formed by the metal electrode can be carried to the cathode by convection or stirring and react there. Since metals can reduce oxygen to hydrogen peroxide (1, 2), and since atmospheric oxygen was present in the above experiments, hydrogen peroxide might be the reducing agent. Samples of an ammonium chloride solution that have been in contact with a silver electrode and air reduce permanganate and oxidize iodide ion, indicating hydrogen peroxide.

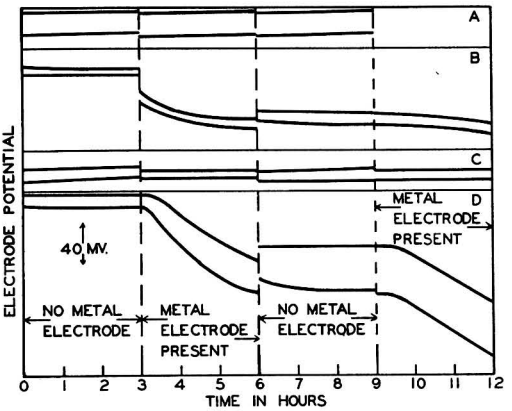

Fig. 1. Effect of a metal electrode on the manganese dioxide electrode potential. A, controls, no metal electrode at any time, ammonium chloride electrolyte; B, silver electrodes in chloride electrolyte; C, silver electrodes in sulfate electrolyte; D, zinc electrodes in potassium chloride electrolyte with phosphate buffer. Dashed line at 3 hr indicates introduction of metal electrode and 12-hr rest period; at 6 hr, removal of metal electrode and 12-hr rest period; at 9 hr, introduction of metal electrode with no rest period.

When an ammonium chloride electrolyte was freed from oxygen by a current of nitrogen before silver and manganese dioxide electrodes were introduced, and a current of nitrogen passed through the cell, the potential of the manganese dioxide electrode was much more nearly constant than when air was present.

Fig. 1C represents a similar experiment with a silver electrode and an ammonium sulfate electrolyte of *p*H 7. The behavior is not enough different from the controls (Fig. 1A) to indicate any effect of the presence of the silver. Appreciable *p*H changes accounted for part of the small potential changes. The test for hydrogen peroxide in the electrolyte was negative.

Zinc in a potassium chloride electrolyte with a phosphate buffer at *p*H 7 was found by Delahay (2) to reduce oxygen to hydrogen peroxide. A cell constructed with this electrolyte showed the most pronounced decrease observed, as shown in Fig. 1D. The procedure was the same as for the cells of Fig. 1B, and the curves are similar, except that no decrease took place during the first night. After standing overnight the zinc electrodes were covered with a loosely adherent gray film. Also, the test for hydrogen peroxide was negative when the cell had stood overnight with the zinc electrode in place. However, it became positive the next day when the solution was stirred.

When a clean zinc electrode was tried in the same way

in an ammonium chloride electrolyte containing zinc chloride and ammonia, *p*H 7, the manganese dioxide electrode showed no change during the 3-day period. A similar electrolyte of *p*H 5 gave indeterminate results, changes little larger than the experimental error. In agreement, the test for hydrogen peroxide in these solutions was negative.

The result for zinc at *p*H 5 does not disagree with Jennings and Vosburgh (5). Their observation of a decrease in potential of a manganese dioxide electrode in the presence of zinc was made over a period of several weeks, and the change per day was small. However, the manganese dioxide was probably reduced by hydrogen peroxide rather than undergoing loss of oxygen as assumed by them.

A clean lead electrode in ammonium sulfate electrolyte of *p*H 7 also caused no observable reduction of the manganese dioxide electrode. Clean lead on which lead sulfate had been deposited electrolytically formed too little hydrogen peroxide for a positive test on standing overnight in ammonium sulfate electrolyte. However, electrodes made of uncleaned sheet lead that had acquired a surface coating of oxide during storage acted like silver in chloride solutions and zinc in phosphate solutions. Such an electrode caused reduction of a manganese dioxide electrode in a cell with an ammonium sulfate electrolyte. Also, ammonium sulfate solutions that had stood overnight with the uncleaned lead electrodes gave positive tests for hydrogen peroxide. In this case the test with titanium(IV) sulfate was positive; it is not sufficiently sensitive in chloride solutions.

Observable amounts of peroxide were formed by the three electrodes that either had a surface coating or formed one as the result of oxygen attack. These were silver in chloride solutions, zinc in phosphate solutions, and uncleaned lead. Clean metals that stayed clean evidently caused catalytic decomposition of the peroxide as fast as formed. A suitable surface film must retard the decomposition more than the formation.

To see whether the self-discharge reaction would go on indefinitely, a cell with silver and manganese dioxide electrodes was allowed to stand for a month during which time the manganese dioxide electrode potential decreased continuously from an initial value of 0.453 to 0.237 v.

Rough measurement of the concentration of peroxide in solutions that had stood two or three days with metal electrodes gave $10^{-4}N$ for both chloride electrolyte with silver and sulfate electrolyte with uncleaned lead.

Errors can be avoided in experiments with manganese dioxide (and perhaps other) electrodes and silver, lead, or zinc electrodes by the use of clean metal and conditions not leading to film formation. Exclusion of oxygen is also effective. If silver electrodes must be used in chloride solutions, a layer of silver chloride thick enough to retard peroxide formation will prevent trouble. Two silver electrodes coated with silver chloride electrolytically with a current of 0.25 ma/cm² for 50 hr and kept in boiling water for 3 hr to insure absence of peroxide caused no significant change in a manganese dioxide electrode when tested as above. Such electrodes seem to be able to acquire some peroxide on standing in water and also from the electrolyte in which they are coated with chloride. Freshly coated silver electrodes not given the boiling water treatment, and electrodes that had stood for some time caused decreases of the order of 10 mv on standing overnight in chloride electrolytes with manganese dioxide electrodes.

Acknowledgments

Part of this work was carried out under Contract Nonr-1016(00) with the Office of Naval Research and part with the help of a fellowship supported by E. I. du Pont de Nemours and Company.

Manuscript received July 11, 1955.

Any discussion of this paper will appear in a Discussion Section to be published in the December 1956 Journal.

References

1. J. W. Mellor, "A Comprehensive Treatise on Inorganic and Theoretical Chemistry," Vol. 1, p. 925, Longmans Green & Co., London (1922).
2. P. Delahay, *This Journal*, **97**, 205 (1950).
3. A. M. Chreitzberg, Jr., D. R. Allenson, and W. C. Vosburgh, *ibid.*, **102**, 557 (1955).
4. D. T. Ferrell, Jr., and W. C. Vosburgh, *ibid.*, **98**, 334 (1951).
5. C. W. Jennings and W. C. Vosburgh, *ibid.*, **99**, 309 (1952).

A Technique for Evaluating Various Cathode Materials

C. K. Morehouse and R. Glicksman

RCA Laboratories, Radio Corporation of America, Princeton, New Jersey

ABSTRACT

An apparatus and technique are described which enables a quick preliminary evaluation to be made of various manganese dioxides and other cathode materials in various electrolytes. Data are presented which show that the capacity of the manganese dioxide electrode exceeds that calculated for its reduction to $Mn_2O_3 \cdot H_2O$ when discharged at low current drains or with a flow of electrolyte over the electrode. It is also shown that the structure of the manganese dioxide material is an important property which determines the performance that is obtained when the electrode is discharged, not only in a NH_4Cl-$ZnCl_2$ type of electrolyte, but also in a basic electrolyte.

Introduction

It is well known that the manganese dioxide cathode is the limiting electrode of the Leclanché dry cell. Manganese dioxide is not a simple compound of constant properties and its value for battery use does not depend merely on its purity (1, 2). The x-ray spectrometer, the electron microscope, differential thermal analysis, and magnetic susceptibility have all thrown new light on its characteristics. In spite of the recent advances, no satisfactory single physical or chemical method of evaluating cathode materials has been developed, and actual trials in operating cells have been necessary to establish their battery quality.

Cahoon (3) suggests the use of the following two electrochemical tests as a means of evaluating a manganese dioxide: (*a*) determination of the *p*H-potential relation in zinc and ammonium chloride electrolyte; and (*b*) determination of the "utilization factor," i.e., the extent of cathodic reduction in a continuous stream of fresh electrolyte.

In this paper a technique for evaluating various cathode materials is presented. The apparatus which was designed for this work is similar to that described by Cahoon (3) for his "utilization test;" however, the procedure and methods of measurement have been considerably modified.

Equipment and Procedure

The apparatus used is shown in Fig. 1, and the procedure used in making cathode polarization studies is as follows.

A piece of filter paper supported by cotton gauze is fastened to a glass cylinder, 1⅝ in. I.D. and 1¾ in. in length, by means of a rubber band. A layer of Acheson No. 615 graphite wet with electrolyte is laid on the filter paper inside the glass cylinder. On top of this is placed 0.5 g of cathode material previously ground with 10% by weight of Shawinigan acetylene black. The cathode material is then covered with a layer of graphite and a perforated graphite disk. A graphite rod, on top of which is placed a 2 kg weight, makes contact with the perforated graphite disk and acts as a terminal electrode for the cathode. A zinc sheet placed outside the reservoir at a controlled distance from the cathode material acts as the anode.

After the cell is assembled, electrolyte is flushed through the cathode chamber to wet completely the cathode material. The cell is then discharged by withdrawing a constant current from the cell, either with electrolyte flowing over the cathode material at a controlled rate or with no flow of electrolyte. In this work measurements were made with no flow of electrolyte, i.e., under static conditions. The inner chamber, containing the cathode material, holds 15–20 ml of electrolyte and the outer chamber approximately 60 ml of electrolyte.

The potential of the cathode or anode is measured by means of a saturated calomel reference electrode which is contained in the outer chamber close to the cathode in a fixed position. Measurements are made at definite time intervals with a L&N type K potentiometer.

The procedure differed from that of Cahoon's in the following ways: (*a*) the cathode material was discharged under static conditions with a fixed quantity of electrolyte; (*b*) measurements were made while the cathode material was discharging.

The results presented are lower than the true polarization values since they include a small constant *IR* drop which is characteristic of the electrolyte, apparatus, and procedure. If necessary, this *IR* drop can be eliminated by using various known procedures (4), or it can be measured by an oscillographic technique (5).

The purpose of this study was to evaluate the performance of various cathode materials, and, since the manner in which the voltage of the electrode changed with time is the most important factor, measurements were made by the simpler technique. In these experiments, a current drain of 0.050 amp was used, which corresponds to a discharge rate of 0.100 amp/g for the 0.5-g sample of cathode material.

Evaluation of Technique

A number of manganese dioxides which are now being used in batteries were tested. It was found that differences in the polarization behavior of the various manganese dioxides were comparable with test results reported for cells containing these oxides. In order to be positive about the method, several samples of manganese dioxide were obtained as unknowns from the Signal Corps Engineering Laboratories. Information about source, structure, and performance in actual cells was withheld until after dis-

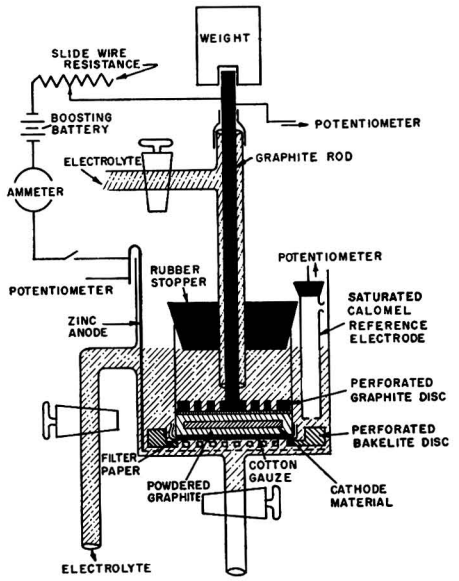

FIG. 1. Apparatus for evaluating cathode materials

the capacity in ampere-minutes per cubic inch for these manganese dioxides. On the basis of the data in Fig. 2 taking a cut-off voltage of +0.5 v for the manganese dioxide, samples were rated for expected performance in dry cells on high current drain applications. Taking a +0.10 v cut-off, samples were also rated for expected performances in batteries on low drain applications. A complete tabulation of the discharge data and rating for high drain applications along with the cell performance data and rating is shown in Table II. Comparative data and rating for low drain applications are given in Table III.

The discharge data presented in these tables are on the basis of ampere-minutes per gram and ampere-minutes per cubic inch of the manganese dioxide materials. Cell discharge data presented were gathered by the Signal Corps Engineering Laboratories.

It should be pointed out that the rating of the manganese dioxide materials based on discharge data expressed in ampere-minutes per cubic inch more closely approaches the rating based on actual cell discharge data than that based on discharge data expressed in ampere minutes per gram since the density factor of the sample is taken into account. This is important because only a certain volume of manganese dioxide can be introduced into a specific cell size.

TABLE I. *Various properties of manganese dioxide materials*

Classification	Electro ore #1 (F)		Electro ore #2 (B)		Electro ore #3 (D)		Chem ore #1 (E)		Chem ore #4 (A)		Chem ore #3 (G)		Chem ore #2 (C)		African ore (J)		Mexican ore (I)	
Method of preparation	Anodic deposition on graphite electrodes from aqueous solution of H_2SO_4 and $MnSO_4$						Reduced African MnO_2, treated with H_2SO_4 solution. The MnO_2 which settles out is filtered and washed free of acid.						Thermal decomp. of $Mn(NO_3)_2$		Naturally occurring			
Available oxygen as % MnO_2	89.2		85.0		65.6		79.9		68.6		85.0		84.6		84–85		70.3	
% Total Mn	57.7		59.0		61.5		55.3		45.8		59.0		58.1		58.0		49.0	
	d	I/I_1	*d*	I/I_1	*d*	I/I_1	*d*	I/I_1	*d*	I/I_1	*d*	I/I_1	*d*	I/I_1	*d*	I/I_1	*d*	I/I_1
Electron diffraction data	4.10	100	2.41	100	4.68		3.53		4.0	37	2.41	100	4.18		4.37	12	3.11	
	3.70	59	2.12	43	3.96		3.11	69	3.68	100	7.14	75	2.39	100	3.11		2.43	100
	2.955	6	1.83		3.16		2.43	100	2.45	5	1.65	50	2.115	83	2.57	100	2.16	72
	2.467	2	1.64	28	2.74	24	2.16	70	1.39	25	1.55		1.63	52	2.43	61	1.83	39
	2.410	1.7	1.495	18	2.43	100	1.83	20			1.44	50	1.415	55	2.16	18	1.70	39
	2.207	10	1.222	9	2.15	65	1.65	51			1.31	25	1.345	50	1.84	35	1.54	
	2.117	1.2	1.165	11	2.04	13	1.54								1.62		1.44	60
	2.052	6	1.065	11	1.84	17	1.42	91							1.54	47	1.37	70
	1.850	2.5	0.85		1.64	53	1.37	32							1.44	23		
	1.743	2.5	0.84		1.54		1.29	12							1.37			
	1.606	1.7			1.44	66	1.05								1.29			
	1.501				1.41	52									1.24			
	1.477				1.31	17												
	1.417				1.17													
	1.389																	
	1.268				1.06													
	1.228				0.99													
	1.116																	
	1.099																	
	1.005																	

charge data on the above equipment had been gathered and the samples rated according to these data. The various types of manganese dioxides are characterized by the chemical and physical data shown in Table I. Fig. 2 shows

These results show that the method is of value in making preliminary evaluations of cathode materials. Large differences should be easily recognized. The method does have limitations in that it tells nothing about the concen-

TABLE II. *Discharge data and ratings of various manganese dioxide materials for use in batteries designed for high drain applications compared with Signal Corps battery data and rating*

Source	Classification	Apparent density g/in.³	Discharge data: 0.5 g MnO_2 material discharged at 0.100 amp constant current per gram to +0.50 v in 20% NH_4Cl-33% $ZnCl_2$-47% H_2O electrolyte				Signal Corps Battery data	
			Weight basis		Volume basis			
			Wt basis amp min/g	Rating	Vol. basis amp min/in.³	Rating	Capacity hr*	Rating
Electro ore #1	F	19.4	5.8–5.4	2	112–105	2	7.9	1
Electro ore #2	B	21.0	5.3	3	111	1	6.5–7.5	2
Chem ore #1	E	16.1	4.9–4.3	4	77–69	4	6.8	3
Chem ore #2	C	11.5	8.8–6.6	1	101–76	3	6.4	4
Chem ore #3	G	18.5	3.0–2.6	5	56–48	5	4.5–5.0	5
Electro ore #3	D	21.8	2.3–2.0	6	50–44	6	4.5	6
African ore (natural)	J	22.5	1.9–1.1	7	43–25	7	4	7
Mexican ore (natural)	I	23.3	0.6	8	14–2.3	8	2.1	8
Chem ore #4	A	13.1	0.3–0.2	9	3.9–2.6	9	Very low	9

* "A" size Leclanché cells discharged continuously through a 16⅔ ohm resistance to 1.00 v/cell.

TABLE III. *Discharge data and ratings of various manganese dioxide materials for use in batteries designed for low drain applications compared with Signal Corps battery data and rating*

Source	Classification	Apparent density g/in.³	Discharge data: 0.5 g of MnO_2 material discharged at 0.100 amp/g to +0.10 v in 20% NH_4Cl-33% $ZnCl_2$-47% H_2O electrolyte				Signal Corps battery data	
			Weight basis		Volume basis			
			Wt. basis amp min/g	Rating	Vol. basis amp min/in.³	Rating	Capacity hr*	Rating
Electro ore #1	F	19.4	12.4–11.3	2	241–219	2	140.9	1
Electro ore #2	B	22.5	11.4–11.1	3	257–250	1	130–135	2
Chem ore #1	E	16.1	11.5–10.7	4	185–172	4	101.3	3
Chem ore #2	C	11.5	18.6–17.5	1	214–201	3	96.8	4
Chem ore #3	G	18.5	7.9–6.8	5	146–126	5	85.9	5
African ore (natural)	J	21.0	6.8–5.8	6	143–122	6	80	6
Electro ore #3	D	21.8	5.2–4.8	8	113–105	7	61.8	7
Chem ore #4	A	13.1	4.7–4.6	9	62–60	9	50	8
Mexican ore (natural)	I	23.3	5.3–2.9	7	123–68	8	36.0	9

* "A" size Leclanché cells discharged through a 116⅔ ohm resistance to 1.13 v/cell.

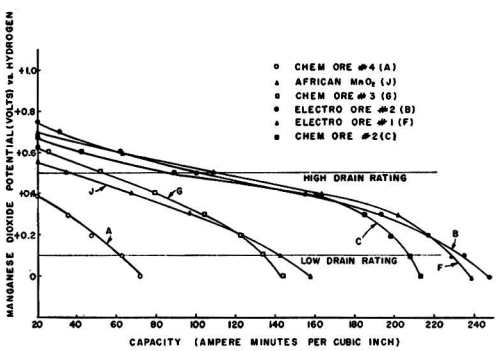

FIG. 2. Capacity in ampere-minutes per cubic inch of various manganese dioxides discharged at 0.100 amp/g in 20% NH_4Cl-33% $ZnCl_2$-47% H_2O electrolyte.

tration of impurities, stability, or solubility of a particular material, such properties being important in designing a cell with a good shelf life. Data of this type will have to be obtained from other measurements or from experimental cells.

CAPACITY STUDIES

The apparatus can also be used to study the effect of various factors on the efficiency of a manganese dioxide electrode. For example, attempts to obtain maximum efficiency from a manganese dioxide electrode were made by reducing the discharge rate, allowing greater chance for ions to diffuse away or to the electrode. Results of these experiments are shown in Fig. 3. In accordance with cell test data, as the current drain is reduced, the ampere-minutes capacity per gram of manganese dioxide to any cut-off voltage is increased. Data also show that if the current drain is low enough, it appears possible to reduce the manganese below its oxidation state in $Mn_2O_3 \cdot H_2O$.

It was reasoned that, by flowing the electrolyte over the manganese dioxide, diffusion effects would be minimized, and in addition the hydrogen ion concentration at the electrode would be kept more constant. Data obtained on an electrode (Electro MnO_2 #2) discharged at a current drain rate of 0.100 amp/g with electrolyte flowing through the cathode chamber at a rate of 6–9 ml/min are shown in Fig. 4. As expected, the capacity of the manganese dioxide is much greater than if it were discharged under static conditions with a constant volume of electrolyte. It should

be noted that the capacity exceeds the theoretical capacity calculated on the basis of reduction to $Mn_2O_3 \cdot H_2O$, but not below Mn_3O_4. An examination of the effluent showed the presence of Mn^{II}, which verifies the findings of other workers (3).

Since the discharge products were not analyzed, the exact reaction mechanism cannot be determined. However, a review of the literature, along with other experimental data, indicates that the following possible reactions could occur which might explain the increased capacity beyond the $Mn_2O_3 \cdot H_2O$ theoretical limit:

$$MnO_2 + 4H^+ + 2e^- \rightarrow Mn^{++} + 2H_2O$$

$$Mn_2O_3 + 2H^+ \rightarrow Mn^{++} + MnO_2 + H_2O$$

$$3Mn_2O_3 + 2H^+ + 2e^- \rightarrow 2Mn_3O_4 + H_2O$$

$$3MnO_2 + 4H^+ + 4e^- \rightarrow Mn_3O_4 + 2H_2O$$

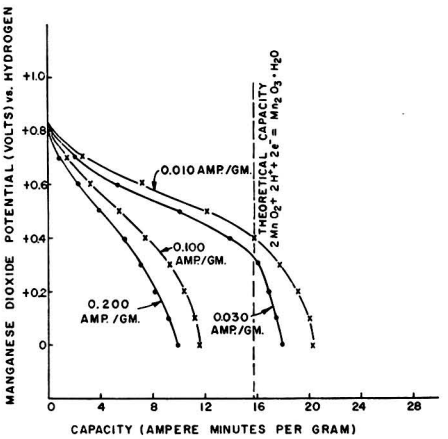

FIG. 3. Capacity in ampere-minutes per gram of Electro Ore #2 (B) discharged at various current drains in 20% NH_4Cl-33% $ZnCl_2$-47% H_2O electrolyte.

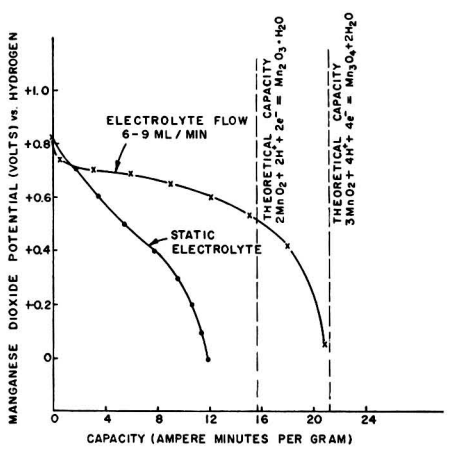

FIG. 4. Capacity in ampere-minutes per gram of Electro Ore #2 (B) discharged at 0.100 amp/g in 20% NH_4Cl-33% $ZnCl_2$-47% H_2O electrolyte, under static conditions and with a continuous flow of electrolyte.

The possibility of the last two reactions occurring is supported by the work of Copeland and Griffith (6).

The technique described in this paper can also be used to study the performance of various cathode materials in different electrolytes. Fig. 5 shows the relative performance of two types of manganese dioxides discharged in acid and basic electrolytes. The manganese dioxide prepared electrolytically gives a greater capacity in both basic and acid electrolytes than the naturally occurring African manganese dioxide. The importance of the structure of manganese dioxide on its performance in Leclanché cells containing an NH_4Cl—$ZnCl_2$ electrolyte has been shown

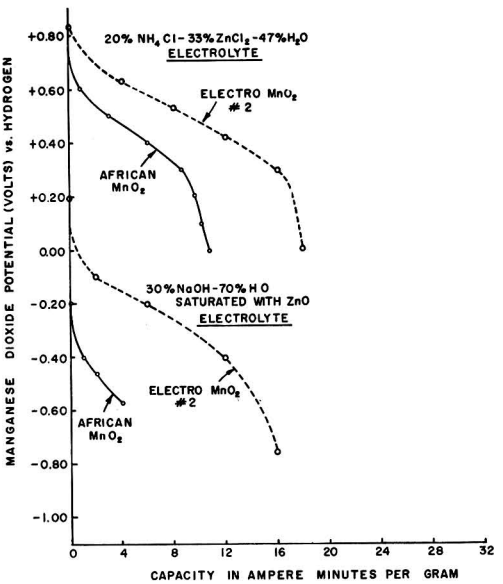

FIG. 5. Capacity in ampere-minutes per gram of Electro Ore #2 (B) and African Ore (J) discharged at 0.030 amp/g in acid and base electrolytes.

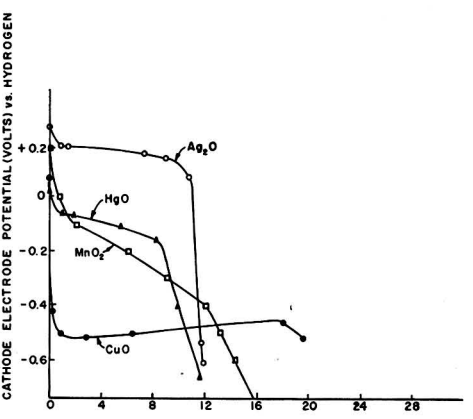

FIG. 6. Various cathode materials discharged at 0.030 amp/g in 30% NaOH-70% H_2O, saturated with ZnO, electrolyte.

previously. It is evident from these data that structure is also an important property with respect to the performance of manganese dioxide in strongly basic electrolytes.

Studies of Other Cathode Materials

Discharge data obtained on other cathode materials which have been used in primary batteries are shown in Fig. 6. It should be noted that the discharge curves and voltage levels of these materials simulate the type and level of discharge curves found in actual cells made with these materials. The cathode potentials are all lower than found in actual cells due to an *IR* drop which is included in the potential measurements. Since the measurements were all made using an electrolyte of the same composition and with the same electrode spacings, this *IR* drop becomes a constant for all measurements enabling comparisons to be made between different materials.

Summary

A convenient method has been devised which enables a quick evaluation to be made of different manganese dioxides and other cathode materials in various electrolytes. Like all methods proposed to date, this method has limitations in that it tells nothing about the concentration of harmful impurities, solubility, or stability of a particular cathode material in the electrolyte. Such data, which are important for the design of a practical cell with a long shelf life, have to be determined by other chemical methods or by experimental cells.

The apparatus and technique can also be of value in obtaining a better understanding of reaction rates and conditions under which maximum cathode efficiency can be obtained.

Acknowledgment

The authors wish to thank the Power Sources Branch of the Signal Corps Engineering Laboratories for making available the dry cell capacity and chemical analysis data of the various manganese dioxides, as well as Dr. J. A. Amick of the RCA Research Laboratories for gathering the electron diffraction data.

Manuscript received June 15, 1955. This paper was prepared for delivery before the Pittsburgh Meeting, October 9 to 13, 1955.

Any discussion of this paper will appear in a Discussion Section to be published in the December 1956 Journal.

References

1. G. Leclanché, *Les Mondes*, **16**, 532 (1868).
2. G. W. Vinal, "Primary Batteries," John Wiley & Sons, Inc., New York (1951).
3. N. C. Cahoon, *This Journal*, **99**, 343 (1952).
4. G. Kortum and J. O'M. Bockris, "Textbook of Electrochemistry," Vol. II, Elsevier Publishing Co., New York (1951).
5. R. Glicksman and C. K. Morehouse, *This Journal*, **102**, 273 (1955).
6. L. C. Copeland and F. S. Griffith, *Trans. Electrochem. Soc.*, **89**, 495 (1946).

The Influence of Nitrogen-Containing Organic Inhibitors on the Electrode Potential of Steel in Sulfuric Acid

R. N. Ride

Department of Supply, Commonwealth of Australia, Victoria, Australia

ABSTRACT

Corrosion inhibition of mild steel in 1*N* sulfuric acid has been studied by observing electrode potentials and corrosion rates for thirteen compounds. The mechanism of inhibition is discussed with special reference to the nature of the adsorption interphase and a revised theory of inhibition is proposed.

From hydrogen overvoltage and other considerations, it is postulated that the inhibitor is mainly physically adsorbed as a second phase on the chemisorbed hydrogen film already present on the metal. Inhibition is due primarily to increased hindrance to the anodic dissolution process, accompanied at higher inhibitor concentrations by a rise in hydrogen overvoltage.

The measurable quantities, electrode potential, inhibitive efficiency, and inhibitor concentration are related in an adsorption equation which can be applied to compounds adsorbed in a single and fixed mode of molecular orientation.

Introduction

Extensive investigations have been made of the corrosion inhibition of steel in acid solutions, due to the presence of small quantities of organic compounds containing nitrogen, oxygen, or sulfur. There are several comprehensive reviews of the literature on earlier work, notably those by Hackerman and his co-workers (1, 2).

Most investigators agree that inhibition occurs as a result of adsorption of the organic compounds on the metal surface. The presence of an adsorbed inhibitor

layer, generally assumed to be monomolecular, has been shown by Rhodes and Kuhn (3) by analytical methods and by Hackerman and Glenn (4) using electron diffraction techniques. Existing theories on inhibition differ principally on the question of whether inhibition is due to adsorption of the inhibitor only at cathodic areas on the metal or to general nonspecific adsorption.

The several investigations of Mann and his co-workers (5–7) and others (8–10) led to the theory of specific adsorption of positively charged inhibitor ions at cathodic sites on the surface. Inhibition was attributed to hindrance of the discharge of hydrogen ions. The compounds examined by Mann, mainly aliphatic and aromatic amines, were supposed to be attached with the chain or ring essentially vertical to the metal surface through forces acting on the positively charged nitrogen atom in the molecule. Inhibition efficiency was claimed to be related to the vertically projected area of the molecules on cathodic sites. Nonsymmetrical substitution of alkyl groups on the benzene ring was found to increase the inhibiting efficiency of the compounds. This was interpreted in terms of the tilting of these molecules, due to attractive forces between the positive alkyl groups and the negative benzene ring, with a resulting increase in projected area of the molecule.

Later investigators (11, 12) have criticized this "cathode screening" theory on the following grounds: (*a*) not all organic compounds showing inhibitive properties are positively charged; (*b*) the difference in electrode potential between anodic and cathodic sites on a freely corroding steel surface in sulfuric acid is likely to be very small; there is, therefore, little reason for assuming preferential and specific attraction to cathodic sites; and (*c*) the degree of electrolytic migration of large charged ions to cathodic points must be negligible in a solution containing a high concentration of hydrogen ions.

The "cathodic screening" theory has been based mainly on results derived from external cathodic polarization experiments on specimens in inhibited acid solutions; proponents of this theory do not appear to have investigated the anodic process by anodically polarizing the specimens. Several investigators (2, 3, 7) have apparently misinterpreted the work of Chappell, Roetheli, and McCarthy (9) in this respect, as showing that no appreciable change in potential occurred on anodic polarization in the presence of the inhibitor. It is quite clear from their report that Chappell and his co-workers did not anodically polarize their specimens, their "anode potential" being simply the normal corrosion potential of a specimen with no externally applied current. This anode potential was found to be slightly more cathodic in the presence of their inhibitor, a certain indication that the inhibitor affects the anodic process.

The experimental basis for the cathodic screening theory is also open to question on several grounds. Even if external cathodic polarization at current densities up to some fifty times greater than the normal local action current density could be justified as a valid basis for interpretation, the apparent increase in hydrogen overvoltage does not exclude the possibility of considerable anodic polarization. As pointed out by Hoar (11), Mann's (7) correlation of relative efficiencies of inhibitors from cathodic polarization and weight loss data merely indicated that the fraction of the surface covered with inhibitor molecules is the same as when no current is applied.

Recent work supports the view that inhibition is the result of general adsorption of inhibitor molecules on the metal surface, whereby both the anodic and cathodic reactions are affected. Hoar (11) and Hackerman and Sudbury (1) showed that, for a large number of compounds in sulfuric acid, steady-state potentials invariably moved in the cathodic direction relative to specimens in uninhibited acid, which indicates a greater degree of anodic than cathodic self-polarization (11). Hackerman and Sudbury (1), externally polarizing specimens both cathodically and anodically, and Cavallaro (13) in galvanic tests with copper-iron and iron-zinc couples, concluded that both anodic and cathodic sites are involved in the inhibition mechanism.

The present work on nitrogen-containing organic inhibitors was undertaken to investigate: (*a*) the individual contribution of each of the two electrode processes to the inhibited state; (*b*) the relationship between the concentration and efficiency of the dissolved inhibitor; (*c*) the significance of the difference in the steady-state potentials between specimens in inhibited and noninhibited solutions.

Experimental

Method of investigation.—The behavior of steel in inhibited 1*N* H_2SO_4 solutions was studied by observing average corrosion rates and changes in steady-state electrode potentials. The measurement of electrode potentials under steady-state conditions ($(\Delta e/\Delta t) < 1$ mv/hr), as discussed by Gatty and Spooner (14), is of considerable importance in systems of this type in which $\Delta e/\Delta t$ is initially large. It was found that the electrode potential of the specimen reached a steady-state condition after about 2.5 hr; all experiments in inhibited solutions were conducted on specimens which had been allowed to corrode freely for this period in a noninhibited 1*N* H_2SO_4 solution.

This pretreatment followed Hoar's recommendation (11) in removing the original abraded surface, but was found to give more reproducible electrode potentials (±1 mv) after the 2.5 hr period than his HNO_3 treatment.

Materials and equipment.—Mild steel rod (C 0.10%, Mn 0.65%, Si 0.02%, S 0.03%, P 0.03%) of 0.24 in. diameter was used as the test material. Specimens 5½ in. long were rotated in a chuck at 1400 rpm and abraded with "Hydrodurexsil" 280 C and 400 grade emery paper. They were then swabbed with acetone and distilled water, dried with a clean cloth, and stored for approximately 20 hr in a desiccator over potassium hydroxide.

Electrode potential measurements were made against a saturated calomel reference electrode. Electrical connection was made from the calomel electrode via a saturated KCl-agar bridge to an isolating tube containing 1*N* H_2SO_4 and thence by filter paper strips moistened with 1*N* H_2SO_4 to seven specimen tubes. All specimen tubes and the reference electrode assembly were maintained at 25° ± 0.25°C throughout the test.

A four-stage double-channel d-c amplifier with a high

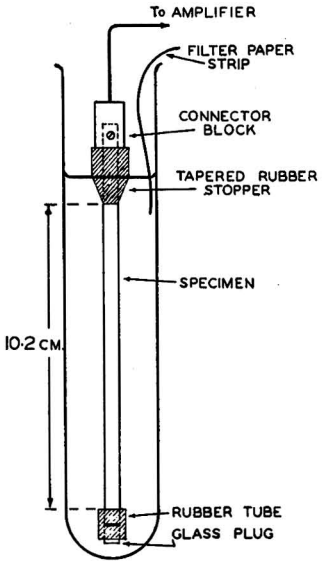

FIG. 1. Test assembly

input impedance [modified from a design by Shepard (15)] was used to measure electrode potentials. The amplifier input connection was made via a selector switch to brass connector blocks from which the specimens were suspended in the solution (Fig. 1). A voltage-backing network in the amplifier permitted an arbitrary zero to be fixed at a convenient reference level. This was maintained at a constant value throughout of −0.405 v with respect to the reference electrode; potentials quoted in the text are negative with respect to this level. As the tests were concerned only with potential differences, no corrections were made for liquid junction potentials; individual differences in liquid junction potentials between each of the seven tubes and the reference electrode were less than 1 mv.

All inhibitors were either of Analytical Reagent grade or were fractionally redistilled. The quinoline and quinaldine were synthesized and redistilled. Inhibitors were dissolved in 1*N* H_2SO_4 (A.R.) at the highest concentrations required; this solution was then diluted with 1*N* H_2SO_4 to give the appropriate lower concentrations.

Procedure.—For each inhibitor, seven concurrent tests covered a range of concentrations. Specimens were weighed and assembled as in Fig. 1.

A short length (approximately ½ in.) of close-fitting rubber tubing containing a short glass plug in one end was placed over the bottom end of the specimen. A rubber stopper, ground as shown in Fig. 1, was then placed on the rod so that a length of exactly 4 in. was exposed between the adjacent edges of the rubber tube and stopper. The taper prevented hydrogen bubbles collecting on the underside. The specimen was suspended in a test tube (8 in. long, 1½ in. diameter) containing 110 ml of the test solution so that the liquid level covered the tapered edge of the stopper. This method of assembly restricted the specimen under test to a cylindrical surface with an area of 3.01 in.² (19.4 cm²).

Specimens were inserted in the tubes containing uninhibited 1*N* H_2SO_4 at 5-min intervals. After exactly 2.5 hr, during which the specimens corroded freely, an electrode potential reading was taken. The uninhibited acid in each tube was sucked into separate flasks, together with 50 ml of 1*N* H_2SO_4 added to the tubes for rinsing, and the tubes were refilled immediately with 1*N* H_2SO_4 containing the dissolved inhibitor. One tube, acting as a control, was refilled with noninhibited 1*N* H_2SO_4. This changeover operation occupied less than 1 min. The electrode potential was read within 2 min of changing the solutions and at intervals of 20–30 min thereafter.

After a second 2.5-hr period, each specimen was removed in turn from its solution, washed thoroughly, dried, and weighed.

If w_i = weight of iron dissolved during the period in the inhibited solution, this is given by $w_i = W - w_0$, where W = total loss of weight (in 5 hr), and w_0 = weight dissolved in the first 2.5 hr (determined volumetrically with 0.02*N* potassium dichromate on the extracted solution in the flasks).

The apparent efficiency of the inhibitor is determined from the usual equation,

$$\text{efficiency} = 100 \cdot \frac{w_b - w_i}{w_b} \%$$

where w_b = weight of iron dissolved in the control (noninhibited) solution during the second 2.5-hr period.

A test period of 2.5 hr in the inhibited solution was chosen because the corrosion rate of the control specimen was found to be almost constant during this time. Tests over longer periods showed that the average corrosion rate changed from about 0.3 mg/min after 2.5 hr, to about 0.5 mg/min after 23 hr, probably due to the increase in surface area. The short test period resulted in a proportionately lower weight loss on the control specimen and, hence, lower efficiency values for a given inhibitor than have been reported by other investigators using much longer times.

RESULTS

The following nitrogen-containing organic compounds were investigated: aniline, ethylaniline, dimethylaniline, diethylaniline, pyridine, quinoline, quinaldine (2-methylquinoline), β-naphthoquinoline, diethylamine, di-*n*-butylamine, piperazine, tetramethyldiamino-diphenyl methane, and brucine.

The various relationships between efficiency, concentration, and electrode potential are given in Fig. 2 to 10.

Reproducibility of results was satisfactory as is shown in duplicate tests on β-naphthoquinoline, diethylamine, and tetramethyldiamino-diphenyl methane.

DISCUSSION

Introductory Comments on Inhibitor Efficiency, Concentration, and Potential Curves

Fig. 2–7 show curves typical of those found by other investigators. Several attempts have been made to relate either inhibitor efficiency (6, 7, 11) or electrode potential (1) with inhibitor concentration through adsorption isotherms of the Langmuir or Freundlich type. The usual

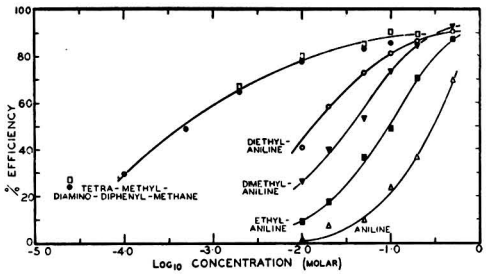

FIG. 2. Relationship between inhibitor efficiency and concentration.

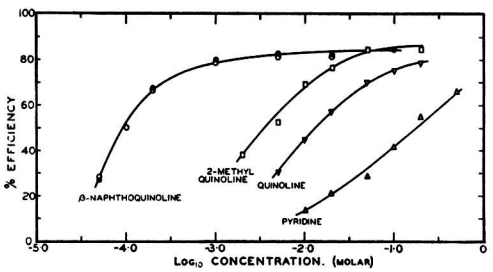

FIG. 3. Relationship between inhibitor efficiency and concentration.

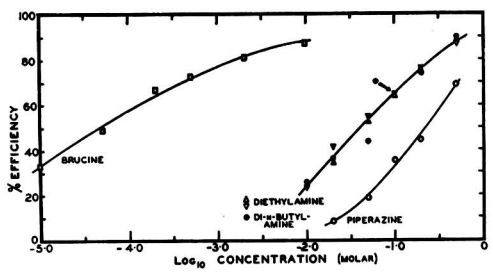

FIG. 4. Relationship between inhibitor efficiency and concentration.

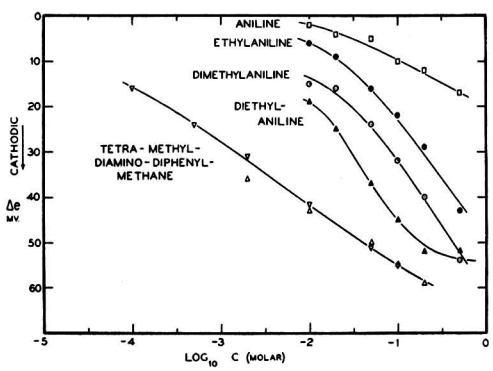

FIG. 5. Change in electrode potential as a function of inhibitor concentration.

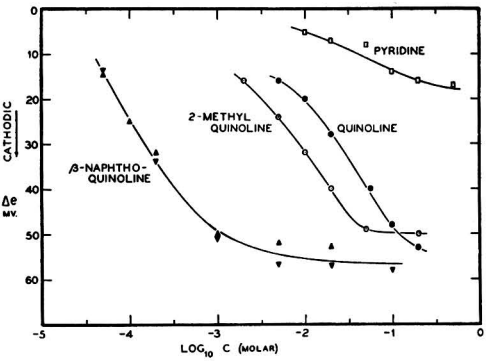

FIG. 6. Change in electrode potential as a function of inhibitor concentration.

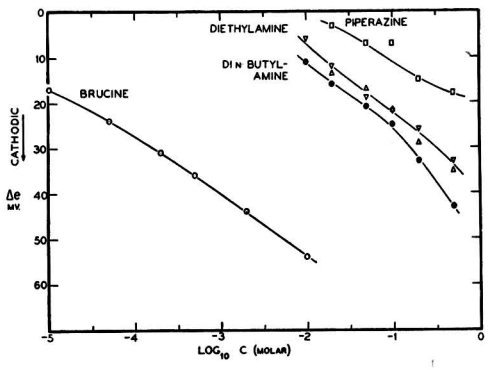

FIG. 7. Change in electrode potential as a function of inhibitor concentration.

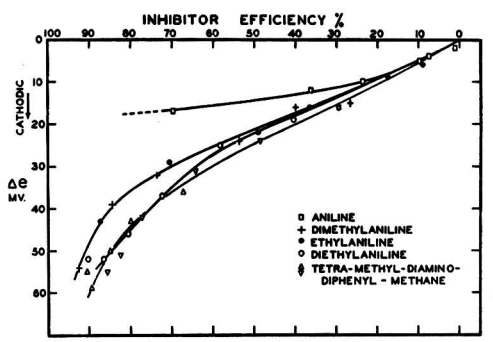

FIG. 8. Change in electrode potential related to inhibitor efficiency.

assumptions made in these calculations are that inhibitor efficiency or change in electrode potential is proportional to the fraction of the surface covered by the inhibitor. In later discussion, it will become evident that these assumptions are oversimplified.

Fig. 8–10 have been drawn so as to show the relation between the change in electrode potential and inhibitor efficiency in terms of the conventional potential vs. corrosion current-type curves. (Plotting inhibitor efficiency in a

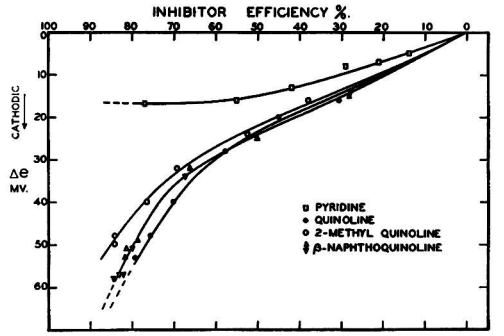

FIG. 9. Change in electrode potential related to inhibitor efficiency.

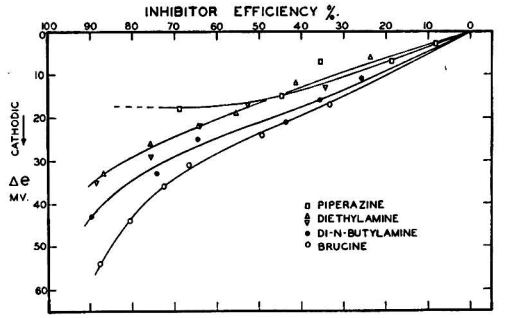

FIG. 10. Change in electrode potential related to inhibitor efficiency.

negative sense is equivalent to plotting percentage weight loss and, hence, corrosion current in the positive sense.)

The change in electrode potential, Δe, is

$$\Delta e = E_p - E_i$$

where E_p = corrosion (steady-state) potential of the specimen in noninhibited acid, and E_i = average potential (integrated and averaged over the "inhibition" period of the test)[1] for the specimen in a solution containing an inhibitor at a specified concentration.

The curves show that (*a*) the over-all movement in potential for each inhibitor is in the cathodic direction, indicating predominantly anodic hindrance to the corrosion process; and (*b*) the value of electrode potential *for a given efficiency* (*current*) differs for each compound. If all inhibitors acted in a purely anodic manner, the observed potentials for all compounds would be identical and would correspond to a point on the cathodic polarization (hydrogen overvoltage) curve. The present observation can only mean that each compound produces a characteristic degree of cathodic polarization.

Taking both observations, it is evident that the inhibitor is adsorbed generally or, at least, in a manner which affects both electrode reactions, rather than specifically at cathodic areas, as Mann and others have suggested.

[1] At higher concentrations of a few inhibitors, a slow drift in potential of a few millivolts occurred during the test period; for this reason, all potentials were integrated on a time basis and averaged. It was assumed that a corresponding slow change occurred in the corrosion rate which would, however, be included in the term weight-loss, itself an integrated quantity.

Nature of the Electrode Surface

Before proceeding to a detailed interpretation of the results, it is necessary to summarize the existing theory on the probable nature of the electrode surface at which adsorption occurs. Except for Hoar and Holliday's paper (16), little consideration appears to have been given to this important aspect.

Most modern theories on hydrogen overvoltage agree that an electrode evolving hydrogen is almost completely covered with a chemisorbed monolayer of atomic hydrogen (17–19). Hickling and Salt (17) state that any electrode at which hydrogen is present is to be regarded simply as an atomic hydrogen electrode, the pressure of atomic hydrogen determining the electrode potential according to the electrode material and the experimental conditions.

Gatty and Spooner (20), in their comprehensive studies of corroding systems, consider the nature of the electrode surfaces in detail. They have produced substantial evidence (on grounds other than overvoltage) from which they infer that, in air-free acid solutions, the surface of many metals (including iron) undergoing corrosion is almost completely covered with an adsorbed atomic hydrogen film. Anodic dissolution takes place only through pores in this film; the continuous change in location and magnitude of these pores accounts for the uniform etching of the whole surface. The total instantaneous area of the anodic sites comprises only a very small fraction of the total surface and, certainly for iron, anodic polarization is very high, even in noninhibited solutions (20, 21).

According to the theory of overvoltage, the hydrogen discharge process, essentially

$$M{-}H + H_3O^+ + e \rightarrow M + H_2 + H_2O$$

takes place on the adsorbed hydrogen film. From Gatty and Spooner's conclusions, it follows that, where hydrogen is being evolved as a result of corrosion in acid solution, the cathodic current density will be very small compared with that at the anodic pores, because of the very large difference in cathode and anode areas.

The following experimental evidence indirectly supports this view of the conditions at the electrode surface. Kuznetzov and Iofa (22) concluded from their inhibitor studies that hydrogen evolution occurred from the whole surface, whereas dissolution of iron occurred only at the edges of grains. Hoar and Havenhand (23), investigating 36 steels in noninhibited citric acid, found that all materials under a wide variety of test conditions had approximately equivalent cathodes and that the different rates of corrosion were due to widely differing anodes. Further, Frumkin (24) quotes experimental work indicating that the factors governing hydrogen overvoltage (including the constants in the Tafel equation) are not necessarily altered by the simultaneous existence of a metal dissolution process.

The probable nature of the surface of an iron electrode

undergoing corrosion in air-free[2] acid solutions may therefore be summarized as follows: (*a*) the cathodic field consists of a chemisorbed atomic hydrogen film which almost completely covers the electrode surface; (*b*) anodic dissolution occurs at pores in the cathodic field. These pores occupy a very small fraction of the total surface and the anodic reaction is highly polarized.

Adsorption of the Inhibitor and Mechanism of Inhibition

Most of the evidence available favors the view that adsorption of nitrogen-containing inhibitors from acid media is mainly physical rather than chemical. The following typical adsorption characteristics, taken together, indicate the probability of van der Waal's forces being involved: (*a*) asymptotic increase in adsorption (judged on inhibitor efficiency) with increasing concentration; (*b*) adsorption is rapid (in the present work, it was observed that on adding the inhibitor, the change in electrode potential to a fairly steady value was almost instantaneous); (*c*) reversibility [although not always complete (1)]; (*d*) low heats of adsorption (16); and (*e*) decreasing adsorption with increasing temperature (1, 16).

On the other hand, there is little doubt from the theory of overvoltage that the hydrogen film is chemically adsorbed. For a chemisorbed hydrogen film on iron at −96° to −78°C, Emmett and Harkness (25) found the heat of adsorption to be about 10,400 cal/g mole. At 25°C, the value should be rather larger. While heat of adsorption data for organic inhibitors is meager, Hoar and Holliday (16) quote values of approximately 3,000–8,500 cal/g mole for several quinoline compounds.

It is important to note that, hitherto, adsorption of the inhibitor has been either directly or implicitly assumed to occur on the bare metal surface. Since, however, the chemisorbed hydrogen film will not be displaced by a process involving physical adsorption especially if, as is likely, the heat of adsorption is less, it is necessary to consider the possibility that the inhibitor is physically adsorbed on top of the hydrogen film.

As already mentioned, the rapid movement in electrode potential on first adding the inhibitor indicates that it evidently experiences no difficulty in becoming adsorbed. Benton and White (26) and Insley (27) have shown that, for iron and other metals, hydrogen can be physically adsorbed on a pre-existing chemisorbed hydrogen monolayer. The possibility of inhibitor adsorption in an analogous manner does not appear to have been considered previously. While further experimental evidence is required, this inference appears a necessary and logical outcome from preceding considerations.

It is visualized, therefore, that the inhibitor is physically adsorbed on the cathodic hydrogen field and covers, at the same time, the small anodic pores possibly by "bridging." The possibility of direct physical or chemical adsorption of the inhibitor on the bare metal at sufficiently large anodic pores is not excluded. This may, in fact, account for the small residual of undesorbed inhibitor observed by Hackerman and Sudbury (1).

The effect of the inhibitor film on the separate electrode reactions is now examined.

Anodic polarization.—The presence of the inhibitor film, even at very low concentrations, markedly hinders the outward migration of ferrous ions from the anodic pores. Whether this is due to concentration polarization or increased diffusion resistance is not yet clear. Machu's resistance measurements (28) appear to support the latter view. This further hindrance, added to the already existing high state of polarization at anodic sites, will determine almost exclusively the magnitude of the local action current. On the other hand, at these low inhibitor concentrations, very little increase in polarization of the large cathodic field occurs.

The predominantly anodic behavior of the inhibitor is shown in Fig. 11. Here, the change in electrode potential, Δe, is plotted against the logarithm of the corrosion rate (in relative units). For a purely anodic inhibitor, the movement in electrode potential with decreasing corrosion rate would follow the cathodic polarization (hydrogen overvoltage) curve, represented by the usual Tafel expression

$$\eta = a + b \log_{10} (\text{current density})$$

where η = overvoltage and a, b are constants. In Fig. 11, b has been assigned the usual value for iron = 0.12 (29). (In earlier experiments in this series, using applied current, approximate values of b between 0.12 and 0.16 were obtained.) The proximity of the inhibitor curves, in the early stages of inhibition, to the overvoltage curve is indicative of substantially increased anodic polarization.

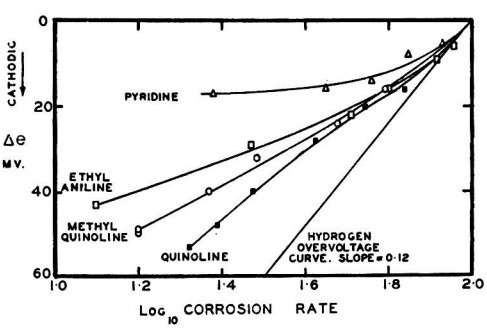

FIG. 11. Change in electrode potential vs. log corrosion rate for several inhibitors in relation to the hydrogen overvoltage curve for iron.

[2] Though probably not air-free in the strict sense, it is unlikely that the present solutions contained more than very small amounts of dissolved oxygen. Hydrogen was continuously evolved from almost all specimens and the solutions were quiet with an air-liquid interphase of less than 1 cm². It is also interesting to note that, within certain limits, conditions at the metal surface controlling hydrogen evolution are not materially affected by appreciable amounts of dissolved oxygen. Thus, saturation of the solution with oxygen does not affect hydrogen overvoltage values (on copper amalgam) at current densities greater than about 10^{-4} amp/cm² (33). In the present low oxygen solutions, current densities were of the order of 10^{-3} amp/cm². Uhlig (34) observed a difference of only 1 mv in the electrode potential shift due to the addition of an inhibitor to acid solutions bubbled with either oxygen or nitrogen. Also, in low *p*H solutions, where hydrogen evolution is the main cathodic reaction, small amounts of oxygen have a negligible effect on corrosion rate (35).

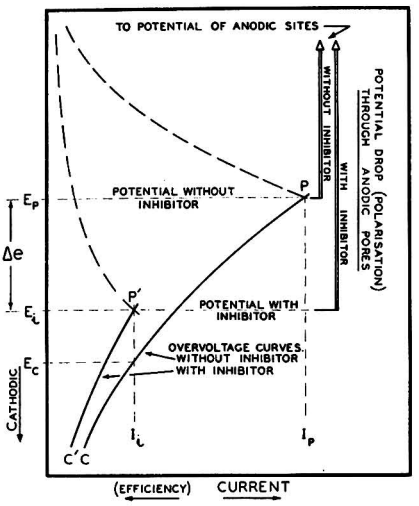

FIG. 12. Schematic potential-current relationship for inhibited and noninhibited surfaces.

The gradual divergence of the curves with increasing efficiency points to an increasing effect of the inhibitor on the kinetics of the cathodic process.

Cathodic polarization and the significance of the change in electrode potential.—It is recognized that the observed electrode potential of a corroding surface is influenced by the relative areas of the anodic and cathodic zones (30). Where, as in the present study, the cathodic field covers almost all the metal surface, the observed potential will be approximately that of the cathodic film (20). The observed potential, in either inhibited or noninhibited solutions, is therefore virtually independent of the potential of the anodic sites and approximately equal to that of an iron electrode evolving hydrogen at a rate depending on its normal overvoltage characteristics and the current. The latter is essentially determined by the degree of anodic polarization. The relationship is shown diagrammatically in Fig. 12. *PC* and *P'C'* are the hydrogen overvoltage curves for noninhibited and inhibited solutions, respectively.

The significance of the change in cathodic polarization potential, E_c to E_i, on adding the inhibitor to the system can now be examined. E_c and E_i are the potentials of noninhibited and inhibited surfaces, respectively, at which hydrogen is being discharged at a rate corresponding to a current I_i in each case.

Adsorption of the inhibitor on to the chemisorbed hydrogen film may conceivably increase cathodic polarization by increasing (*a*) the diffusion resistance; (*b*) the activation energy required for the overvoltage process; (*c*) the current density.

(*a*) From their overvoltage measurements by the direct and indirect methods, Bockris and Conway (31) found no appreciable increase in film resistance in the presence of inhibitors. Also calculations in connection with the present work show that, for the idealized case of a complete monolayer of plane circular molecules, disposed in an ordered manner to give greatest packing density, the proportion of free space (area not covered by inhibitor) is about 5%. The diffusion resistivity through such a monolayer would need to be improbably high to account for changes in potential observed. It is most unlikely in any case that the proportion of free space would ever approach such a small value in view of the irregular shape of most molecules and the dynamic nature of the adsorption process.

(*b*) Except for Bockris and Conway's conclusions, there is no evidence to date in favor of increased activation energy causing the change in potential. It is interesting to note that, for magnesium in acid solution, Hurst and Jermyn (32) showed that the activation energy was of the same order in either inhibited or noninhibited acid. They concluded that while a proportion of the surface was isolated by the inhibitor, the residual reaction was the same as in noninhibited acid.

(*c*) The view that increased cathodic polarization may be due simply to reduction in the total area available for hydrogen discharge, with a corresponding rise in the current density on the free area, was proposed by Mann and his school to explain the "specific cathodic adsorption" theory. Machu (28) has also admitted the feasibility of this mechanism. This approach has been applied to the "general adsorption" argument developed here and leads to an adsorption isotherm expression which is substantially supported by present experimental data.

Derivation of Equation Relating Electrode Potential, Inhibitor Efficiency, and Concentration

It is assumed that the rise in overvoltage from E_c to E_i is due solely to an increase in current density (the inhibitor film having reduced the available cathode area) and that no change in activation energy is involved. The usual Tafel equation then still applies with its constants unchanged. In Fig. 12, this means that for a given current I_i, $E_i - E_c$ corresponds to the difference between two values of the Tafel equation containing only different current density terms.

For a noninhibited surface

$$E_c = a + b \log_{10} \frac{I_i}{A_p}$$

where A_p = the cathode area.

For an inhibited surface

$$E_i = a + b \log_{10} \frac{I_i}{A_i}$$

where A_i = the uncovered area (free space) of the cathode surface corresponding to the current I_i

$$A_i = A_p(1 - \theta)$$

where θ = the fraction of the surface covered by the inhibitor.

Taking A_p as unit area, and $E_i > E_c$, and since the current is the same in each case

$$E_i - E_c = b \log_{10} \frac{1}{A_i}$$

$$= b \log_{10} \frac{1}{1 - \theta}$$

from which

$$\frac{\theta}{1-\theta} = \text{antilog}\,\frac{(E_i - E_c)}{b} - 1$$

From Fig. 12,

$$\frac{E_i - E_c}{b} = \frac{(E_p - E_c) - \Delta e}{b}$$

where Δe is the observed difference in potential between noninhibited and inhibited surfaces for current I_i.

Thus

$$\frac{E_i - E_c}{b} = \frac{1}{b}\left[\left(a + b\log_{10}\frac{I_p}{A_p}\right) - \left(a + b\log_{10}\frac{I_i}{A_p}\right)\right] - \frac{\Delta e}{b}$$

$$= \log_{10}\frac{I_p}{I_i} - \frac{\Delta e}{b}$$

Hence

$$\frac{\theta}{1-\theta} = \text{antilog}\left(\log_{10}\frac{I_p}{I_i} - \frac{\Delta e}{b}\right) - 1$$

$$= \frac{I_p}{I_i}\,\text{antilog}\left(-\frac{\Delta e}{b}\right) - 1$$

Following the form of the Langmuir isotherm used by Hoar (11, 16) in which

$$\log_{10}\frac{\theta}{1-\theta} = \log_{10} K + \log_{10} c - \frac{Q}{2.3\,RT}$$

where c = bulk concentration of the inhibitor, Q = heat of adsorption, and K = constant, one may write

$$\log_{10} c = \log_{10}\left[\frac{I_p}{I_i}\,\text{antilog}\left(-\frac{\Delta e}{b}\right) - 1\right] - \log_{10} K + \frac{Q}{2.3\,RT}$$

Now we have an isothermal equation relating electrode potential, concentration, and inhibitor efficiency, which depends primarily on the two assumptions: (*a*) that increased overvoltage is due to increased current density; and (*b*) that inhibitor adsorption follows the Langmuir theory.

Application of Equation to Present Data

In Fig. 13 to 15, $\log_{10} c$ has been plotted[3] against $\log_{10}[I_p/I_i\ \text{antilog}\,(-\Delta e/b) - 1]$ (denoted by $\log_{10} F$) for the inhibitors studied. For the nine compounds, aniline, ethylaniline, dimethyl- and diethylanilines (except for the points of lowest concentration), diethyl- and dibutylamines, pyridine, piperazine, and 2-methyl quinoline, data are in good linear agreement with the equation. For pyridine, dibutylamine, and dimethylaniline, the slopes of the curves are close to unity, as is required by the equation. While the slopes for the other six compounds are generally of the right order, it is evident that adsorption is also influenced by an additional unknown factor characteristic of each compound.

[3] Least squares lines have been drawn to all data, except for the point of lowest concentration for each of the anilines which was not included in the calculations. The value of the Tafel constant b was taken as 0.12. The linearity of the expression is independent of b and the slope of the curves is only slightly affected by adopting an approximate value.

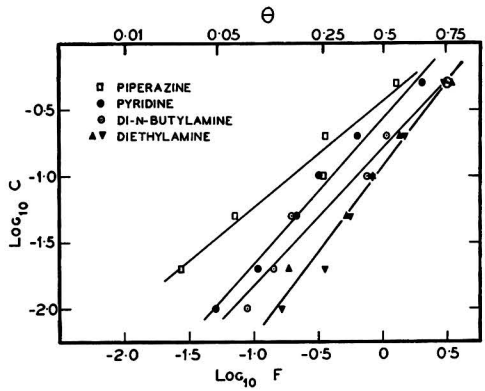

FIG. 13. Adsorption isotherms relating inhibitor concentration (log C) with electrode potential and corrosion current (log F).

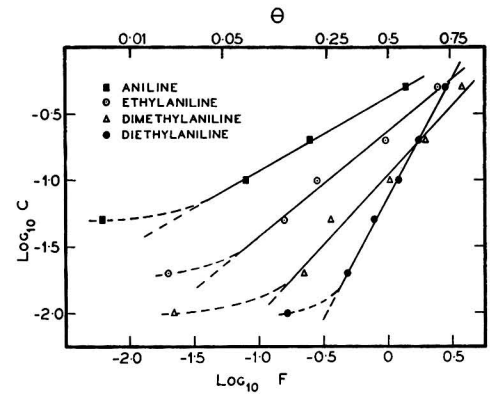

FIG. 14. Adsorption isotherms relating inhibitor concentration (log C) with electrode potential and corrosion current (log F).

The case of the lowest concentration points of the anilines is of special interest. While the position of these points is less certain because of the relatively large effect of small experimental errors in measuring Δe, the fact that all points fall on the same side of the linear curve is probably significant. The present theory assumes that, as the inhibitor concentration increases, the current density at the cathodic field also rises. If, however, at low inhibitor concentrations, the fractional decrease in corrosion current due to anodic polarization very nearly equals the fractional decrease in cathode film area, the current density over this range of concentration will be nearly constant. The equation, which relates changing current density with concentration, will then not apply and calculated data will fall to the left of the equation line as occurs for the anilines. This reasoning implies that, at low concentrations, anilines have a slightly stronger anodic influence than other compounds of this group, although the cause of this behavior is not yet clear.

Molecular orientation.—Except for pyridine, the compounds showing substantial agreement with the equa-

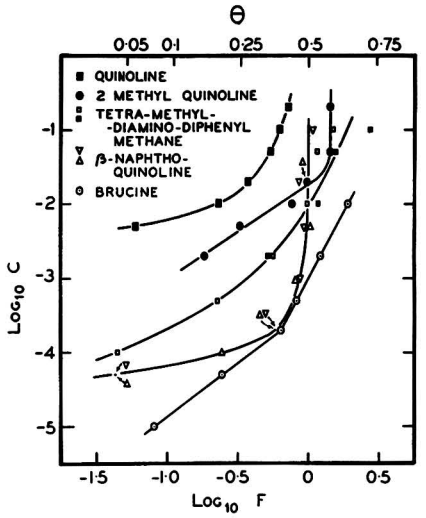

FIG. 15. Adsorption isotherms relating inhibitor concentration (log C) with electrode potential and corrosion current (log F).

tion contain the nitrogen atom "within" the structure of the molecule. If, as is generally agreed, the adsorption forces are directed mainly to this atom, these molecules, on adsorption, should exhibit only a single mode of orientation. Ring compounds, like ethylaniline, for example, should only be oriented "flat" or parallel to the adsorbent surface.

Pyridine, quinoline and β-naphthoquinoline have the nitrogen atom located on the outside of the ring structure. In this position it is always accessible to the adsorption forces so that these molecules are capable of adsorption in either the "flat," "inclined," or "vertical" modes of orientation, depending on surface concentration.[4] It is not surprising, therefore, that quinoline and β-naphthoquinoline do not conform to the equation, since the fraction of the surface covered depends not only on the bulk concentration but also on the molecular orientation which will vary with surface concentration. This behavior was not observed for pyridine which is a relatively weak inhibitor and evidently exhibits a single (possibly preferred) orientation at the comparatively lower surface concentrations existing.

For 2-methyl quinoline, the position of the methyl group (adjacent to the nitrogen atom) should permit adsorption of the molecule only in the flat orientation. Closer observance of the data to the equation for this material compared to the parent compound quinoline supports this view. The vertical section of the 2-methyl quinoline curve suggests that a state of maximum adsorption has been reached.

Brucine may be adsorbed through either of its two nitrogen atoms, although not through both at the one time. The two linear sections of the brucine curve appear to indicate two distinct modes of orientation.

The nonconformity of tetra-methyl-diamino-diphenyl methane with the equation is not unexpected as adsorption is possible through either or both of its nitrogen atoms. As the surface concentration increases, the 'single atom' mode of orientation should predominate, since it requires a smaller area for adsorption.

Revised Theory on the Mechanism of Inhibition[5]

It has been suggested that the true picture of the mechanism of inhibition probably involves aspects of both the "cathodic screening" theory typified by Mann and the "general adsorption—mainly anodic inhibition" theory of Hoar, Hackerman, and others. The present argument embraces the main features of both these theories and, with the additional evidence, presents a more complete account of the probable inhibition mechanism than has been available previously.

The theory is also consistent with modern views on hydrogen overvoltage.

It can be summarized as follows:

1. A steel surface corroding in an acid solution is covered with a chemisorbed atomic hydrogen film which comprises the cathode area of the corrosion process. Anodic dissolution takes place only at pores in this film.

2. The inhibitor is physically adsorbed on to the hydrogen film. Anodic pores are also covered, probably by bridging, although at sufficiently large pores, some direct adsorption, either physical or chemical, may occur.

3. Reduction in the local action current is primarily due to increased polarization at the anodic pores.

4. Reduction of the available cathode area by the adsorbed inhibitor causes a rise in hydrogen overvoltage due to increased current density.

5 For adsorbed nitrogen-bearing inhibitors having only one mode of orientation, the relation between bulk concentration, corrosion current, and electrode potential can be expressed quantitatively for the most part by the derived equation

$$\log_{10} c = K' \log_{10}\left[\frac{I_p}{I_i}\,\text{antilog}\left(-\frac{\Delta e}{b}\right) - 1\right] - \log_{10} K + \frac{Q}{2.3\,RT}$$

where c = molar concentration, I_i and I_p = current (corrosion rate) with and without the inhibitor, respectively, Δe = difference in electrode potentials of inhibited and uninhibited surfaces for current I_i, b = Tafel overvoltage constant, Q = heat of adsorption, and K and K' = constants; ideally K' should equal unity.

The over-all picture of the mechanism of inhibition is still incomplete in many respects. The kinetics of anodic polarization of iron with and without inhibitors require

[4] Hackerman and Glenn's (4) electron diffraction studies on an alkyl pyrrolidine-dione, which has a similarly placed nitrogen atom, obtained evidence indicating that the orientation of the adsorbed molecules changed from the flat to inclined mode as the surface concentration increased.

[5] The theory is, for the moment, restricted to compounds containing only nitrogen as the active atom for adsorption. Sulfur-bearing compounds like the thioureas not only exhibit a different electrode potential behavior but stimulate corrosion at very low concentrations. See also Hoar and Holliday (16).

further elucidation as does the effect of molecular structure and adsorbed orientation on inhibition. The collection of additional experimental data to confirm or modify the present views on the nature of the adsorbent interphase and the manner of adsorption appears to be the next step toward interpreting other complex aspects of inhibition.

ACKNOWLEDGMENT

This paper is published with the permission of the Chief Scientist, Department of Supply, Australia.

Manuscript received July 23, 1954.
Any discussion of this paper will appear in a Discussion Section to be published in the December 1956 JOURNAL.

REFERENCES

1. N. HACKERMAN AND J. D. SUDBURY, *This Journal*, **97**, 109 (1950).
2. N. HACKERMAN AND H. R. SCHMIDT, *Corrosion*, **5**, 237 (1949).
3. F. H. RHODES AND W. E. KUHN, *Ind. Eng. Chem.*, **21**, 1066 (1929).
4. N. HACKERMAN AND E. E. GLENN, *J. Phys. Chem.*, **54**, 497 (1950).
5. C. A. MANN, B. P. LAUER, AND C. T. HULTIN, *Ind. Eng. Chem.*, **28**, 1048 (1936).
6. C. A. MANN, *Trans. Electrochem. Soc.*, **69**, 115 (1936).
7. S. J. CH'IAO AND C. A. MANN, *Ind. Eng. Chem.*, **39**, 910 (1947).
8. E. JIMINO, I. GRIFOLL, AND F. R. MORRAL, *Trans. Electrochem. Soc.*, **69**, 105 (1936).
9. E. L. CHAPPELL, B. E. ROETHELI, AND B. Y. MCCARTHY, *Ind. Eng. Chem.*, **20**, 582 (1928).
10. L. E. SWEARINGEN AND A. F. SCHRAM, *J. Phys. Chem.*, **55**, 180 (1951).
11. T. P. HOAR, "Pittsburgh International Conference on Surface Reactions," p. 127, Corrosion Publishing Co., Pittsburgh (1948).
12. N. HACKERMAN, *Corrosion*, **8**, 143 (1952).
13. L. CAVALLARO, *Métaux & corrosion*, **23**, 184 (1948).
14. O. GATTY AND E. C. R. SPOONER, "The Electrode Potential Behaviour of Corroding Metals in Aqueous Solutions," Chap. 1, Clarendon Press, Oxford (1938).
15. W. G. SHEPARD, *Electronics*, **20**, (10), 174 (1947).
16. T. P. HOAR AND R. D. HOLLIDAY, *J. Appl. Chem. London*, **3**, 502 (1953).
17. A. HICKLING AND F. W. SALT, *Trans. Faraday Soc.*, **38**, 474 (1942).
18. P. J. HILLSON AND E. K. RIDEAL, *Proc. Roy. Soc. London*, **A199**, 295 (1949).
19. N. K. ADAM, "The Physics and Chemistry of Surfaces," pp. 326 and 330, Oxford University Press, London (1941).
20. O. GATTY AND E. C. R. SPOONER, *op. cit.*, pp. 314-5 and Chap. 1.
21. S. GLASSTONE, "An Introduction to Electrochemistry," p. 462, D. Van Nostrand Co., Inc., New York (1942).
22. V. A. KUZNETZOV AND Z. A. IOFA, *J. Phys. Chem. U.S.S.R.*, **21**, 201, (1947); *C. A.*, **41**, 6115c (1947).
23. T. P. HOAR AND D. HAVENHAND, *J. Iron Steel Inst. London*, **133**, 239 (1936).
24. A. FRUMKIN, Discussions of the Faraday Society No. 1, "Electrode Processes," p. 57 (1947).
25. P. H. EMMETT AND R. W. HARKNESS, *J. Am. Chem. Soc.*, **57**, 1631 (1935).
26. A. F. BENTON AND T. A. WHITE, *ibid.*, **54**, 1373, 1820 (1932).
27. E. G. INSLEY, *J. Phys. Chem.*, **39**, 623 (1935).
28. W. MACHU, *Trans. Electrochem. Soc.*, **72**, 333 (1937).
29. A. HICKLING AND F. W. SALT, *Trans. Faraday Soc.*, **36**, 1226 (1940).
30. W. J. MULLER, *Trans. Electrochem. Soc.*, **76**, 167 (1939).
31. J. O'M. BOCKRIS AND B. E. CONWAY, *J. Phys. Chem.*, **53**, 527 (1949).
32. R. HURST AND M. A. JERMYN, *J. Chem. Soc.*, **1950**, 158.
33. A. HICKLING AND F. W. SALT, *Trans. Faraday Soc.*, **37**, 319 (1941).
34. H. H. UHLIG, *Ind. Eng. Chem.*, **32**, 1490 (1940).
35. O. GATTY AND E. C. R. SPOONER, *op. cit.*, pp. 276-7

Oxidation of Tungsten

WATT W. WEBB,[1] JOHN T. NORTON, AND CARL WAGNER

Department of Metallurgy, Massachusetts Institute of Technology, Cambridge, Massachusetts

ABSTRACT

Two oxide layers form during the oxidation of tungsten between 700° and 1000°C. The outer layer is porous, powdery, yellow tungstic oxide, WO_3, and the inner layer is a dense, thin, dark-blue, tightly adherent oxide of uncertain composition. The oxidation reaction follows initially the parabolic rate law, but eventually there is a transition to the linear rate law. The rate of formation of the inner oxide is presumably inversely proportional to its thickness. The inner oxide seems to transform to the outer oxide at a constant rate. Upon combining the rate laws of the two individual processes, an overall rate equation covering the whole range is obtained. The thickness of the inner layer tends to a limiting value when the rate of its formation is equal to the rate of transformation to the outer layer.

INTRODUCTION

The oxidation of tungsten has been investigated by several authors. Gulbransen and Wysong (1) found the parabolic rate law applicable under most conditions up to 550°C. Likewise Dunn (2) found the parabolic rate law to hold between 700° and 1000°C. In contrast, Scheil (3) reports a linear rate law between 500° and 900°C. Results obtained by Nachtigall (4) and Kieffer and Kölbl (5) suggest an intermediate rate law. To clarify, the oxidation

[1] Allegheny Ludlum Steel Co. Fellow, 1953-1955; present address: Metals Research Lab., Electro Metallurgical Co., Union Carbide and Carbon Corp., Niagara Falls, N. Y.

of tungsten has been re-investigated between 700° and 1000°C. Seemingly conflicting observations have been resolved by covering a wide span of time ranging from several minutes up to more than one day.

Gulbransen and Wysong (1) noted appreciable volatility of tungsten oxides only under good vacuum above 800°C. Millner and Neugebauer (6) reported that tungsten trioxide is not volatile at 1000°C in oxygen, argon, or in a vacuum of 1 μ mercury. However, they found that tungsten trioxide volatilized in the presence of water vapor in excess of 30 volume per cent. The present investigation confirms that volatilization of tungsten oxides in dry oxygen up to 1000°C is insignificant, and, therefore, oxidation can be followed by measuring the weight gain of specimens.

Hickman and Gulbransen (7) have studied the crystal structures of the oxides formed on tungsten up to 700°C. Below 700°C they found only WO_3, but at 700°C both WO_2 and WO_3 were reported. According to studies of phase relations in the system tungsten-oxygen, especially x-ray investigations. the occurrence of other phases may also be expected. The following stable phases have been reported (8–15):

αWO_3 triclinic pseudo-orthorhombic (stable below 720°C),
$\alpha' WO_3$ tetragonal (stable above 720°C),
$\beta W_{20}O_{58} = WO_{2.90}$ monoclinic,
$\gamma W_{18}O_{49} = WO_{2.72}$ monoclinic,
δWO_2 monoclinic.

Each of these phases is supposed to exist in a finite homogeneity range, the limits of which are temperature dependent.

In addition, there is a cubic phase, W_3O (15), which however does not seem to be stable above 700°C.

The available thermodynamic data on the tungsten oxides have been summarized by Coughlin (16).

Experimental

The weight of tungsten specimens suspended in a tube furnace by quartz filaments from a standard analytical balance was read periodically as the oxidation proceeded. Since all the oxide remained on the surface of the specimens, the amount of oxide formed was thus obtained. Specimens of 0.05-cm thick tungsten sheet weighing from

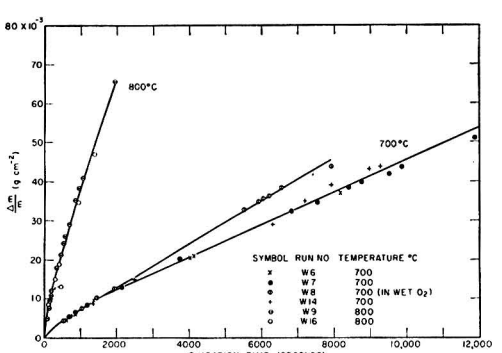

Fig. 1. Oxidation of tungsten at 700° and 800°C

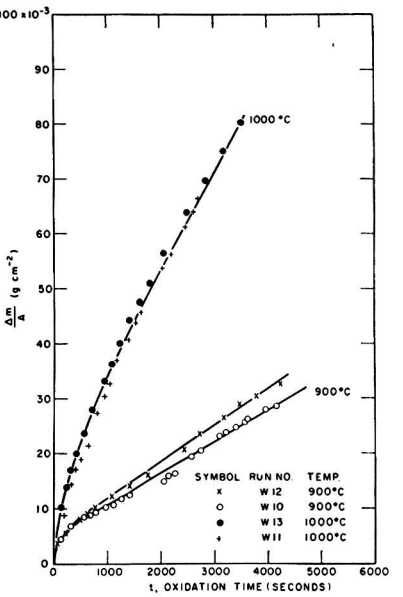

Fig. 2. Oxidation of tungsten at 900° and 1000°C

2 to 10 g with surface areas from 4 to 10 cm² were polished on 120-mesh Alundum abrasive paper and washed with C.P. acetone. U.S.P. tank oxygen was passed over "Ascarite," $CaSO_4$, and "Anhydrone" for purification before being admitted to the furnace at flow rates of 2–5 liter/hr.

To start a run, the specimen was raised from a cold zone below the bottom of the furnace into the oxygen-filled hot zone maintained at the desired temperature within ±5°C. About 1 min was required for the specimens to reach the desired temperature. The alternative method of initiating runs by introducing oxygen into the furnace with the specimen already at reaction temperature in an inert atmosphere was rejected since calculations indicated that, in this case, initial evolution of the heat of formation of the oxide would produce significant overheating of the specimen and hence give spurious results.

Tungsten sheet from the A. D. McKay Company was reported to be 99.9% pure. An analysis revealed the following impurities: 0.002% Fe, 0.005% Si, 0.01% Al, 0.033% C, and 0.004% sulfur.

Experimental data are presented in Fig. 1 and 2. No allowance is made for the time required to reach the reaction temperature. Deviations between duplicate runs had about the same magnitude as the scatter of points during an individual run. Points at short oxidation times have been omitted for clarity.

The weight gain curves start out with a steep slope which gradually decreases and tends to a limiting value corresponding to a virtually constant rate. This suggests that a parabolic rate law may represent the data for a short time at the beginning of the experiments. Subsequently, transition to a linear law seems to occur. On this basis, limiting rate constants k_2 and k_1 have been evaluated

TABLE I. *Rate constants for the oxidation of tungsten*

Temp, °C	Run No.	k_2	k_1	y_{max}	d_{max}	$t_{0.5}$
		g^2/cm^4sec	g/cm^2sec	g/cm^2	cm	sec
700	6	2.5×10^{-9}	3.9×10^{-7}			
700	7	‡	3.9×10^{-7}			
700	8*	2.5×10^{-9}	5.6×10^{-7}			
700	14†	‡	4.3×10^{-7}			
700	best values	2.5×10^{-9}	4.0×10^{-7}	3.1×10^{-3}	2.0×10^{-3}	1490
800	9	3.0×10^{-8}	3.2×10^{-6}			
800	16	3.0×10^{-8}	3.0×10^{-6}			
800	best values	3.0×10^{-8}	3.2×10^{-6}	4.7×10^{-3}	3.1×10^{-3}	280
900	10	1.0×10^{-7}	5.8×10^{-6}			
900	12†	1.3×10^{-7}	7.5×10^{-6}			
900	best values	1.0×10^{-7}	6.0×10^{-6}	8.4×10^{-3}	5.5×10^{-3}	264
1000	11	7.3×10^{-7}	1.8×10^{-5}			
1000	13	7.3×10^{-7}	1.8×10^{-5}			
1000	best values	7.3×10^{-7}	1.8×10^{-5}	2.0×10^{-2}	1.35×10^{-2}	214

* Oxidized in O_2 saturated with H_2O at 23°C.

† Large edge-to-area ratio.

‡ No value of k_2 has been obtained in view of irregularities at small oxidation times.

and are tabulated in the third and the fourth column of Table I. The parabolic rate constants k_2 are in general agreement with those of Dunn (2) whose runs did not exceed 3 hr. Scheil (3) found that the linear rate law applied when specimens were oxidized up to 90 hr at 700°C. This is also in agreement with the results of the present investigation because for such long oxidation times the transition from the parabolic to the linear rate law is virtually complete.

Two experiments were made in order to determine the effect of variations in the experimental conditions which may be expected to be critical.

In view of the reported volatility of WO_3 in water vapor (6), one run was made in oxygen saturated with H_2O at 23°C. The only significant difference was a slight increase in the constant oxidation rate approached after long times. No deposit of oxide appeared at the exit of the furnace.

Since preferred oxidation at edges and corners was noticed, specimens with an exceptionally large ratio of edge length to surface area were oxidized. They showed some small irregularities in rate, but, as a whole, results did not differ widely from results for standard samples.

On the outer surface of the specimens a thick, powdery, porous layer of the yellow tungstic oxide, WO_3, appeared. The oxide appeared to have grown outward perpendicular to the flat surfaces of the specimens as has previously been observed by Scheil (3). After the yellow oxide had reached a thickness of the order of 1 mm, preferred oxidation near the edges was quite evident, particularly at the higher temperatures where eventually the yellow oxide layer projected from the edges like petals. Weight gain data were not taken after the preferred oxidation became evident since, by that time, the effective area of the specimens had changed excessively. The porosity of this layer was clearly evidenced by rapid absorption of ink from a fountain pen point touched to the oxide surface, and by microscopic examination (see Fig. 3). Pycnometric density measurements indicated about 30% porosity. Absorption of water or glycerin during density determinations was slight, apparently due to poor wetting of the oxide. X-ray diffraction powder patterns taken with a Geiger counter spectrometer revealed only WO_3. Presumably, the α' structure was formed above 710°C but transformed on cooling.

On scraping the yellow oxide from the surface, a hard, dark-blue substrate was found which yielded an x-ray diffraction pattern different from tungsten and different from that for any of the known tungsten oxides. The observed diffraction lines coincided with some of the lines observed for WO_3 and with some of those reported for the blue tungsten oxide listed as W_4O_{11} in the ASTM x-ray diffraction data cards. The five lines that appeared were

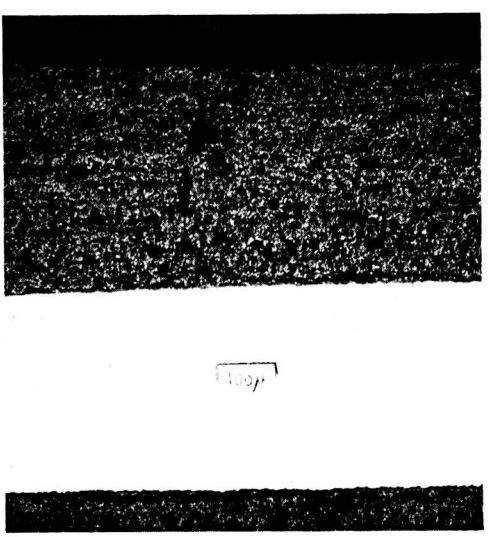

FIG. 3. Tungsten oxidized at 700°C showing porosity in the yellow oxide (no etch). The light area is unoxidized metal.

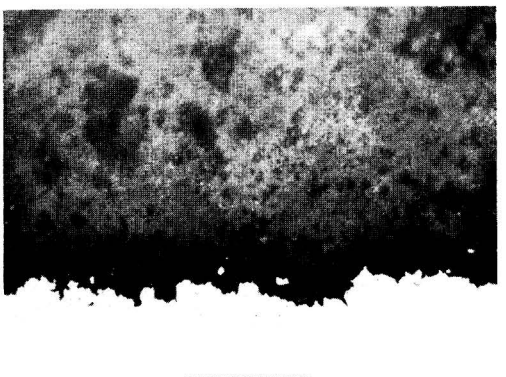

FIG. 4. Tungsten oxidized at 700°C for 4 hr observed with oil-immersion objective (no etch). The dark, irregular band in the middle is the 4- to 15-μ thick "blue oxide" layer between yellow WO_3 at the top and metal at the bottom. The distinct identity of the blue oxide is emphasized by examination with a polarizing microscope or with a sensitive tint plate.

all sharp and could be indexed on the assumption of a cubic lattice with a parameter of 3.77 Å. The composition and structure were not definitely determined, but it may be surmised that this oxide is a metastable modification of one of the intermediate oxide phases.

The thickness of the blue oxide formed by protracted oxidation at several temperatures was estimated roughly from the relative integrated intensities of diffraction lines from the blue oxide layer and from the underlying tungsten. At 700°C, the estimated thickness was of the order of 15 μ. At 900°C, the thickness was roughly two times greater. The thickness found at 700°C is close to an estimate of 10 μ obtained by microscopic observation of a cross section, part of which is shown in Fig. 4.

Specimens oxidized for about 5 min at 700°C were found to have almost the same thickness of the blue oxide as those oxidized for extended periods but only a very thin, powdery layer of yellow oxide. This indicates that the blue oxide forms quite rapidly during the early stages of oxidation but later ceases growing.

DISCUSSION

According to Loriers (17) the transition from the parabolic to a linear rate law occurs when the primary oxidation product is a nonporous oxide which transforms to another porous oxide by take-up of additional oxygen. The formation rate of the primary oxide is assumed to be inversely proportional to its thickness, whereas the rate of transformation to the porous oxide is assumed to be constant. Then one has the rate equations

$$dy/dt = a/y - b \qquad \text{(I)}$$

$$dz/dt = fb \qquad \text{(II)}$$

where y is the mass of oxygen in the barrier layer per unit area at time t, z is the mass of oxygen in the outer porous oxide layer, f is the ratio of the oxygen content per gram-atom metal in the outer layer to that in the inner layer, and a and b are constants.

The total amount of oxygen per unit area, equal to the increase in mass per unit area, is

$$\Delta m/A = y + z \qquad \text{(III)}$$

For short times, when the barrier layer is thin and thus y is relatively small, the first term on the right-hand side of equation (I) predominates. Consquently, the constant a may be calculated as

$$a = \lim_{t=0}\left\{\frac{1}{2}\frac{d}{dt}\left[\left(\frac{\Delta m}{A}\right)^2\right]\right\} = \frac{1}{2}k_2 \qquad \text{(IV)}$$

Hence a is one-half the rate constant, k_2, of the parabolic rate law of Pilling and Bedworth (18). At longer times, the amount of oxygen in the barrier layer tends to a limiting value y_{max} when the rate of formation of this layer is equal to the rate of transformation to the nonporous oxide. From equation (I), it follows that

$$y_{max} = a/b \qquad \text{(V)}$$

If $y = y_{max}$, the rate of change in mass per unit area is essentially equal to dz/dt. Hence, in view of equation (II),

$$bf = \lim_{t=\infty}\left[\frac{d(\Delta m/A)}{dt}\right] = k_1 \qquad \text{(VI)}$$

where k_1 is the rate constant of the linear rate law valid for long oxidation times.

On this basis, Loriers has explained qualitatively the gradual transition from a parabolic to a linear rate law observed for cerium (17). Subsequent measurements by Cubicciotti (19) are in accord herewith. The same behavior has been found for the oxidation of uranium (20).

In the case of tungsten, it is also possible to represent the experimental data with the help of equations (I) and (II) at intermediate times when neither limiting rate law applies.

Integration of equations (I) and (II) yields

$$\ln(1 - by/a)^{-1} - by/a = b^2t/a \qquad \text{(VII)}$$

$$z = bft \qquad \text{(VIII)}$$

whereby the values of y and z in equation (III) as functions of time are determined.

Introducing the auxiliary values

$$X = \ln(1 - by/a)^{-1} \qquad \text{(IX)}$$

$$Y = b^2t/a \qquad \text{(X)}$$

we may rewrite equation (VII) as

$$X - (1 - e^{-X}) = Y \qquad \text{(XI)}$$

and plot log Y calculated from equation (XI) vs. log X. With the help of this plot, one may obtain the value of X for a given value of $Y = b^2t/a$.

Substitution of equations (VII) and (VIII) in equation (III) yields

$$\Delta m/A = (a/b) \ln (1 - by/a)^{-1} + b(f-1)t = (a/b)[X + Y(f-1)] \quad \text{(XII)}$$

In this way, one may calculate $\Delta m/A$ for any time t for a comparison with observed values in order to check the applicability of the rate laws assumed in equations (I) and (II). If the inner oxide had the approximate composition $WO_{2.75}$, the value of f would be 1.09. Since the actual composition of the inner oxide is uncertain, however, f has been taken as unity for the sake of simplicity. Hence, a is equal $\frac{1}{2}k_2$ and b is taken as equal to k_1 according to equations (IV) and (VI). Values of k_1 and k_2 are listed in Table I.

Fig. 5 shows that the observed oxidation curves generally agree with the calculated curves within the limits of uncertainty. Deviations at short times which are emphasized by the logarithmic scale are due to an uncertainty of about 30 sec in fixing the effective starting time of the experiments and to an uncertainty in the calculation of the limiting parabolic rate constant.

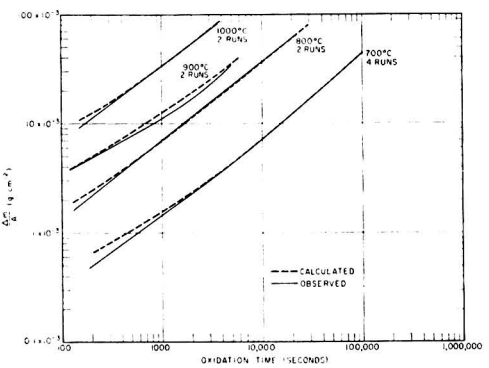

FIG. 5. Comparison of calculated and observed values of $\Delta m/A$ for the oxidation of tungsten.

In addition, the value of y_{max} calculated from equation (V) may be used in order to obtain the maximum thickness of the inner oxide film,

$$d_{max} = y_{max} M/16x\rho \quad \text{(XIII)}$$

where M is the formula weight of the inner oxide involving one atom of tungsten, x is the number of oxygen atoms per tungsten atom, and ρ is the density of the inner oxide. The evaluation of equation (XIII) has been based on the formula WO_3, although the actual value of x is smaller than 3. Calculated values of d_{max} agree with the observed values within a factor of two which is about the magnitude of the experimental uncertainty. The observed trend of d_{max} with temperature is in accord with the calculations.

From equations (V) and (VII), one may also calculate the time $t_{0.5}$ required for $y = 0.5\ y_{max}$ when half the limiting thickness of the protective oxide layer has been reached,

$$t_{0.5} = (a/b^2)(\ln 2 - 0.5) = 0.19(a/b^2) \quad \text{(XIV)}$$

Values of $t_{0.5}$ listed in Table I show that most of the inner oxide layer is built up in a rather short time, especially at higher temperatures. This shows the difficulties of obtaining an adequate value of k_2.

Manuscript received August 25, 1955. This paper was prepared for delivery before the Pittsburgh Meeting, October 9 to 13, 1955, and is based in part on a thesis submitted by W. W. Webb in partial fulfillment of the requirements for the D.Sc. degree from Massachusetts Institute of Technology.

Any discussion of this paper will appear in a Discussion Section to be published in the December 1956 JOURNAL.

REFERENCES

1. E. A. GULBRANSEN AND W. S. WYSONG, *Trans. Am. Inst. Mining Met. Engrs.*, **175**, 611 (1948).
2. J. S. DUNN, *J. Chem. Soc. (London)*, **1929**, 1149.
3. E. SCHEIL, *Z. Metallkunde*, **29**, 209 (1937).
4. E. NACHTIGALL, *ibid.*, **43**, 23 (1952).
5. R. KIEFFER AND F. KÖLBL, *Z. anorg. u. allgem. Chem.*, **262**, 229 (1950).
6. T. MILLNER AND J. NEUGEBAUER, *Nature*, **163**, 601 (1949).
7. J. W. HICKMAN AND E. A. GULBRANSEN, *Trans. Am. Inst. Mining Met. Engrs.*, **171**, 371 (1947).
8. H. BRAKKEN, *Z. Krist*, **78**, 484 (1931).
9. O. GLEMSER AND H. SAUER, *Z. anorg. u. allgem. Chem.*, **252**, 144 (1943).
10. G. HÄGG AND A. MAGNELI, *Arkiv Kemi, Mineral. Geol.*, **19A**, No. 2, (1944).
11. A. MAGNELI, *ibid.*, **24A**, No. 2, (1946).
12. A. MAGNELI, *Arkiv Kemi*, **1**, 223, 513 (1949).
13. R. UEDA AND T. ICHINOKAWA, *Phys. Rev.*, **80**, 1106 (1950); **82**, 563 (1951).
14. W. L. KEHL, R. G. MAY, AND D. WAHL, *J. Appl. Phys.*, **23**, 212 (1952).
15. N. SCHÖNBERG AND G. HÄGG, *Acta Cryst.*, **7**, 351 (1954).
16. J. P. COUGHLIN, *U. S. Bur. Mines Bull. 542* (1954).
17. J. LORIERS, *Compt. rend.*, **231**, 522 (1950).
18. N. B. PILLING AND R. E. BEDWORTH, *J. Inst. Metals*, **29**, 529 (1923).
19. D. CUBICCIOTTI, *J. Am. Chem. Soc.*, **74**, 1200 (1952).
20. J. LORIERS, *Compt. rend.*, **234**, 91 (1952).

Oxidation Studies in Metal-Carbon Systems

WATT W. WEBB,[1] JOHN T. NORTON, AND CARL WAGNER

Department of Metallurgy, Massachusetts Institute of Technology, Cambridge, Massachusetts

ABSTRACT

A general analysis of the characteristics of the oxidation of alloys containing carbon or carbides is given. Evolution of gaseous CO and CO_2 may rupture oxide films which, in the absence of carbon, are highly protective. On the other hand, if the base metal has a high affinity for oxygen, carbon may be retained in the alloy, or carbon may diffuse across the oxide layer. Experimental data are reported for the systems Ni—C, W—C, Mn—C, and Ti—C.

INTRODUCTION

A determining factor for the oxidation resistance of hard metals based on metal carbides and of carbon-bearing alloys may be the presence of carbon which may yield gaseous reaction products, CO and CO_2. Some carbon-bearing materials are of industrial interest due to their high strength at elevated temperatures, but, for widest applicability, their oxidation resistance must also be sufficiently high (1). In general, oxidation resistance of a metal is due to the formation of a solid protective metal oxide film which acts as a diffusion barrier and limits the rate of oxidation (2), but the formation of gaseous reaction products such as CO and CO_2 may disrupt the protective oxide film. Therefore, the oxidation of various metal-carbon systems has been investigated to clarify this situation.

Oxidation of a metal such as nickel or manganese at elevated temperatures yields an oxide layer virtually without pores, and the rate is controlled by diffusion of ions and electrons across the oxide film. If carbon is present as an alloying element, the formation of CO or CO_2 at the alloy-oxide interface may rupture the oxide layer and, therefore, change the kinetics of the oxidation process.

If the metal oxide adjacent to the alloy has the formula MeO_y, evolution of CO and CO_2 may be due to the reactions

$$C(\text{alloy}) + 1/y\ MeO_y = CO(g) + 1/y\ Me(\text{alloy}) \quad (I)$$

$$C(\text{alloy}) + 2/y\ MeO_y = CO_2(g) + 2/y\ Me(\text{alloy}) \quad (II)$$

The corresponding equilibrium partial pressures of CO and CO_2 are

$$p_{CO} = K_1 a_C/(a_{Me})^{1/y} \quad (III)$$

$$p_{CO_2} = K_2 a_C/(a_{Me})^{2/y} \quad (IV)$$

where K_1 and K_2 are the equilibrium constants of reactions (I) and (II), respectively, and where a_{Me} and a_C are the activities of metal and carbon, respectively, at the alloy-oxide interface.

The following two principal cases are to be considered.

Case I.—If metal Me has a relatively low affinity for oxygen and, accordingly, the sum $p_{CO} + p_{CO_2}$ [calculated from equations (III) and (IV) with the carbon activity of the original alloy] is much greater than the surrounding pressure P, outburst of CO and CO_2 is likely to rupture the oxide film. Then molecular oxygen may diffuse through the resulting cracks toward the alloy-oxide interface so that the oxidation of the metal may proceed much more rapidly than in the absence of carbon unless the oxide layer shows a very good "healing tendency."

Under these conditions, the activity of carbon at the alloy-oxide interface will be much lower than in the bulk alloy. In view of the porosity of the oxide, the sum of p_{CO} and p_{CO_2} may be assumed to be virtually equal to the surrounding pressure P,

$$p_{CO} + p_{CO_2} = P \quad (V)$$

The CO_2/CO ratio is given by the reaction

$$1/y\ MeO_y + CO = 1/y\ Me + CO_2 \quad (VI)$$

with the equilibrium condition

$$p_{CO_2}/p_{CO} = K_3/(a_{Me})^{1/y} \quad (VII)$$

Upon combining equations (V) and (VII), one may calculate the values of p_{CO} and p_{CO_2} and finally, on using equations (III) or (IV), the activity of carbon at the alloy-oxide interface.

The following possibilities under Case I are to be considered.

(*A*) A much lower carbon activity at the alloy-oxide interface than in the bulk alloy may result in diffusion of carbon toward the oxide-alloy interface and, therefore, in preferential oxidation of carbon. This has been found in the system Ni—C.

(*B*) In spite of depletion of carbon at the metal-oxide interface, diffusion of carbon may be negligible. By and large, the rate of diffusion in a single phase is determined by the product of a diffusion constant and a concentration gradient which, in turn, is essentially proportional to the homogeneity range of the phase. Therefore, if the homogeneity ranges of the phases of the Me—C system which are involved are very small and the rate of oxide formation is high, diffusion of carbon will be insignificant as can be shown by calculations omitted in this paper. Thus, non-preferential oxidation of carbon is expected as has been found in the system W—C.

Case II.—In systems involving a high absolute value of the standard free energy of formation of metal oxide per gram-atom of oxygen, the sum $p_{CO} + p_{CO_2}$ calculated

[1] Allegheny Ludlum Steel Co. Fellow, 1953–1955; present address: Metals Research Lab., Electro Metallurgical Co., Union Carbide and Carbon Corp., Niagara Falls, N. Y.

from equations (III) and (IV) with the carbon activity of the original alloy is less than the surrounding pressure unless the temperature is very high. Under these conditions, carbon may be retained in the alloy underneath a dense oxide film, but it is also possible that carbon is oxidized as is shown below. The following possibilities under Case II are to be considered.

(*A*) Carbon rejected at the alloy-oxide interface may diffuse backward into the bulk alloy as has been found in the system Mn—C. Possibly, phases richer in carbon than that in the original alloy may form. If the sum $p_{CO} + p_{CO_2}$ calculated from equations (III) and (IV) with the carbon activity prevailing at the alloy-oxide interface does not exceed substantially the surrounding pressure, no rupture of the oxide film is to be expected and the oxidation rate is supposed to be essentially the same as in the absence of carbon except for a small effect due to the lower activity of the metal.

Enrichment of carbon at the alloy-oxide interface, however, may in some systems result in a large increase in the activity of carbon and a pressure $p_{CO} + p_{CO_2}$ which is substantially greater than the surrounding pressure. Thus, after a certain amount of carbon-rich alloy or, eventually, graphite has been formed, rupture of the oxide film may occur. Access of oxygen will decrease the carbon activity with following healing of the ruptured oxide film and accumulation of carbon until once more the critical activity of carbon for rupture of the oxide film has been reached. Thus, periodic changes of the oxidation rate would occur. So far, no experimental evidence for this type of oxidation is available.

(*B*) Backward diffusion of carbon will not occur if the alloy is saturated with graphite and, accordingly, there is no activity gradient of carbon. In this case, more graphite may be formed at the alloy-oxide interface. If graphite appears in disperse form, the cross section of oxide available for migration of ions and electrons is changed only to a minor extent and so the oxidation rate may not differ widely from that for a system free of carbon. No example can be quoted at the present.

(*C*) In special cases, outward migration of carbon across an "oxide layer" may occur if carbon is sufficiently soluble therein. The presence of carbon in the oxide may increase or decrease the concentration of lattice defects which are decisive for the rate of migration of ions and electrons in the oxide and, therefore, may increase or decrease the rate of oxidation of the metal. Dissolution of carbon in oxide may be considered as an important factor when TiC is oxidized because TiC and TiO are known to be mutually soluble, and there may be some carbon solubility in TiO_2. So far, however, no direct experimental proof has been obtained.

The foregoing discussion is based on the assumption of attainment of thermodynamic equilibrium at the various phase boundaries. It is possible, however, that the breakup of metal-carbon bonds in a carbide phase requires a high activation energy and thus becomes the rate-determining step. Under these conditions, oxidation of a carbide may follow a linear rather than a parabolic rate law and is substantially slower than the oxidation of the corresponding metal under comparable conditions during a certain span of time. Although there is no direct evidence, this may be an important possibility to account for the oxidation resistance of some carbides and other constituents in hard metals such as borides and nitrides.

These general principles for the oxidation of metal-carbon systems are illustrated by investigations on the systems Ni—C, W—C, Mn—C, and Ti—C.

Experimental Procedure

The weight change of specimens heated in dry oxygen of atmospheric pressure was measured in the same manner as for the oxidation of tungsten (3). In view of the loss of carbon, however, the weight change is not a direct measure of the oxidation rate. Therefore, the amount of carbon being oxidized was determined separately in parallel runs. The gas passed over the specimen was led into an auxiliary furnace with cupric oxide as a catalyst, where CO was converted into CO_2 which was finally collected in weighing bottles containing Ascarite and Anhydrone. The oxygen take-up per unit surface area $\Delta m_{ox}/A$ may then be calculated as

$$\Delta m_{ox}/A = \Delta m/A + (12/44)(\Delta m_{CO_2}/A) \quad \text{(VIII)}$$

where $\Delta m/A$ is the observed change in mass of the sample per unit area and $\Delta m_{CO_2}/A$ is the amount of CO_2 per unit area collected during the same time.

If metal and carbon are oxidized nonpreferentially, we have the equation

$$(1 - x)\text{Me} + x\text{C} + \left[\frac{1}{2}(1 - x)y + x\right]\text{O}_2 = (1 - x)\text{MeO}_y + x\text{CO}_2 \quad \text{(IX)}$$

where x is the mole fraction of carbon in the original alloy or carbide, and y is the average number of oxygen atoms per metal atom in the oxide layer.

From equation (IX) it follows that

$$\frac{\Delta m_{CO_2}/A}{\Delta m/A} = \frac{44x}{16(1 - x)y - 12x} \quad \text{(X)}$$

if neither metal nor carbon is oxidized preferentially.

If equation (X) holds, the oxygen take-up per unit area may be calculated directly from the weight change of the sample. Upon substitution of equation (X) in equation (VIII), it follows that

$$\frac{\Delta m_{ox}}{A} = \frac{16(1 - x)y}{16(1 - x)y - 12x}\frac{\Delta m}{A} \quad \text{(XI)}$$

Conversely, $\Delta m_{ox}/A$ may also be calculated from the amount of CO_2. Substitution of equation (X) in equation (XI) yields

$$\frac{\Delta m_{ox}}{A} = \frac{16(1 - x)y}{44x}\frac{\Delta m_{CO_2}}{A} \quad \text{(XII)}$$

Values calculated from equations (VIII), (XI), or (XII) have been used in order to calculate the parabolic rate constant as $(\Delta m_{ox}/A)^2/t$ in g^2cm^{-4} sec^{-1} as far as the parabolic rate law applies.

Equations (VIII) and (X) involve data from parallel runs since the weight change of a sample and the amount

of CO_2 were not determined simultaneously. The applicability of equations (VIII) and (X) requires, therefore, a sufficient reproducibility. Checks showed that deviations between different runs were of the same order of magnitude as the weighing errors in an individual run (about ± 0.001 g corresponding to an error of 0.0002 g/cm^2 in $\Delta m/A$ or $\Delta m_{CO_2}/A$ for a sample of 5 cm^2 area).

The System Ni—C

When pure nickel is oxidized at 1000°C, the parabolic rate law is obeyed, i.e., a protective layer of NiO is formed. For nickel saturated with graphite and coexisting with nickel oxide, NiO, the sum $p_{CO} + p_{CO_2}$ calculated from equations (III) and (IV) and data compiled by Coughlin (4) is of the order of 10^6 atm at 1000°C. This suggests that CO and CO_2 formed by reactions (I) and (II) will rupture a nickel oxide film. This is confirmed by a comparison of the oxidation rates of pure nickel and a Ni-C alloy containing 2.3% carbon at 1000°C. Data are presented in Fig. 1.

Virtually pure nickel was obtained from Vacuum Metals Corporation, Cambridge, Massachusetts. A nominal analysis indicates the presence of the following impurities: 0.004% C, 0.002% O, 0.0045% S, 0.003% Co, 0.003% Si.

In accordance with previous investigations (5, 6, 7), pure nickel was found to oxidize very slowly. The parabolic rate constant was found to be 4×10^{-10} g^{2}cm^{-4} sec^{-1} at 1000°C.

A Ni-C alloy with 2.3% C was prepared by melting pure nickel with carbon in an induction furnace and sucking the liquid alloy into a Vycor tube. Thus, rods with a diameter of 0.4 cm were obtained. Since the solubility of graphite in nickel amounts to only 0.27% at 1000°C (8), the alloy consisted of nickel saturated with graphite and excess graphite in nodular and flake form as was found by microscopical examination. In oxidation tests, samples showed a weight decrease rather than a weight increase because the mass of carbon being oxidized exceeded the oxygen take-up due to formation of nickel oxide. Analogous observations have been made by Gulbransen and Hickman (9) when carbon-containing alloys were exposed to much lower oxygen pressures of the order of 1 μ.

The amount of CO_2 collected during the first few hours, which is shown as the uppermost curve in Fig. 1, clearly indicates preferential oxidation of carbon. Only after longer exposure when the CO_2 evolution had ceased, a weight increase of the Ni-C alloy was observed.

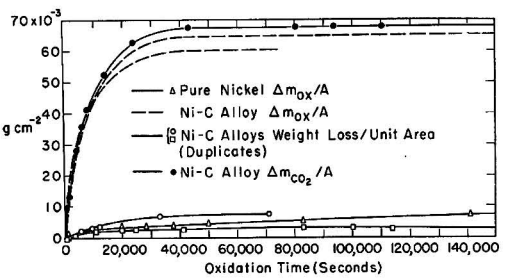

FIG. 1. Oxidation of nickel and a nickel-carbon alloy at 1000°C.

From equations (III), (V), and (VII) it follows that the carbon concentration at the alloy-oxide interface is virtually zero. Thus there is formed a one-phase alloy with a variable carbon content, ranging from zero to 0.27% C, between the alloy-oxide interface and the core of the original two-phase alloy. In view of the concentration gradient in the one-phase region, carbon diffuses outward, and the boundary between the one-phase and the two-phase region is shifted inward because excess graphite dissolves. A similar situation occurs during the decarburization of Fe-C alloys in a H_2O-H_2 atmosphere according to Pennington (10). A mathematical analysis for a plane sample has been given by Jost (11). The decarburization rate observed in the present experiments is somewhat higher than the value estimated from the diffusion constant of carbon in nickel, which has been reported to be 3×10^{-7} cm^2/sec at 1000°C (8).

A photomicrograph of a sample after oxidation for 17 hr confirmed virtually complete decarburization in accordance with the end of the CO_2 evolution. Voids were found instead of the original graphite inclusions.

The rate of formation of nickel oxide on the alloy depends on the damage done to the protective layer by gas evolution. No detailed mechanism can be suggested. Thus the observed oxidation rate cannot be related to other data. The fact that the rate of nickel oxide formation after complete decarburization drops to values lower than those observed for pure nickel after equal times indicates that the damage to the oxide caused by gas evolution later disappears by some kind of "healing process." Microscopical examination of oxidized samples showed an inner oxide layer consisting of a porous aggregate of fine grains whereas the outer layer was more coherent. It is probable that the porous part of the oxide was formed during the early stages of oxidation while gas was evolved rapidly and that the less porous outer part was formed later when gas evolution was slow or had ceased.

To summarize, the oxidation of a Ni-C alloy containing 2.3% carbon is an example for Case I(*A*) considered above.

The System W—C

In the system W—C, two carbides, W_2C and WC, of nearly invariable composition are found. The solubility of carbon in tungsten is very low. Thus virtually no diffusion of carbon and no preferential oxidation of carbon can be expected. From previous investigations (12), it is already known that W_2C and WC are oxidized at a high rate, but no quantitative evaluation is possible since only the weight change of samples was determined but not the loss of carbon.

In view of the general program outlined above, the rate of oxidation of the compound WC was investigated for a comparison with the rate of oxidation of pure tungsten. Outburst of CO and CO_2 is likely to occur at 1000°C but thermodynamic calculations for lower temperatures are not conclusive in view of uncertainties of the free energies of formation of WC and the various oxides.

Specimens of WC were prepared by hot-pressing pure WC powder obtained from A. D. McKay Company. The resulting material had a relative density of about 90%.

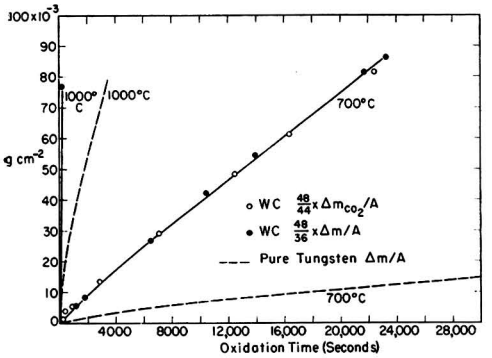

FIG. 2. Oxidation of tungsten and tungsten carbide

Data for the oxidation of WC are shown in Fig. 2 and are compared with data concurrently obtained for tungsten (3). At 700°C, the oxidation of WC follows the linear rate law. The rate constant is 4×10^{-6} g cm^{-2}sec^{-1}. Results for 1000°C are rather of a qualitative nature in view of the exceedingly high rate. The amount of CO_2 collected indicates nonpreferential oxidation of carbon corresponding to the over-all reaction

$$WC + 2.5\ O_2 = WO_3 + CO_2$$

The higher rate for the oxidation of WC in comparison to that of tungsten suggests rupture of the oxide film due to formation of CO and CO_2. Thus the oxidation of WC follows the pattern for Case I(*B*) considered above.

An examination of the oxide film formed on WC at 700°C revealed only the presence of yellow WO_3, but no blue oxide was found in contrast to the finding with pure tungsten (3).

The System Mn—C

Manganese has a high affinity for oxygen. Therefore, it is expected that during the oxidation of Mn-C alloys no CO or CO_2 is formed, but carbon is retained in the alloy.

The oxidation of pure manganese has been studied by Gurnick and Baldwin (13), who overcame the tendency of manganese samples to disintegrate on heating by electroplating manganese on a strong base material. The parabolic law was followed during oxidation in air between 400° and 1100°C. The parabolic rate constant was found to be 5×10^{-8} g^{2}cm^{-4}sec^{-1} at 1000°C. About 10% MnO and 90% Mn_3O_4 were formed.

The manganese-carbon phase diagram has been studied by Isobe (14) and by Vogel and Döring (15) who have shown that there is a high temperature γ phase, similar to γ iron, which dissolves carbon up to about 2 wt % at 1000°C. At higher carbon contents, there seems to be a carbide with a homogeneity range from about 3 to 4 wt % carbon at 1000°C. The available information on the manganese carbides has been summarized by Kuo and Persson (16).

A sample of manganese obtained from Electro Metallurgical Company, New York, New York, contained 0.92% Fe, 0.21% Si, and 0.21% C. A Mn-C alloy containing 1.33% C was prepared by melting manganese and chips of spectroscopically pure carbon in an alumina crucible

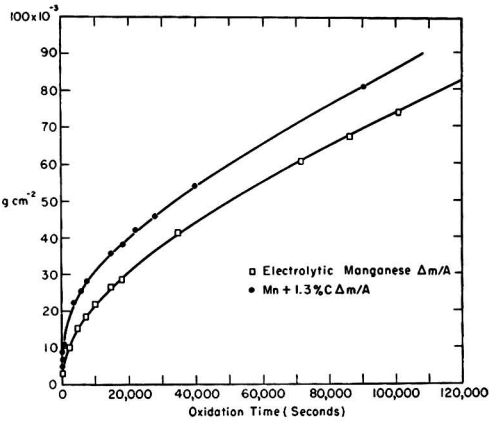

FIG. 3. Oxidation of manganese and a manganese-carbon alloy.

under a purified argon atmosphere. Rods were obtained by sucking the liquid metal into Vycor tubes. Oxide-free surfaces resulted, but specimens of both manganese and the manganese-carbon alloy invariably cracked during cooling. However, it was possible to select suitable pieces, cut them to size, abrade their surfaces, and reheat them for oxidation experiments without disintegration.

Data for 1000°C are presented in Fig. 3. Unalloyed manganese was found to oxidize according to the parabolic rate law with a constant of 5×10^{-8} g^{2}cm^{-4}sec^{-1} in agreement with Gurnick and Baldwin (13). The Mn-C alloy oxidized at a somewhat higher rate.

Only small amounts of CO_2 were collected. A stoichiometric calculation indicates that 0.17 g CO_2/1 g O take-up should be collected if neither manganese nor carbon were oxidized preferentially. After 90,000 sec, a weight increase of 0.08 g/cm^2 was found, whereas the amount of CO_2 collected amounted to only 0.00027 g/cm^2 which is 2% of the amount expected for nonpreferential oxidation. In another run of 44 hr (160,000 sec), the amount of CO_2 was $\frac{1}{20}$ the amount expected for nonpreferential oxidation.

That nearly all the carbon does remain in the manganese during oxidation was confirmed by a carbon analysis of a representative sample of the metallic core from another test after 25 hr (90,000 sec) of oxidation. The analysis showed 2.15 wt % carbon in exact agreement with the amount expected, assuming that all carbon remains in the specimen. Metallographic examination revealed the presence of a distinct layer, about 100 μ thick at the surface of the metallic core. Presumably, there was a carbide phase stable at 1000°C which transformed on cooling to other phases stable at lower temperatures. In the oxide layer, no pores were visible.

To summarize, the oxidation of a Mn-C alloy containing 1.33% carbon is an example for Case II(*A*) considered above.

The System Ti—C

Titanium also has a high affinity for oxygen and accordingly the sum $p_{CO} + p_{CO_2}$ at the alloy-oxide interface is expected to be low so that rupture of the oxide film on Ti-C alloys should not and did not occur. Nevertheless,

nonpreferential oxidation similar to that of WC was found.

The titanium-carbon system has a narrow, terminal solid solution and a very stable carbide, TiC, with a substantial homogeneity range (17).

The titanium-oxygen system is characterized by a large terminal solid solubility of oxygen in titanium and by at least three oxides: TiO, Ti_2O_3, and TiO_2 (18, 19)

Oxidation of pure titanium has been studied by several authors and the references through 1954 are given by Simnad, Spilners, and Katz (20). The parabolic rate law is obeyed fairly well. There are essentially two simultaneous processes, namely, solution of oxygen in titanium, and formation of a layer of titanium oxides, mainly TiO_2. Simnad, Spilners, and Katz have separated the rates of these processes.

In what follows, comparative values for the oxidation of pure titanium, TiC, and carbon-deficient TiC are reported.

Titanium metal specimens were cut from swaged rods of vacuum-melted iodide titanium. Commercially pure titanium carbide powder was hot-pressed into specimens having apparent densities in excess of 97%. Carbon deficient titanium carbide containing 15.8 wt % carbon was made by reacting stoichiometric TiC with titanium powder reported to be 99.9% pure (A. D. McKay Company) at 1600°C in vacuo for 1 hr. This material was crushed in order to obtain a uniform powder. The carbon content corresponded to the formula $TiC_{0.63}$. Hot-pressed specimens were rather porous and contaminated by carbon from the graphite die at their outer surfaces. Contamination was removed by grinding.

Upon comparing weight change and CO_2 evolution during oxidation, it was found that essentially equation (X) holds, i.e., titanium and carbon are oxidized nonpreferentially. Therefore, the oxygen take-up was calculated from weight gain measurements and from the amount of CO_2 with the aid of equations (XI) and (XII), respectively. Results are shown in Fig. 4.

At 1000°C, the oxygen take-up corresponding to the formation of TiO_2 is about the same for titanium metal and $TiC_{0.63}$ but is somewhat lower for TiC. The parabolic law does not apply strictly. The rate found for pure titanium is somewhat greater than that found by Simnad, Spillners, and Katz (20) for both pure titanium and oxygen-saturated titanium.

Oxidized $TiC_{0.63}$ samples showed no internal oxidation in spite of the porosity of the original sample.

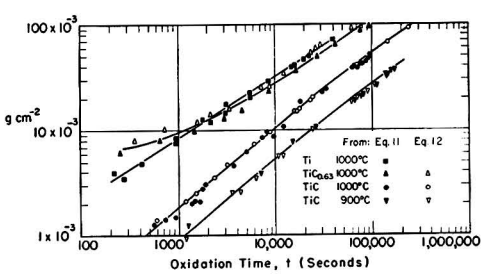

FIG. 4. Oxidation of titanium and titanium carbides

The structure of the scale on both titanium and titanium carbide was investigated by metallographic techniques and x-ray diffraction.

The only oxidation product was TiO_2, with the exception of one experiment in which pure titanium was oxidized for about one week and an intermediate layer of TiO was found. The TiO structure was ascertained by x-ray diffraction.

On titanium carbide oxidized for 24 hr at 1000°C, two conjugate layers were found microscopically. Both layers had the rutile structure. Using the polarizing microscope, it was seen that the outer layer was composed of large grains most of which extended all the way through it, whereas the inner layer consisted of much smaller grains and many pores. The layer structure was similar to that described by McDonald and Dravnicks (21) in their discussion of the "Zone of Metal Phase Consumption." The occurrence of a porous zone is not consistent with diffusion of oxygen ions only via vacancies in TiO_2. Chemical analysis of a portion of the outer layer without any visible TiC gave a value of 0.05% carbon. This is an indication that carbon may dissolve in TiO_2 and diffuse outward.

In an attempt to establish whether carbon escapes from the sample by solution in and diffusion through titanium dioxide, slices from a single crystal of rutile were packed in titanium carbide powder and heated in helium at 900° and 1000°C for two days and then were cleaned and analyzed for carbon. The crystals were reduced as was indicated by the change in color. The analysis did not reveal the presence of carbon in excess of that in a blank (0.005% carbon).

The mechanism of carbon transport across the oxide layer, therefore, remains open to question because diffusion in the form of CO or CO_2 is unlikely, nor has diffusion of carbon atoms been ascertained.

Oxidation of Some Hard Metals

Oxidation of a commercial hard metal consisting of titanium carbide bonded with 20% nickel gave results similar to those obtained for pure titanium carbide. Titanium and carbon are oxidized nonpreferentially, whereas nickel is left over in metallic form near the alloy-oxide interface. This indicates that the chemical potential of oxygen at the alloy-oxide interface is very low and the TiO_2 layer is essentially nonporous.

A commercial hard metal in which tantalum and niobium had been added to the carbide in order to improve the oxidation resistance also showed nonpreferential oxidation of titanium and carbon. After oxidation for 10,000 sec at 1000°C, the oxygen take-up per unit area was found to be four times less than that found for TiC. An alloy containing about the same amounts of the metallic elements without carbon showed a similar improvement of the oxidation resistance in comparison to pure titanium, presumably because of a lower concentration of oxygen ion vacancies in the TiO_2 layer due to the presence of Nb_2O_5 and Ta_2O_5.

As a whole, the presence of carbon seems to have a relatively minor effect on the oxidation characteristics of hard metals based on titanium carbide.

Conclusions

In this paper, an attempt has been made to show the large variety of possibilities which may occur when alloys containing carbon or carbides are oxidized, but detailed investigations have been deferred. In particular, further investigations are desirable in order to determine the effect of carbon concentration on the oxidation rate of alloys in which evolution of CO and CO_2 ruptures an oxide layer. Moreover, the mechanism of carbon migration through a TiO_2 layer needs clarification.

Note added in proof: The curves in Fig. 1 labeled $\Delta m_{ox}/A$ actually show the weight of nickel oxide formed per unit area, i.e., $4.67 \times \Delta m_{ox}/A$.

Manuscript received August 25, 1955. This paper was prepared for delivery before the Pittsburgh Meeting, October 9 to 13, 1955, and is based in part on a thesis submitted by W. W. Webb in partial fulfillment of the requirements for the D.Sc. degree from Massachusetts Institute of Technology.

Any discussion of this paper will appear in a Discussion Section to be published in the December 1956 Journal.

References

1. P. Schwarzkopf and R. Kieffer, "Refractory Hard Metals," Macmillan Co., New York (1953).
2. O. Kubaschewski and B. E. Hopkins, "Oxidation of Metals and Alloys," Academic Press, New York (1953).
3. W. W. Webb, J. T. Norton, and C. Wagner, *This Journal*, **103**, 107 (1956).
4. J. P. Coughlin, *U. S. Bur. Mines Bull.* 542 (1954).
5. O. Kubaschewski and O. von Goldbeck, *Z. Metallkunde*, **39**, 158 (1948);
   O. Kubaschewski and B. E. Hopkins, *loc. cit.*, p. 177.
6. W. J. Moore and J. K. Lee, *Trans. Faraday Soc.*, **48**, 916 (1952).
7. E. A. Gulbransen and K. F. Andrew, *This Journal*, **101**, 128 (1954).
8. J. J. Lander and A. L. Besch, *J. Appl. Phys.*, **23**, 1305 (1952).
9. E. A. Gulbransen and W. Hickman, *Pittsburgh Intern. Conf. Surface Reactions*, p. 222 Corrosion Publishing Co., Pittsburgh (1948).
10. W. A. Pennington, *Trans. Am. Soc. Metals*, **37**, 48 (1946).
11. W. Jost, "Diffusion in Solids, Liquids, Gases," pp. 69 ff., Academic Press, New York (1952).
12. R. Kieffer and F. Kölbl, *Z. anorg. u. allgem. Chem.*, **252**, 229 (1950).
13. R. S. Gurnick and W. M. Baldwin, Jr., *Trans. Am. Soc. Metals*, **42**, 308 (1950).
14. M. Isobe, *Sci. Repts. Res. Inst. Tohoku Univ.*, **3A**, 468 (1951).
15. R. Vogel and W. Döring, *Arch. Eisenhüttenw.*, **9**, 247 (1935).
16. K. Kuo and L. E. Persson, *J. Iron Steel Inst.*, **178**, 39 (1954).
17. P. Schwarzkopf and R. Kieffer, *loc. cit.*, p. 83.
18. P. Ehrlich, *Z. Elektrochem.*, **45**, 362 (1939).
19. E. S. Bumps, H. D. Kessler, and M. Hansen, *Trans. Am. Soc. Metals*, **45**, 1008 (1953).
20. M. Simnad, A. Spillners, and O. Katz, *J. Metals*, **7**, 645 (1955).
21. H. J. McDonald and J. Dravnieks, *This Journal*, **94**, 139 (1948).

Spectral Energy Distribution Curves of ZnS:Ag and ZnCdS:Ag after Thermal Vacuum Treatment

C. H. Bachman, M. L. Sawner, and Wm. Allen

Physics Department, Syracuse University, Syracuse, New York

Abstract

Liquid settled screens of ZnS:Ag and of ZnCdS:Ag of thickness comparable to those of cathode ray tubes were subjected to various temperatures in vacuum. The temperatures ranged from 300° to 800°C and exposure times from 5 to 30 min. Spectral energy distribution curves were then obtained for these phosphors under electron bombardment. Intensity changes, color shifts, and the appearance of new emission bands are noted. These seem to be related to the diffusion and evaporation rates of the phosphor components and the effects depend upon screen thickness as well as time and temperature of exposure.

Introduction

A major problem in the development of cathode ray tubes has been the appearance of blemishes on the luminescent screens due to the bombardment of the screens by ions in the supposedly pure electron beam. These "ion burns" were especially detrimental in obtaining lasting picture quality in television tubes and therefore much attention has been directed to the study of the nature and origin of ions in cathode ray tubes. This phase of the problem has been most recently discussed by Bachman, Hall, and Silberg (1). As a result of such studies, various means have been devised for trapping negative ions before they can strike the screens, and modern cathode ray tubes incorporate some device of this sort. Thus, most of the objectionable blemishes have been removed, although continued electron bombardment can also produce deterioration of the screens.

Although the cause of screen blemishes has been determined and at least partially removed, the actual mechanism for destruction of luminescent efficiency by the ions is unknown. Observations on ion burned screens indicate that the destruction is due to energy transferred from the

fast moving particles to the phosphor screen. Both positive and negative ions will produce a burn, and the degree of burn is roughly proportional to the beam intensity. The burns are usually neutral in color, or exhibit the same color as unburned phosphor but with reduced intensity; however, some have been observed to be violet or green. No correlation between such colors and the ions of any particular element is apparent. The amount of destruction of luminescence seems to be controlled in part also by the penetrating power of the particles, since electrons produce burns at a much slower rate than the more massive ions. Also, aluminum backed screens are less susceptible to ion burning, with burns due to heavier ions diminished more effectively than those due to the lighter ones. Such considerations lead to the hypothesis that ion burns might be due to a localized heating at the point of bombardment. Since phosphors are in general poor heat conductors, dissipated energy would be largely confined to the region near the point of bombardment. Thus it might be that high local "temperatures" are produced on or near the surfaces of the screens. As well as being dependent on the beam intensity, such local temperatures would also depend on the penetrating power of the particles, as determined by their energy and size.

Actual ion burns are difficult to analyze since only the surface portions of the thin screen are affected, and any tests are masked by the predominance of unburned phosphor. A new approach seemed necessary and, following the assumption that local temperatures at the point of ion bombardment could be duplicated on bulk material, the possibility of using thermal vacuum treatment as means of simulating ion burns has been investigated. Such treated materials can be obtained in sufficient quantity for analysis, and studies of their luminescent characteristics can be compared to actual ion burned samples to establish the validity of the approach. Early experiments of this sort showed that thermal vacuum treatment does produce permanent changes in both the color and intensity of luminescence not unlike those observed on ion burned screens. These experiments also established that the changes could not be due to contamination such as by copper. For example, effects were produced on the surface of a phosphor layer which was heated in vacuum by infrared focused on the surface through an infrared transmitting window. In other studies of nearly enclosed pellets of phosphor there occurred gradations in color of luminescence through the pellet, pointing to the importance of the diffusion and evaporation of the phosphor components as factors in thermal destruction. These preliminary experiments which will not be detailed here established that the phosphors could be changed by thermal vacuum treatment and the purpose of this paper is to present data describing such changes.

To gain more quantitative information about this thermal destruction, apparatus was constructed to measure the spectral energy distributions of treated phosphors under cathode ray excitation. Screens of about the standard cathode ray tube thickness were studied. Preliminary experiments of this sort, as well as the pellet study mentioned above, indicated that the screen thickness was an important factor, and must be considered as one of the variables.

On these typical screens the effect was predominantly surface only, as a result of the diffusion and evaporation. It is the authors' intent to look for any correlation between such screens and ion burned screens, but as yet no such correlation has been proven. The data presented are of interest in themselves since the conditions are to some extent encountered in commercial phosphor applications.

The following is then an account of the effects of thermal vacuum treatment on the luminescence of ZnS:Ag and ZnCdS:Ag as controlled by the time and temperature of the heat treatment and the thickness of the screen.

Experimental Procedure

Phosphor screens were prepared on Vycor slides, heated in a vacuum furnace, and finally spectral energy distributions were measured relative to untreated samples under cathode ray excitation. In all handling of phosphors great care was taken to insure that any changes in color or intensity depended only on the thermal treatment, and not on such external factors as contamination, nonuniform screens, or varying properties of the cathode ray tube during measurements.

The phosphors were settled in water on Vycor slides, each of which had an area of about 3 cm^2. These slides were placed on glass rod platforms in the bottom of glass beakers. From a stock suspension of 1 gram of phosphor in 100 ml of water, 10, 20, and 40 ml were added to three 100 ml beakers containing the slides, together with enough water to fill the beakers completely. After allowing the particles to settle for about 30 min, the water was drained off with a capillary tube siphon. Two screens were prepared

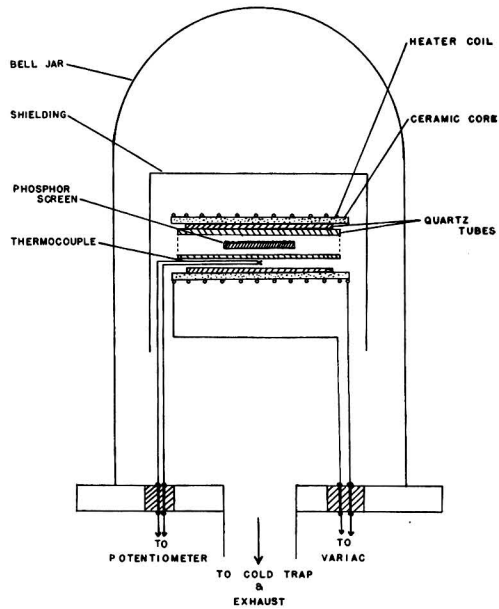

Fig. 1. Thermal vacuum treating apparatus

in each settling so that every treated screen could have an identical untreated standard for comparison. Samples prepared in this way had uniform screen densities of about 2.5 mg/cm², 4.5 mg/cm², and 9 mg/cm². (These will be denoted by I, II, and III in later parts of this paper.)

Thermal treatments were carried out in a bell jar vacuum system evacuated with a metal oil diffusion pump provided with a cold trap (see Fig. 1). Dry ice and acetone were used as the refrigerant. The furnace consisted of a nichrome heater coil surrounded by stainless steel shielding. To guard against any material being ejected from the walls of the furnace onto the sample, the sample was held in a quartz tube within the heater coil. An iron-constantan thermocouple was used for measuring the temperature within the coil. As it required from one to five minutes for the furnace to come to the desired temperature, time measurements were started when the sample reached this temperature. With only manual control the temperature could be maintained to within 10°C. At the end of the heating period, the system was allowed to cool to below 100°C before admitting air to the system. Some uncertainty is introduced here, since some changes in the phosphor constitution affecting luminescence might occur during the heating and cooling periods, which required different times for different temperatures.

The arrangement for measuring the spectral energy distribution of the treated samples is shown in Fig. 2. In brief, the system consisted of a demountable cathode ray tube in which any one of several samples could be viewed at will under irradiation by a diffuse, ion-free, electron beam accelerated to about 1000 v. Our preparation of the phosphor screens results in a surface effect. The ion burn is also a surface effect and the use of this low voltage accentuates the phenomenon by giving greater contrast.

At any time the treated sample could be replaced by its companion standard without varying the exciting electron beam. Thus it was possible to compare the intensity of a treated sample with a standard at any wave length under equivalent conditions of electron beam voltage and current density. The emitted light was analyzed by a prism spectrometer provided with a photo cell. Photocurrents were read with an RCA microammeter and corrections were made for the nonlinear response of the phototube. Such corrections were obtained by making observations

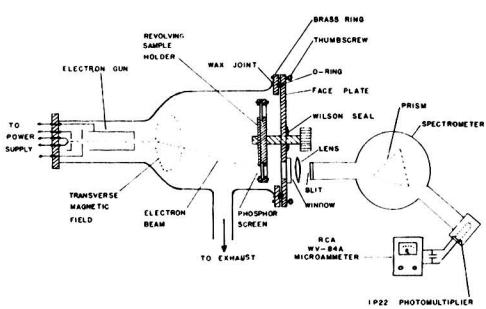

FIG. 2. Arrangement of apparatus for obtaining spectral energy data under electron bombardment.

on a ribbon tungsten filament of known temperature, and determining multiplying factors to fit the photocurrent vs. wave-length curve to the black body curve corrected for the emissivity of tungsten.

In running an energy curve, repeated reference to the intensity of some particular wave length was necessary to detect any small changes which might occur in the cathode ray tube or phototube circuits. Such repeated references at the peak intensity seldom showed variations of more than 3 or 4%. Photocurrent data were then corrected by assuming that these small changes in intensity varied linearly during the short time between references. The intensity standardization was made by observing the photocurrent at the peak wave length for an untreated sample, then immediately rotating the treated sample into view for a similar measurement. Several ratios of intensity of the treated screen to that of the standard at this wave length were averaged. Except at very low intensities (ratios less than 0.2) these ratios showed variations about the average of less than +5%. Calling the peak intensity of the standard unity, this average was then the relative intensity of the treated sample at this wave length. The rest of the distribution was then adjusted to be proportional to this relative intensity at the standardizing wave length. All intensity measurements are therefore relative to a similar untreated sample.

RESULTS

Spectral energy distribution (S.E.D.) curves from treated phosphors are shown in the accompanying illustrations. The intensity relative to the peak intensity of an untreated screen of like thickness is plotted vs. wave length, for screens of three different thicknesses for each temperature and time interval. The phosphors used in this study were furnished by the General Electric Company. The yellow component was 53% CdS and 47% ZnS. Both phosphors contained 0.05% Ag by weight and also 0.015% Cl, 0.05% Na, and 0.04% ZnO. Average particle size was 9 microns. The ZnCdS was, of course, hexagonal, and the ZnS was cubic with a trace of hexagonal form as determined by x-ray diffraction studies.

The effects of the heat treatment on the S.E.D. of ZnS:Ag is shown in the curves of Fig. 3. As can be seen from these the most prominent effect observed is the appearance of two new emission bands, one (5380 Å) appearing at 600°C, the other (5140 Å) appearing at 700°C. Treatments below 500°C have little effect on the intensity or color of luminescence. Samples run at 400°C (not shown in the figure) showed less than a 20% drop in intensity for all three screens. Also, higher temperatures do not cause as large a decrease in the intensity of the blue emission band. There was a slight indication of a more complex structure of the blue emission band, or a possible shift to a slightly longer wave length. This is not shown in the curves but, while points near the peaks usually did not deviate from a smooth rounded curve, slight deviations were noted in the peaks of the samples treated above 600°C.

The results for ZnCdS:Ag are shown in Fig. 4. This phosphor is more sensitive to the treatments, temperatures as low as 300°C lowering the intensity by as much as 50%.

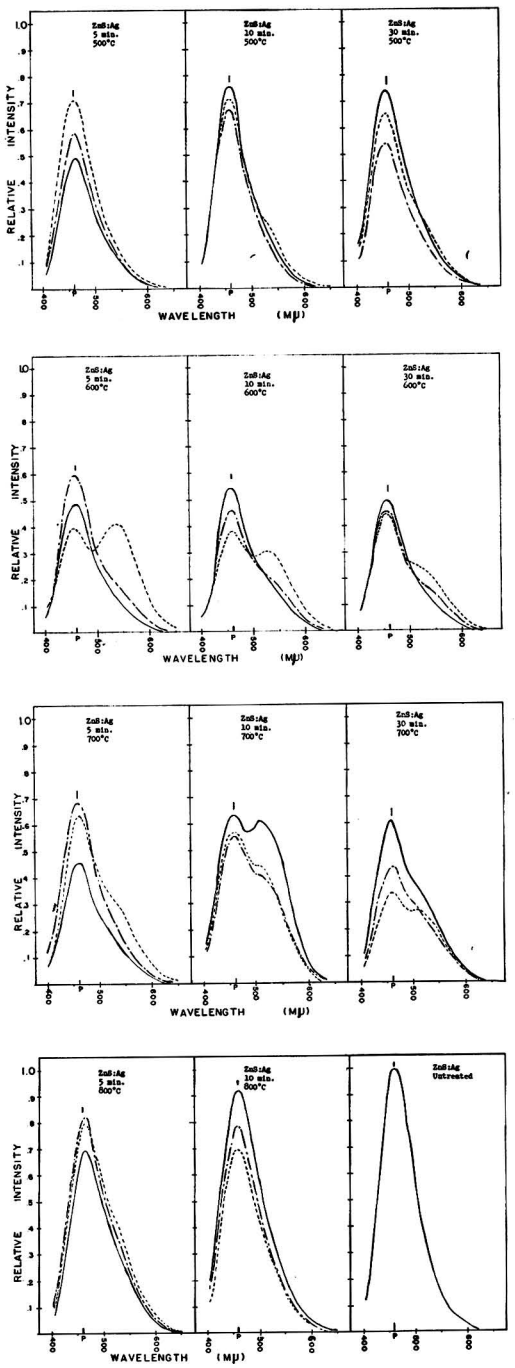

FIG. 3. Spectral energy distribution curves for ZnS:Ag after various thermal vacuum treatments. Dotted lines are for thin screens, broken lines for medium screens, and solid lines for thick screens (see text). "P" indicates peak wave length.

This is of practical interest since such temperatures are used in the industrial processing of cathode ray tubes. There is a tendency for the emission band to shift to shorter wave lengths. Visually, screens treated for 30 min at 700°C fluoresced grayish-blue with a very low intensity. Note that at 300° and 400°C, and also for the longer treatments at 500° and 600°C, the thin screens have a higher intensity than the medium. This might be an indication of a new emission band similar to those observed in treated ZnS:Ag. The long wave-length side of the emission band is broadened for these screens, and a minor emission band appears in the red portion for one of these samples. For both phosphors, material was observed deposited on the inner sur-

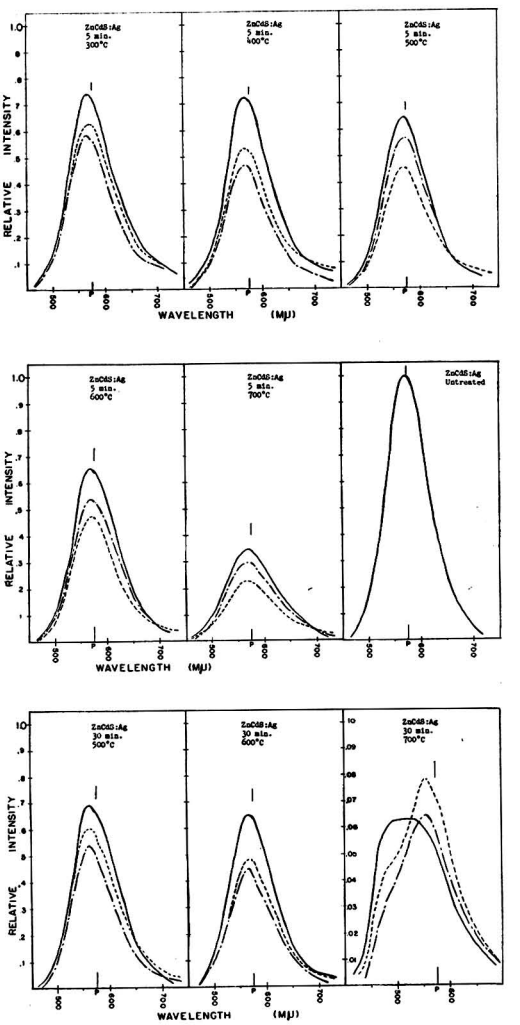

FIG. 4. Spectral energy distribution curves for ZnCdS:Ag after various thermal vacuum treatments. Dotted lines are for thin screens, broken lines for medium screens, and solid lines for thick screens (see text). "P" indicates peak wave length.

face of the quartz tube in which samples were treated, but the amount was insufficient for analysis.

Discussion

Various tests were conducted on treated ZnS:Ag phosphors in an effort to account for the appearance of the two green emission bands. To determine whether they were due to the formation of ZnO, treated samples were washed in acetic acid to dissolve any traces of a surface oxide layer. This affected neither of the bands. X-ray diffraction studies failed to show any observable changes in the crystal structure.

Recent work by Smit and Kroger (2) indicates that a green band peaking at 5140 Å may be produced by heating ZnS in a reducing atmosphere. This band is evidently due to an excess of zinc over the exact stoichiometric composition. It seems quite probable that the 5140 Å band observed in the authors' samples treated at 700°C is due to such an excess produced by evaporation of sulfur. However, a longer wave-length green band (5380 Å) was also observed, most prominent on thin screens treated at 600°C. This might indicate that excess zinc atoms can produce two slightly different emission bands depending on their position in the lattice. At the lower temperatures sulfur may be removed, leaving the zinc atoms more or less in their original positions. At the higher temperatures, zinc may volatilize appreciably, and upon cooling recrystallization might force any extra zinc atoms into interstitial positions. Therefore, one might attribute the longer wavelength green band to excess zinc at normal lattice sites with sulfur vacancies, and the other band to excess zinc atoms in interstitial positions.

Since the longer wave-length green band is attributed to defects in the normal crystal lattice, this emission might be expected to resemble that produced by a substitutional impurity, in contrast to the shorter band, which would be similar to foreign interstitial activation. Leverenz (3) points out that there is evidence indicating a rather clear distinction between the luminescences associated with substitutional and interstitial activation, and has listed the characteristics of phosphors usually associated with the two types of impurity center. Observations on the treated phosphors here seem to be in agreement with this distinction, on two accounts at least. The treated phosphor having the 5140 Å band was observed to have a rather long persistence, usually associated with interstitial activation. The optimum concentration for a substitutional activator is generally much greater than that of an interstitial one. As can be seen in the curves, the 5380 Å band was most prominent on thin screens, appearing on the thicker screens only after long treatment. At higher temperatures zinc may volatilize, thus lowering the effective concentration of the excess zinc activator. Any interstitial zinc produced upon cooling would have a low concentration, lowest on thick screens, where this band is most prominent.

Kroger's theory of self-activated ZnS attributes the blue emission band to zinc vacancies. The presence of silver stimulates the formation of these vacancies, and shifts the emission band to a slightly shorter wave length. Vaporization of sulfur would account for any lowering in the intensity of the blue emission band but, at higher temperatures where sulfur evaporation would be greater, this blue emission is less affected, indicating that a constructive process is also taking place. Assuming the correctness of Kroger's theory, and the above hypothesis concerning the green band, the various emission bands which might occur in a thermally treated ZnS:Ag phosphor are:

(*A*) The original Ag-activated band (4550 Å);

(*B*) A green band due to sulfur vacancies (5380 Å);

(*C*) A green band due to interstitial zinc (5140 Å);

(*D*) The blue emission of self-activated ZnS due to the zinc vacancies not influenced by association with Ag (4700 Å).

The results indicate that each of these emission bands may be produced. The formation of the green bands, and the lowering of intensity of the blue emission band may both be attributed to sulfur evaporation. At the higher temperatures, appreciable zinc evaporation will occur, and zinc vacancies may be produced in certain parts of the crystals. Such vacancies may be produced in the neighborhood of a Ag atom, and hence add to the original emission band, or they may be independently formed, having an emission band of a slightly longer wave length. Such occurrences would account for the apparently enhanced blue emission, and the complex structure of this band noted in the samples treated at the higher temperatures. The dependence of the formation or destruction of the various emission bands on time, temperature, and screen thickness must finally be accounted for by the different rates of evaporation and diffusion of the phosphor components.

The lowering of intensity of the yellow emission of ZnCdS:Ag must presumably be of the same character. However, since there is no apparent reinforcement of intensity at higher temperatures, evidently the rates of diffusion and evaporation are such that there is no tendency for cation vacancies to form. There is only a slight indication that anion vacancies, or interstitial Zn or Cd may produce a new luminescent band. Perhaps certain temperatures and times intermediate to those tested here might bring out these more distinctly. The general tendency for the emission band to shift to shorter wave lengths is due to the higher rate of evaporation of cadmium, this tending to revert the emission band to that of pure ZnS. The odd shaped S.E.D. curve for samples treated at 700°C for 30 min could be due to the presence of regions of the screens which have been predominantly freed of cadmium.

Several interesting observations were noted on treated screens. One of the samples having the 5140 Å band showed signs of deterioration under the short exposure to electrons during measurement. Grotheer has shown (4) that electron burning is most noticeable on phosphors having long persistence, and this is considered an indication that deterioration is enhanced when the luminescent centers are excited. Untreated ZnS:Ag is not electroluminescent, but treated samples with and without the green bands were found to exhibit a weak luminescence excited by an electric field. Samples having the 5140 Å band flashed brightly for a brief instant upon application of the field, indicating the presence of an effective electron trapping mechanism in this phosphor.

Conclusion

The original reason for studying thermal vacuum treatments of phosphors was an attempt to gain further insight into the destruction of luminescence by ion bombardment. Although the validity of the hypothesis that ion burns are due to high local "temperatures" at the point of ion impact has not been firmly established, these studies do indicate that the destruction produced thermally is caused by the ejection of material from the phosphor, such as might be expected to occur with ionic impact.

However, there seems to be one clear distinction between thermally induced destruction and ion burns, especially with the ZnS:Ag. With this phosphor, a constructive process appears at high temperatures, and thus the intensity of the samples was not lowered to less than 70%. Visual observations on ion burned samples of ZnS:Ag seem to indicate a much more pronounced lowering of intensity. If ion burns were completely like thermal burns, one would expect that under some conditions of ion bombardment this constructive process might take place and give rise to a permanent enhancement of luminescence. This has not been noted, and here the analogy between the two types of destruction may fail. The ion burn is an extremely localized affair, and the diffusion and evaporation picture must appear quite different from the case of the more evenly distributed thermal energy of heat treatments. Therefore, the chance of forming zinc vacancies without accompanying anion vacancies would be less, since the formation of these vacancies under thermal treatment is apparently closely connected with the rate of diffusion of zinc through the samples. The chance occurrence of zinc being ejected by the ions may, however, account for the occasional temporary increase of light output sometimes noted on ion bombarded screens.

In addition to possibly furthering the understanding of ion burn phenomena, thermal vacuum treatments such as described here might also be useful in studying the self-activation of other phosphors, and might also lead to the appearance of new emission bands and other luminescent properties such as the green bands and the electroluminescent effects noted here.

Manuscript received June 17, 1955. Portions of this work were sponsored by the office of Ordnance Research, U. S. Army.

Any discussion of this paper will appear in a Discussion Section to be published in the December 1956 Journal.

References

1. C. H. Bachman, G. L. Hall, and P. A. Silberg, *J. Appl. Phys.*, **24**, 427 (1953).
2. N. W. Smit and F. A. Kröger, *J. Opt. Soc. Amer.*, **39**, 661 (1949).
3. H. W. Leverenz, "Excitation and Emission Phenomena in Phosphors," Preparation and Characteristics of Solid Luminescent Materials, Cornell Symposium of Am. Phys. Soc., John Wiley & Sons, Inc., New York (1948).
4. W. Grotheer, *Z. Phys.*, **112**, 541 (1939).

Electrophotoluminescence Effects

Frank Matossi

U. S. Naval Ordnance Laboratory, White Oak, Maryland

and

Sol Nudelman

U. S. Naval Ordnance Laboratory, White Oak, Maryland and University of Maryland, College Park, Maryland

Abstract

Various electrophotoluminescence effects of phosphors continuously excited by ultraviolet radiation were studied for their dependence on field strength and frequency. These effects include luminescence stimulations at application and removal of alternating electric fields, quenching, and a periodic fluctuation of luminescence (ripple) during the field application. For some electroluminescent phosphors, the gradual transition from the quenching ripple to the electroluminescence brightness wave was observed, indicating that the brightness waves and the ripple patterns are produced by independent processes. The observations are discussed in the light of previous theoretical considerations.

Introduction

If electroluminescent or nonelectroluminescent phosphors of the zinc-sulfide type are excited to luminescence by ultraviolet radiation (or by x-rays), the application of an alternating electric field modifies the luminescence. This modification, either during continuous excitation by radiation or during phosphorescence afterglow, is called, according to Destriau (1) "electrophotoluminescence." It is a complex phenomenon consisting of several partial effects (2–4), which are indicated in Fig. 1. During "field on," the intensity varies periodically with twice the frequency of the field. This "ripple" is superimposed on a stimulation

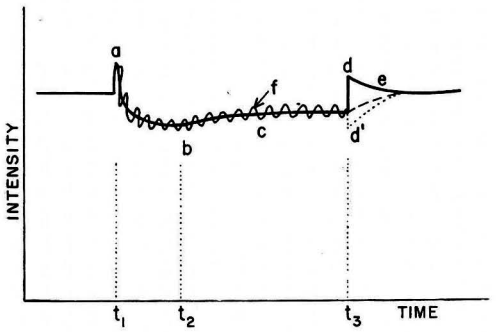

FIG. 1. Electrophotoluminescence, schematical. t_1, field on; t_3, field off; a, electric or first stimulation; b (at t_2), maximum quenching; c, intermediate recovery to steady quenching; d, cut-off or second stimulation (———), sometimes missing (-------) or replaced by d', cut-off quenching (·····); e, final recovery; f, ripple. Time scale distorted: $t_3 - t_2 \gg t_2 - t_1$.

at the instance of field application and on a quenching that exists during field application. The quenching is particularly strong just after the field is applied. The maximum of the first stimulation occurs after a few periods of the field; maximum quenching is reached after about $\frac{1}{10}$ sec; the intermediate recovery takes many seconds; the final recovery, a few seconds.

This paper is mainly concerned with a study of the frequency and field strength dependence of the stimulations, the quenching effect, and the ripple amplitudes of electrophotoluminescence. In addition, for electroluminescent phosphors, the transition from ripple pattern to brightness wave with increasing field strength will be described. It will be shown that the ripple pattern and the brightness wave have independent origins.

Experimental Procedure

Twenty-eight ZnS-phosphors of cubic or hexagonal structure, made with or without flux, and with a variety of activators were examined in this investigation. For detailed quantitative work, only about half of this number was used. These include commercial products such as the electroluminescent phosphors Q62-2666 (du Pont de Nemours & Co., Wilmington, Del.), 3-310 (General Electric Co., Cleveland, Ohio), and Sylvania Panelescent Lamps (Sylvania Electric Products Inc., Salem, Mass.), and the nonelectroluminescent phosphors 1402 (du Pont), 2301 (New Jersey Zinc Co., Palmerton, Pa.), and MB-19 (Stroblite Co., New York, N. Y.). Among the noncommercial phosphors, the most extensively used corresponded to electroluminescent Sylvania type of phosphors. They were prepared in this Laboratory according to the methods of Homer and co-workers (5) and include a green phosphor (No. 23), a blue-green (No. 22), and a yellow phosphor (No. 11).

All phosphors were embedded in parlodium (except the Sylvania Lamps, which were used as delivered) and investigated in cells of the usual construction (3), with about 5 cm² area and about 0.2 mm thickness of the phosphor layer. A d-c-operated argon lamp with a Wratten filter No. 18A transmitting from 2900 to 3900 Å served as the ultraviolet source. Other filters between the cell and the 1P21 photomultiplier separated the green and blue luminescence emission (Wratten No. 21, transmitting above 5300 Å, or Wratten No. 3 and Corning 5850, transmitting from 4300 to 4800 Å).

The output of the photomultiplier was observed either with an oscilloscope or with a vacuum tube voltmeter in an averaging circuit. The last method was used in particular for the measurements of the steady-state quenching, while oscilloscopic observations served for the measurement of the phenomena of short duration. Photographic records or direct readings on the screen were utilized for the oscilloscopic measurements.

The electric field was applied after the ultraviolet excited luminescence had reached its equilibrium value. Ultraviolet excitation was maintained continuously during field application. The applied field was obtained from sinusoidal generators together with power amplifiers. The output of these systems could be varied from zero to 500 v (rms) in the frequency range from 100 cps up to 10 kcps. At higher and lower frequencies the output voltage decreased appreciably. In a few instances, square wave fields from an appropriate generator were used. Except for the square wave fields, all potential differences refer to rms-values.

The measurements of the first stimulation were difficult at low frequencies. Below about 50 cps, they become very sensitive to the phase at which the field is applied to the phosphor. Since this was not regulated, measurements varied sometimes by as much as 25%. Other measurements were reproducible to better than 3%. At frequencies below a few kilocycles per second, the large ripple amplitude during the application of the field also interferes with accurate measurements of stimulation effects.

Results

All phosphors exhibit the two stimulations, the quenching, and the ripple. Frequency and field strength dependence of these effects, however, show notable quantitative differences for the various phosphors. These differences, however, did not show any systematic dependence on the method of preparation (kind of activator or flux) or on other luminescence properties such as time of afterglow or whether electroluminescent or not.

Stimulation.—The first stimulation always decreases with increasing frequency up to about 10 kcps, then either slowly increases or remains nearly constant. The typical behavior is shown in Fig. 2. The values at frequencies below 2 kcps are too high because the large ripple amplitude could not be separated, in these measurements, from the stimulation effect proper.

The cut-off stimulation consists of two components. A very sharp peak, not illustrated in Fig. 1, is followed by a tail ("final recovery") of long duration (Fig. 3). The tail has the shape of the solid or dashed curves at e in Fig. 1. The dashed curve is normally observed only at frequencies below several hundred cps. But for two phosphors, No. 11 and MB-19, this behavior was found at all frequencies. In these cases (Fig. 3B), the peaks were observable down to about 1000 cps, while usually (Fig. 3A) the peaks

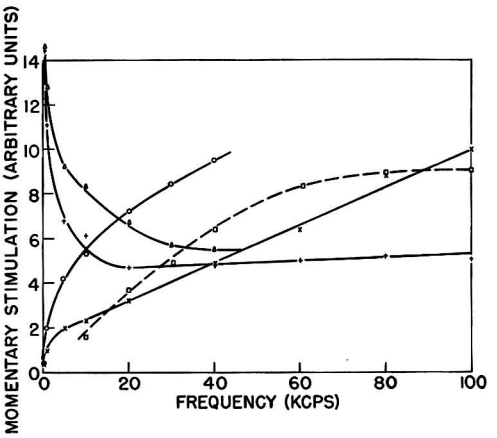

FIG. 2. Stimulation vs. frequency.

△ —— △ 1st stimulation, 105 v
+ —— + 1st stimulation, 53 v } phosphor
○ —— ○ 2nd stimulation, 105 v } 3-310
× —— × 2nd stimulation, 53 v
□ - - - □ 2nd stimulation, 40 v Green Sylvania Lamp

The experimental points for frequency zero correspond to 60 cps.

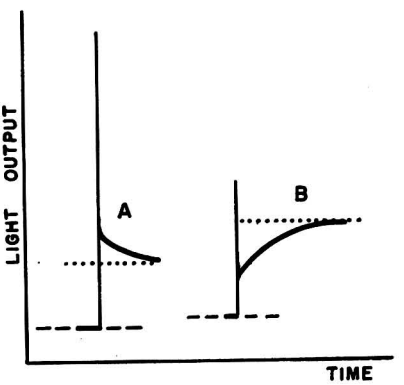

FIG. 3. Cut-off stimulation. A, Green Sylvania Lamp, 4 kcps; B, Phosphor MB-19, 9 kcps; - - - steady-state quenching; ··· output without field.

appeared only above 5 to 10 kcps. The peak intensity increases with frequency and for some phosphors (in particular for the Sylvania Lamps) reaches a saturation value. This saturation occurs sooner with higher applied voltage. The "tail intensity" also increases with frequency at the low frequencies but does not vary appreciably after the peaks can be observed. The curves shown in Fig. 2 for the second stimulation refer to the maximum peak height above the reference level (output without field). The large ripple amplitude at low frequencies prevented the use of the steady quenching level as reference level for the cut-off effects.

All phosphors showed the stimulation. In one case, the cut-off stimulation was reversed into a cut-off quenching (*d'* in Fig. 1). This happened with phosphor No. 22 at low frequencies. At other frequencies, this phosphor behaved like all others. Stimulation effects become stronger at higher field strengths, but the increase with field strength is not very pronounced.

Quenching.—The typical frequency dependence of the maximum quenching and of the steady-state quenching is illustrated in Fig. 4. The curves for phosphor 2301 represent the most generally observed type. A minimum of the quenching at a frequency of the order of 5 to 10 kcps, as shown for MB-19, is observed only for a few other phosphors, notably for No. 11 and 3-310. All these are cubic phosphors, although other cubic phosphors did not show this behavior. The electroluminescent green Sylvania phosphors produced even more complicated curves. It may be pointed out that Destriau (6) recently observed quenching in some fast-decaying phosphors even with d-c fields.

Larger fields increase the quenching with an almost linear dependence on field strength in most nonelectroluminescent phosphors. In electroluminescent phosphors, however, quenching begins to diminish at some field strength, since high fields will produce electroluminescence in these phosphors. The transition from quenching to electroluminescence will be described below.

For many phosphors, the quenching effect appears only in the green emission, although stimulation effects can be observed also in the blue. Phosphors with predominantly blue emission, however, showed quenching also in the blue region.

Ripple amplitude.—In Fig. 5, the frequency dependence of the amplitude of the ripple during the steady-state quenching and of the electroluminescence brightness waves are shown. The maximum of the ripple near 100 cps

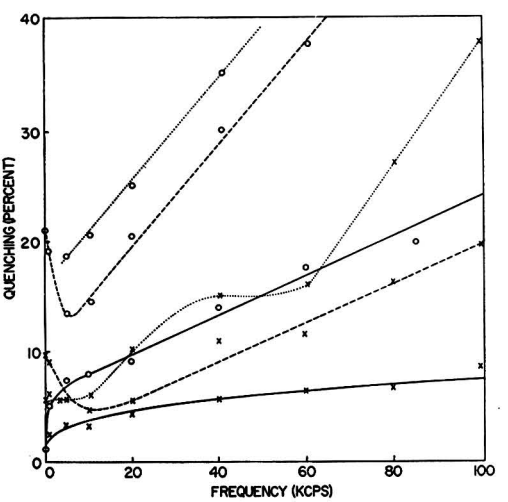

FIG. 4. Quenching vs. frequency (per cent of output without field). XXX Steady-state quenching; OOO maximum quenching; —— Phosphor 2301, green emission; - - - Phosphor MB-19, blue emission; ···· Green Sylvania Lamp, green emission. Frequency zero corresponds to 20 cps.

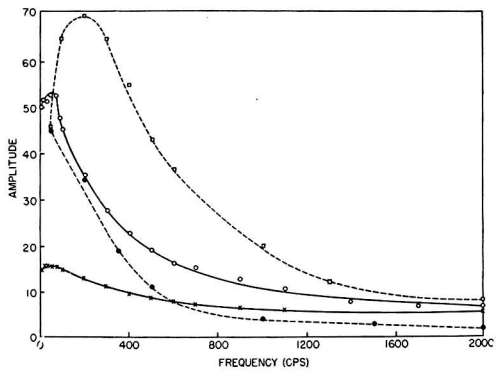

FIG. 5. Ripple and brightness wave amplitude vs. frequency.

——— Ripple amplitudes (per cent of output without field)
○○○ green band } of Sylvania Lamp
××× blue band }
– – – Brightness wave amplitude in arbitrary units (units different for green and blue band)
●●● green band } of phosphor 22
□□□ blue band }

occurs also in other phosphors. This behavior is quite different from that of the brightness wave amplitudes, where maxima occur above or below this frequency in the blue and green bands, respectively. Immediately after the field is applied, i.e., during the first stimulation and the decline to maximum quenching, the amplitudes of the ripple are, in general, much larger than in the steady state.

Transition from quenching to electroluminescence.— Fig. 6 presents a series of oscillograms obtained for increasing potential difference. They show two periods of the ripple during steady-state quenching. It can be seen that the quenching occurs actually only during part of the period and that the two peaks per period are of very unequal height. Increasing the voltage will at first increase the net quenching. Then, at a potential difference that would be just sufficient to produce electroluminescence in the same cell in the absence of ultraviolet radiation, a new peak begins to develop (marked by arrows in Fig. 6). This peak grows with increasing potential difference and finally takes over entirely. At the same time, the total light output increases until the quenching effect has disappeared and an electroluminescence brightness wave is obtained. It shows the usual phase shift of brightness waves, since it slightly precedes the field, whereas the ripple peaks during pure quenching have a phase shift in the opposite direction. The phase change from ripple to brightness wave is not a gradual shift, but it is the result of different relative intensities of two independent peaks whose individual phases remain constant.

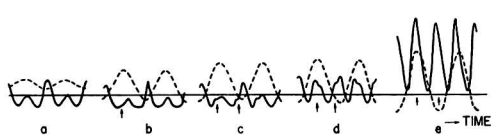

FIG. 6. Oscillograms for Green Sylvania Lamp excited by 60 cps field and ultraviolet. --- field; — ripple pattern. *a*, 26; *b*, 90; *c*, 110; *d*, 125; *e*, 160 volts rms. The continuous solid line: intensity without field. Arrows: brightness wave peaks.

There is, however, an important difference between the brightness waves of Fig. 6*e* and those obtained without any ultraviolet radiation. Only one peak per half-period appears in Fig. 6*e*, while in a brightness wave very often two are observed. Actually, an additional small peak appears slowly if the ultraviolet radiation is cut off. The shape of this normal brightness wave (without ultraviolet) is seen in Fig. 7, where the peaks are named B and C peaks (in phase and out of phase with the field, respectively) in accordance with the designation of similar peaks observed with nonsinusoidal fields (7). The time required for the C peaks to attain a constant height varies from several minutes to a quarter of an hour after removal of the radiation. By applying ultraviolet again, the additional peaks disappear at once. These effects have been observed for various other electroluminescent phosphors.

The ultraviolet radiation tends, for some electroluminescent phosphors, to unbalance markedly the light output for successive half-periods of the field. This was most pronounced in phosphor 3-310 (Fig. 8), a phosphor that did not exhibit C peaks with sinusoidal fields.

Fig. 9 shows a series of oscillograms similar to Fig. 6 but for square wave fields. Again there are marked quali-

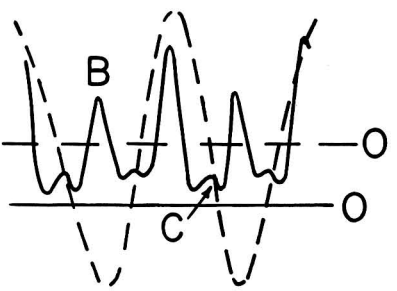

FIG. 7. Brightness wave without u.v., 60 cps, Green Sylvania Lamp. --- Field; — brightness wave.

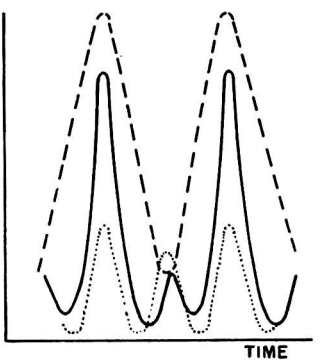

FIG. 8. Dissymmetry of brightness waves, 60 cps, phosphor 3-310. --- Field; — light output with u.v.; ···· light output without u.v.

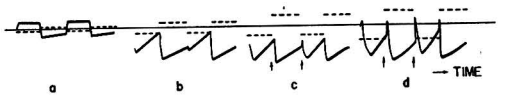

FIG. 9. Oscillograms for Green Sylvania Lamp excited by 60 cps square wave field and ultraviolet. --- Field; — ripple pattern. *a*, 5; *b*, 35; *c*, 53; *d*, 80 volts. Continuous solid line: intensity without field. Arrows: brightness wave peaks.

tative differences between the two half-periods. At low voltages, the one half-period does not seem to be affected at all, while in the other a maximum quenching is followed by a partial recovery. At a certain critical potential difference (again the voltage for which electroluminescence would begin to appear), spikes begin to develop. These spikes grow gradually with increasing field, and the ripple pattern transforms to the brightness wave of square wave excited electroluminescence (7).

DISCUSSION

Several theoretical aspects of electrophotoluminescence effects in a continuously ultraviolet-excited phosphor have been discussed previously (8). This treatment leaves sufficient freedom to accommodate the variety of behavior found for the different phosphors. The basic assumptions and conclusions may be briefly reviewed:

(*A*) The field may empty the traps; this is the main contribution to the first stimulation.

(*B*) The field induces radiationless transitions of conduction electrons; this is the main contribution to quenching.

(*C*) These two processes describe the behavior between t_1 and t_2 of Fig. 1. After this time, the induced radiationless transitions become relatively ineffective, the centers available to them becoming filled. These centers may be assumed to be near the surface, to which the electrons are drawn by the field. Continuous excitation by ultraviolet of the phosphor in this state of intermediate equilibrium, at the time of maximum quenching, yields a growth curve that reaches a final equilibrium different from that without field, equivalent to steady quenching. It is not necessary to assume actual recombinations for the quenching mechanism. If electrons are trapped at the surface, they may attract holes so that these holes cannot be trapped in activator levels, thus diminishing the possibility of radiative transitions of conduction electrons with empty activator levels. This process is mathematically equivalent to the field-induced radiationless transitions assumed above.

(*D*) Excess charges accumulate in the conduction band during field application; their release at field removal produces the cut-off stimulation. These excess charges may in part be due to polarization charges trapped near the surface and released only after final removal of the field. Evidence for such quasi-permanent polarization has recently been offered from quite different experiments (9). The observations shall be discussed in the light of these assumptions and conclusions.

As mentioned above, the intermediate recovery was interpreted (8) as a growth curve. But there is another possibility, viz., the existence of two quenching processes, a fast one with high efficiency and a slow one with low efficiency. The fast process is assumed to be the same as that described above, radiationless transitions of conduction electrons to empty centers or deflection of holes from centers by surface-trapped electrons. This process ceases to be effective after a certain time, i.e., after all surface traps have been filled, equivalent to maximum quenching. The slow process remains and is the only process acting in the steady-state quenching. The intermediate recovery then is the gradual transition to this state. This slow process might be the one assumed by Zalm and co-workers (10), i.e., emptying of hole traps with subsequent radiationless recombinations of the released holes with electrons in traps. It can be shown, by considerations similar to those used in (8), that the ratio of the time constants of the two processes is equal to the ratio of the number of conduction electrons to the number of empty centers, which was assumed to be small.

The slow component of the second stimulation (the final recovery) can readily be ascribed to the slow release of trapped polarization charges as mentioned above. The sharp overshoot, however, requires another source of excess electrons. Curie (11) has pointed out that the lifetime of the cloud of free electrons created by excitation of electroluminescence effects may be several 10^{-4} sec. (In Curie's paper, this time is referred to as the lifetime of an electron in the conduction band, but its real significance is with respect to the cloud and not to an individual electron.) This estimate may be assumed to be valid also for electrophotoluminescence effects. Therefore, at frequencies higher than a few kcps, some free electrons will be retained in the conduction band at every period of the field, with the result that, over many periods, an excess charge is accumulated that increases with frequency for a fixed time of observation. The dumping of these free excess electrons at "field off" should give the observed sharp peak. At frequencies much higher than the reciprocal of the lifetime of the cloud, which is also a measure for the build-up time, saturation may be expected, since the cloud will not be regenerated sufficiently fast.

The disappearance of the quenching and of the slow component of the cut-off stimulation at low frequencies is attributed (8) to the possible existence of currents. This would compensate any loss of electrons and also drain off any excess electrons, maintaining a constant charge density. The individual differences in the quenching behavior at low frequencies (Fig. 4) are, however, difficult to understand from a general viewpoint. Probably, individual surface properties come into play.

It should not be necessary to discuss the frequency dependence of the first stimulation independently since it is intimately connected with that of the quenching (8). If quenching increases with frequency, the first stimulation should decrease if the number of traps emptied per period is considered to be independent of frequency. But this last condition need not hold in all cases and, therefore, no rigorous correspondence between first stimulation and quenching can be expected.

The appearance of certain peaks in electroluminescent phosphors only in the absence of ultraviolet excitation can be ascribed to polarization and diffusion processes

(12). These C peaks, which begin to grow whenever the applied field decreases, were interpreted (7) as being due to polarization charges periodically accumulated by the field and released when the field diminishes. It is plausible that the ultraviolet radiation creates so many free electrons in the bulk of the phosphor particle that the released polarization charges cannot easily diffuse back to empty centers because the charge density gradient has become smaller. Thus, the additional peaks would not appear.

The frequency dependence of the ripple amplitude and of the brightness wave amplitude is due to different processes. While the brightness wave amplitudes are governed mainly by the excitation efficiency and the decay times of the luminescence processes (7), the ripple amplitude depends mainly on the ratio of the transition probabilities from the conduction band to either empty centers or traps. Theory predicts (8) a maximum of the ripple amplitudes at some critical frequency. But since it is doubtful whether the observed maximum (Fig. 5) is actually due to this effect rather than to polarization and possible barrier effects, no numerical evaluation of the probability ratio shall be tried.

Observations on the transition from quenching to electroluminescence also indicate the independent origin of ripple pattern and brightness wave. Both patterns superpose additively. The forward phase shift of the brightness wave is generally assumed to be due to the action of polarization charges (13), although the detailed mechanism of this effect is not yet completely understood since different methods of computing the polarization field lead to different results. The quenching effect is assumed to be due to a loss of free electrons available for luminescence transitions. This loss yields a phase shift in the direction opposite to that caused by polarization effects, as was pointed out by Curie (11) in a simplified consideration of the particle balance.

The assumptions about the cause of the quenching are also supported by the fact that quenching is observed, for many phosphors, in the green emission only. This is true in particular for the green Sylvania phosphor, where two separate emission bands with different excitation mechanisms are established (7, 14) and where only the green band involves conduction electrons. This argument is valid also for the quenching process proposed by Zalm (10) since the trapped electrons come from the conduction band.

No interpretation can yet be given of the unbalancing effect of the ultraviolet radiation. It may be connected with the experimental circumstance that only one side of the cell is exposed to radiation and that the cell is not symmetric with respect to the electrodes.

After submission of this paper for publication, similar work became known (15) in which unbalancing effects were observed under various circumstances. The authors want to point out that such effects do not contradict the model used here (8) since the shape of the ripple pattern is not derived from the model, but is put into the mathematical formalism.

Conclusion

The properties described and discussed in the previous sections, although demonstrated only in a few examples, are typical for all phosphors investigated quantitatively or tested qualitatively. In particular, the qualitative features of the frequency dependence of the electrophotoluminescence effects and the transition to electroluminescence are common to many phosphors, and they agree well with the general picture derived for these effects from other observations and from theoretical considerations. On the other hand, there is a wide spread in the quantitative aspects. Any speculation about the individual differences would be premature. The general properties and their interpretation seem, however, to be well established.

Acknowledgment

The authors thank Dr. J. F. Waymouth, Sylvania Electric Products Inc., for information about the Sylvania panels and Dr. E. Meschter, du Pont de Nemours and Co., for providing two electroluminescent phosphors.

Manuscript received June 30, 1955. This paper was delivered before the Cincinnati Meeting, May 1 to 5, 1955, and is based in part on a dissertation submitted by one of the authors (S. N.) to the University of Maryland in partial fulfillment of the requirements for the Ph.D. degree.

Any discussion of this paper will appear in a Discussion Section to be published in the December 1956 Journal.

References

1. G. Destriau, *Phil. Mag.*, **38**, 700, 880 (1947).
2. G. Destriau and J. Mattler, *J. Phys. radium*, **11**, 529 (1950).
3. F. Matossi and S. Nudelman, *Phys. Rev.*, **89**, 660 (1953).
4. K. W. Olson, *ibid.*, **92**, 1323 (1953).
5. H. H. Homer, R. H. Rulon, and K. H. Butler, *This Journal*, **100**, 566 (1953).
6. G. Destriau, *J. Appl. Phys.*, **25**, 67 (1954).
7. S. Nudelman and F. Matossi, *This Journal*, **101**, 546 (1954).
8. F. Matossi, *Phys. Rev.*, **94**, 1151 (1954).
9. J. F. Waymouth and F. Bitter, *ibid.*, **95**, 941 (1954).
10. P. Zalm, G. Diemer, and H. A. Klasens, *Philips Res. Rpts.*, **9**, 181 (1954).
11. D. Curie, *J. Phys. radium*, **14**, 672 (1953).
12. F. Matossi, *Phys. Rev.*, **98**, 434 (1955).
13. D. Curie, *J. Phys. radium*, **14**, 510 (1953).
14. L. Burns, *This Journal*, **100**, 572 (1953).
15. W. Low, I. T. Steinberger, and E. Alexander, *also*, R. E. Halsted, Unpublished papers presented at Symposium on Electroluminescence and Photoconduction in Inorganic Phosphors, Brooklyn Polytechnic Institute, Sept. 9, 1955.

Effect of Zone-Refining Variables on the Segregation of Impurities in Indium-Antimonide

T. C. HARMAN

Battelle Memorial Institute, Columbus, Ohio

ABSTRACT

Upon zone-refining indium-antimonide, ultimate concentrations of two slowly segregating impurities are approached. The most slowly segregating impurity, identified as tellurium, was found to be *n*-type which lowers the melting point of indium-antimonide. The second most slowly segregating impurity, identified as zinc, was shown to be *p*-type which raises the melting point of indium-antimonide. Both impurities originated in the indium. Electrorefining is an effective technique for removal of zinc from indium. Zone-refining is an effective technique for removal of tellurium from indium. There are no indications that deviations from stoichiometry prevent the attainment of extrinsic carrier concentrations below 10^{14}/cm^3 in indium-antimonide.

INTRODUCTION

At the present time, there is considerable interest in the semiconducting compound, indium antimonide. This interest may be grouped broadly under the categories constituting practical applications and those involving basic advances in present knowledge of solid-state phenomena.

Both the fabrication of devices and the carrying out of fundamental studies requires ultra-high purity material with impurity contents of the order of one part per hundred million or less. It is the purpose of this paper to discuss the nature of the problems involved in the preparation of high-purity InSb and to give an account of the solution of such problems.

EXPERIMENTAL

Preparation and Purification of the Compound

Indium-antimonide ingots were prepared by direct reaction of the elements in a Vycor container under a reduced pressure of pure, dry hydrogen. The compound was purified by the zone-melting technique (1). Initially, the ratio of zone length to ingot length was ½ and the rate of travel of the molten zone was 30 cm/hr. These quantities were gradually decreased until the zone length was 2.0–2.5 cm with a 20 cm ingot, and the rate of pass was 1 cm/hr. The final 10–15 zone-melt passes were made under these conditions.

During the course of the zone-refining passes, 1-cm lengths were cut from the impure ends and discarded. Also, specimens were removed from various portions of the ingot for electrical measurements. In addition, the ingot was probed periodically to determine the sign of the thermal emf at room temperature and at 80°K, to ascertain whether *p*- or *n*-type conduction predominated. The electrical measurements indicated that, initially, the entire ingot was *p*-type. However, upon subsequent zone passing, the region at the end of the ingot which was last to freeze became *n*-type. Subsequent passes increased the length of this *n*-type region as determined by electrical measurement at 80°K. After 30 passes, it extended over half the length of the ingot. After a total of 30 or more zone passes, thin slices cut perpendicular to the direction of travel of the molten zone were removed from the ingot. Hall coefficient and resistivity measurements at 80°K were carried out on specimens prepared from these slices. Carrier concentrations, type of conduction, and mobilities were determined from the electrical data. Analyses of the electrical properties as a function of distance along the ingot after a large number of zone passes, as well as information obtained during the course of zone-refining passes, indicated that the most slowly segregating impurity is *n*-type, and that it lowers the melting point of indium-antimonide. The second most slowly segregating impurity is *p*-type; it raises the melting point. Early in the investigation it was found that the final concentration of these two slowly segregating impurities in indium-antimonide depended on the purity of the indium used in the preparation of the compound. In the experiments to be described in this paper, the antimony was zone melted prior to use in preparations of indium-antimonide. However, recent measurements show that concentration of these troublesome impurities is much lower in high-purity antimony than it is in the indium.

Zinc Impurity in InSb

Fig. 1 shows how the purity of indium-antimonide, after 17 zone-melt passes, is affected by the purity of the indium. As indicated in the figure, indium-antimonide was prepared from as-received indium and indium further purified by zone refining and by electrorefining. Both electrorefining and zone refining of the indium are effective in removing the *p*-type impurity. The *p*-type impurity concentrates at the front of the InSb ingot during zone refining. Spectrographic analyses on the ends of an indium-antimonide ingot after five and nine zone passes showed that zinc segregates to the portion of the ingot first to crystallize, while copper, lead, tin, and nickel segregate to the portion of the ingot last to freeze. These results suggest that the unknown *p*-type impurity is zinc.

Confirmatory evidence was obtained by a zinc-doping experiment. An ingot of pure indium-antimonide (total impurity concentration less than 10^{16} at./cm^3) was doped with 2.6×10^{18} zinc at./cm^3. After five zone-leveling passes,

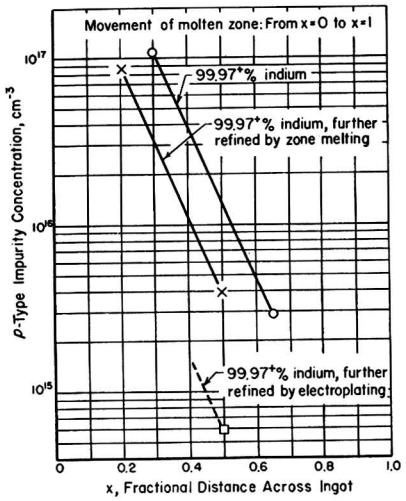

FIG. 1. Effect of indium purification on the concentration of the second most slowly segregating impurity found in InSb after 17 zone-melt passes.

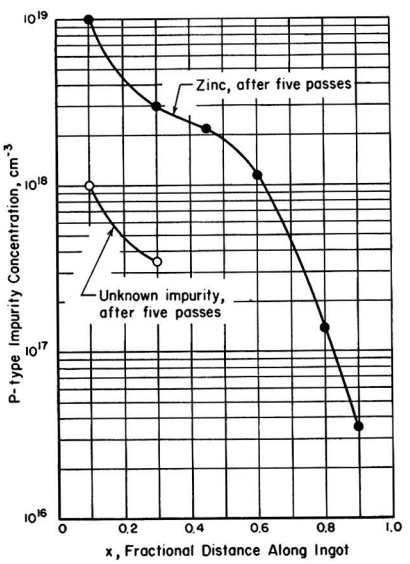

FIG. 2. Effect of five zone-melt passes on the distribution of zinc atoms in InSb.

the carrier concentration varied from 1.7×10^{18} cm^{-3} to 3.1×10^{18} cm^{-3}, indicating that each zinc atom had contributed one hole.

The distribution after five zone-melt passes is shown in Fig. 2. The lower curve gives the distribution of the slowly segregating p-type impurity found in indium-antimonide after five zone-melt passes. Thus, it is further verified that zinc is the slowly segregating p-type impurity in indium-antimonide and has a segregation coefficient greater than one.

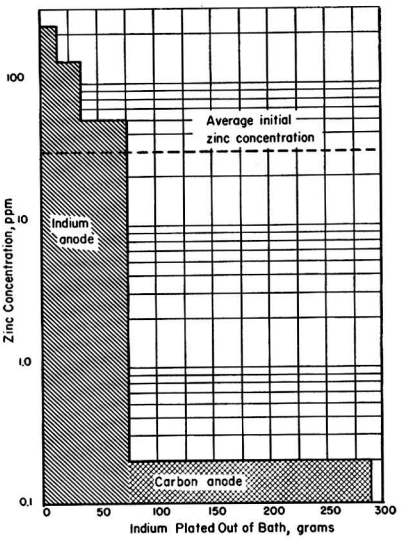

FIG. 3. Segregation of zinc from indium by electroplating.

Another important consequence of this experiment is that the information obtained can be used to determine the concentration of zinc in indium. This is done in the following manner. An indium-antimonide ingot prepared from indium with an unknown concentration of zinc and pure antimony is given five zone-melt passes. From a comparison of the concentration of the p-type impurity in this ingot with the concentration measured in the zinc-doped ingot, the zinc concentration in the indium can be calculated. Using this technique, it was found that the 99.97+ % purity indium obtained from the Indium Corporation of America has a zinc concentration of 20–30 ppm.

Results of studies of electrorefining processes for the reduction of the zinc impurity in the indium are shown in Fig. 3. The zinc concentration, as determined by the technique just described, is plotted as a function of the amount of material plated out of the bath. The electroplating cell consists of an indium anode, an indium fluoborate electrolyte, and a steel cathode upon which the indium is plated. For the first 75 g, additional indium is being dissolved in the electrolyte and zinc-rich indium is plated out of the bath. Then, the indium anode is replaced by a carbon anode and the pure indium remaining in the electrolyte is plated out.

n-Type Impurities in Insb

The most slowly segregating impurity found in indium-antimonide also was investigated. As discussed previously, it is n-type and segregates to the rear of the indium-antimonide ingot during zone melting. Fig. 4 shows the effect of the further purification of indium on the concentration of the n-type impurity in indium-antimonide. To minimize compensation effects caused by the p-type impurity, a large number of zone passes were given to move the zinc to the front of the ingot. The mobilities at 80°K of speci-

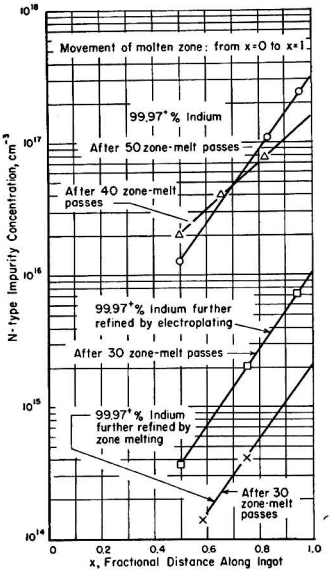

FIG. 4. Effect of indium purification on the concentration of the most slowly segregating impurity in InSb.

mens whose impurity concentrations are given in Fig. 4 varied from 500,000 cm²/volt-sec to 40,000 cm²/volt-sec in a manner consistent with increasing impurity concentration. This behavior is consistent with a negligible amount of compensation. Further evidence that the material is uncompensated is afforded by extrapolating to this region the *p*-type concentration gradient at the front of the ingot. It is then found that the concentration of zinc is at least an order of magnitude lower than the *n*-type impurity. In general, uncompensated *n*-type specimens of best purity are cut approximately 5 cm from the *p-n* junction in extensively zone-refined ingots of 20 cm length.

As shown by the upper curves, distribution of the *n*-type impurity after 40 zone-melt passes does not differ greatly from the distribution after 50 zone-melt passes. The larger number of zone passes continues to purify the compound, but the process becomes inefficient. Purification efficiency is greatly enhanced by removing the slowly segregating impurity from the indium before the compound is formed. An effective method for removing this impurity was found to be zone melting of the indium. The techniques used in this process are as follows. Approximately 1 lb indium was placed in a high-purity graphite boat 30 cm long. The boat was placed in a sealed Vycor tube under a reduced pressure of hydrogen. Zone lengths of 2.5–5 cm were maintained by means of a resistance heater. Five zone-melt passes were made at 7.5 cm/hr and five additional passes were made at 1 cm/hr. The front and rear sections of this ingot were used to prepare indium-antimonide ingots for extensive zone refining. Analysis of the measurements made on the extensively zone-refined indium-antimonide showed that the front section of the indium ingot contained approximately two orders of magnitude less of the slowly segregating *n*-type impurity than had been present in the rear section. In an effort to identify the unknown impurity, spectrographic analyses were carried out. Even though electrical data indicated the presence of 8 ppm of the unknown impurity, no impurity was detected. Therefore, the impurity is one whose spectrographic detection limit is at a rather high concentration. A possibility which was considered is selenium, since this element has a relatively high detection limit and is known to be an *n*-type impurity in InSb. However, activation analyses for selenium, which were obtained, did not confirm selenium to be the impurity in question.

The rates of segregation of various impurities in a material upon zone melting are usually widely different. Hence, by comparing the distribution of the unknown impurity found in indium-antimonide ingots after five zone passes with the distribution of various known impurities, it should be possible to identify the unknown material. It is known that the Group VI elements are *n*-type impurities in indium-antimonide and that they have high spectrographic detection limits. Work on the segregation coefficients (2) of various impurities in germanium has shown that the smaller atoms usually segregate the more slowly. Since sulfur is a small atom and a Group VI element, it was studied first. Fig. 5 compares the distribution of the sulfur impurity with the unknown impurity after five zone passes as a function of fractional distance along the ingot.

The information about the segregation of the unknown impurity was obtained by zone leveling rear sections of extensively zone-refined indium-antimonide ingots. The impurity concentrations of all other impurities except the unknown are estimated to be below 10^{15}/cm³. After zone leveling, a zone of 2.5 cm was passed along the 20-cm ingot a total of five times. The impurity distribution was then determined by Hall effect measurements at 80°K.

A similar technique was used for determining the distribution of the sulfur atoms. Indium-antimonide of 10^{15}/cm³ purity was doped with 1.2×10^{18}/cm³ sulfur atoms. After zone-leveling, the impurity concentration was

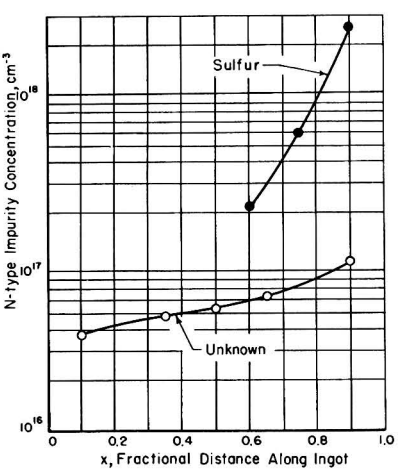

FIG. 5. Behavior of sulfur contrasted with that of the unknown *n*-type impurity in InSb after five zone-melt passes.

relatively uniform, varying from $7 \times 10^{17}/cm^3$ to $1.25 \times 10^{18}/cm^3$. Rate of pass, zone lengths, and ingot lengths were kept constant for the various dopings. By comparing the behavior of the two impurities, one can readily see that sulfur segregates much faster than does the unknown.

Fig. 6 shows the behavior of selenium contrasted to that of the unknown after five zone-melt passes. These results

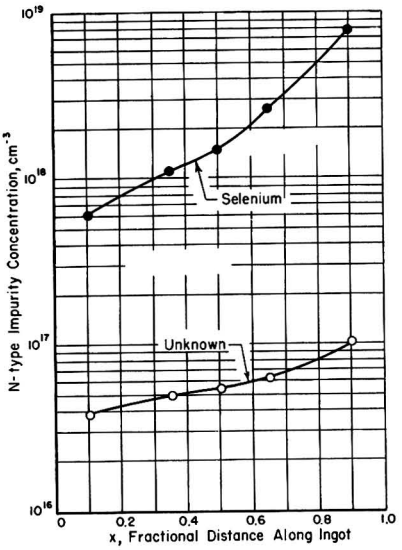

FIG. 6. Behavior of selenium contrasted with that of the unknown n-type impurity in InSb after five zone-melt passes.

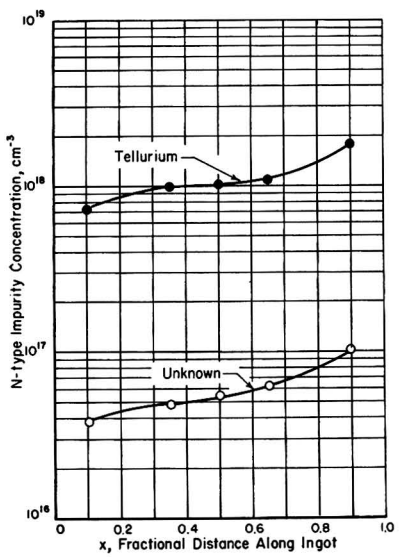

FIG. 7. Behavior of tellurium contrasted with that of the unknown n-type impurity in InSb after five zone-melt passes.

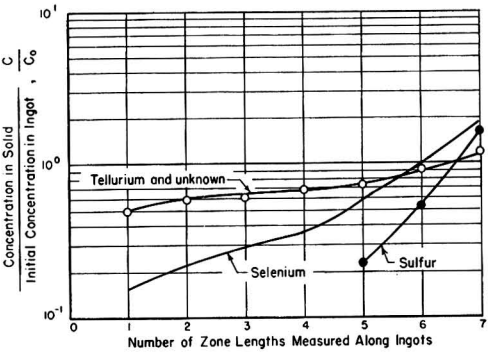

FIG. 8. Normalized values of the concentration along the ingot of some group VI impurities in InSb after five zone-melt passes.

indicate that selenium segregates more slowly than does sulfur but not so slowly as the unknown. This is rather surprising since, in germanium, the segregation coefficients deviate further from unity with increasing atomic number of impurities from Groups III and V of the periodic table (2). Confirmatory evidence that the situation is reversed for some Group VI impurities in indium-antimonide is shown in Fig. 7. Here it is seen that tellurium segregates more slowly than does selenium and that its rate of segregation is, in fact, identical to that of the unknown.

Fig. 8 summarizes the distributions of the principal Group VI impurities in indium-antimonide after five zone passes. Recently, Reiss (3) has developed equations for the redistribution of solute after zone passing. His equations for the case of a finite bar with a segregation coefficient close to unity describe fairly well the distribution of tellurium after five passes when a segregation coefficient of 0.8 is used. Since equations for the case of a finite bar with a segregation coefficient differing appreciably from unity have not been developed, effective segregation coefficients of the other impurities studied can only be roughly estimated. They are 10 for zinc, 0.5 for selenium, and 0.1 for sulfur.

SUMMARY AND CONCLUSIONS

The information obtained on the most slowly segregating p-type impurity found in indium-antimonide is summarized as follows:

1. The impurity is zinc.
2. It has a segregation coefficient greater than 1 in indium-antimonide.
3. It originates in the indium. The concentration in Indium Corporation of America's 99.97+ % purity is 20–30 ppm.
4. It has a segregation coefficient less than 1 in indium.
5. Electrorefining is an effective technique for removal of zinc from the indium.

The information obtained on the most slowly segregating n-type impurity found in InSb is summarized as follows:

1. The impurity is tellurium.

2. It has a segregation coefficient slightly less than 1 in indium-antimonide.

3. It originates in the indium. The concentration in 99.97+ % purity indium is about 1 ppm.

4. It has a segregation coefficient considerably less than 1 in indium.

5. Zone refining of the indium is an effective technique for removal from the indium.

In conclusion, the preceding work has shown that by purifying the elements as well as zone-refining the compound, it is possible to achieve uncompensated extrinsic carrier concentrations of below $10^{14}/cm^3$ in indium-antimonide. For purities in this range, there are no indications that deviations from stoichiometry offer a barrier to the attainment of this low extrinsic carrier concentration.

ACKNOWLEDGMENTS

The author is indebted to H. L. Goering, R. K. Willardson, and A. C. Beer for many valuable discussions, and to W. G. Hespenheide for carrying out the electroplating.

Manuscript received July 21, 1955. This paper was prepared for delivery before the Cincinnati Meeting, May 1 to 5, 1955. The work was supported in part by Wright Air Development Center, Air Research and Development Command, U. S. Air Force.

Any discussion of this paper will appear in a Discussion Section to be published in the December 1956 JOURNAL.

REFERENCES

1. W. G. PFANN, *J. Metals*, **4**, 747 (1952).
2. J. A. BURTON, E. D. KOLB, W. P. SLICHTER, AND J. D. STRUTHERS, *J. Chem. Phys.*, **21**, 1991 (1953).
3. H. REISS, *J. Metals*, **6**, 1053 (1954).

Electrolytic Stream Etching of Germaniun

MILES V. SULLIVAN AND JOHN H. EIGLER

Bell Telephone Laboratories, Inc., Murray Hill, New Jersey

ABSTRACT

A technique has been developed for the electrolytic etching of germanium in a controlled stream of 0.1% potassium hydroxide. By means of a special jig, the etching is restricted to the junction area without the aid of the usual masking waxes.

INTRODUCTION

In the processing of semiconductor materials for use in transistor devices, it is necessary to etch the surface in order to remove all the mechanical debris formed in cutting and shaping operations. This etching also removes any chemical contamination introduced during processing.

In the past, this etching has been done with very corrosive chemicals such as hydrofluoric acid, nitric acid, acetic acid, bromine, and hydrogen peroxide. Because these materials are so very corrosive, it has been necessary to protect solder joints, lead wires, and other portions of the device by masking them with an inert material. The application of this masking material is done under a microscope by a skilled operator and is both difficult and time consuming. The desire to eliminate this masking and the subsequent unmasking operation led the authors to develop a technique of stream electroetching which does not require masking. It will be seen, however, that other advantages have also accrued.

Electroetching of germanium which is submerged in an electrolyte has been previously described (1), but this method requires masking to protect the surfaces which are not to be etched. Jet electroetching of germanium was introduced by Tiley and Williams (2) and has been successfully applied to the fabrication of certain types of transistors, but has not been adapted for use on grown junctions. The technique to be described in this paper is another modification of electroetching in which a stream of electrolyte is allowed to flow over certain portions of the sample to be etched but is restrained from wetting other portions by surface tension between the stream and a special etching jig.

APPARATUS AND PROCESS

Four principles in the process restrict the etching current to the desired areas of the device. First, the use of an electrolyte whose conductivity is lower than that of the material being etched assures one that the most intense etching takes place on those portions of the germanium which are the nearest to the cathode. And since the cathode can be positioned close to the *p-n* junction, one is then able to give the junctions the most intense etching. Second, the use of a close electrode spacing along with the low-conductivity electrolyte results in a rapid etching rate for those areas directly opposite the cathode. Third, the use of a shaped cathode aids considerably in giving a relatively uniform etch to that area of the germanium which is directly opposite the cathode. Fourth, the use of a restricted stream of etchant very definitely limits the etching to those areas which are wetted by the electrolyte.

These restrictions to the etching current permit one to control the etching pattern precisely enough to make it unnecessary to resort to masking in any of the applications of this technique. A convenient jig for maintaining a restricted stream of electrolyte around a typical junction bar is a hairpin-shaped piece of platinum wire (see Fig. 1). The electrolyte which is gravity fed from a nozzle above the hairpin is constrained by surface tension to flow between

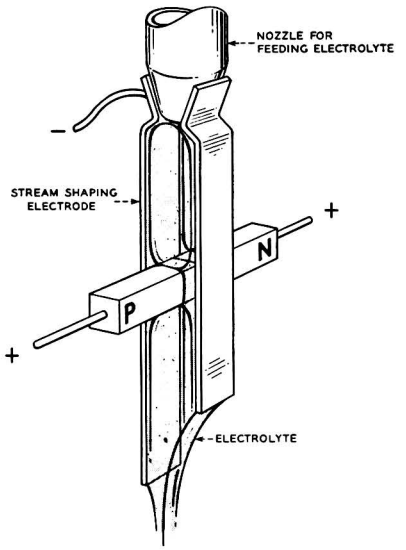

FIG. 1. Stream electrolytic etching a p-n junction

the legs of the hairpin. The germanium bar is brought up from below and placed between and at right angles to the legs of the hairpin. The rate of flow of electrolyte is adjusted to maintain a flow over only that portion of the germanium bar which lies between the hairpin legs but not for any appreciable distance beyond. In this manner the leads which are connected to the ends of the germanium bar are not wetted.

Etching times and currents vary with the material being etched and its past history. With 0.1% potassium hydroxide as the electrolyte, the first etch after the usual mechanical shaping operation requires 1–2 min, whereas a cleanup etch after waxing and dewaxing requires only a few seconds. Etching current densities up to 15 amp/cm² have been employed although most of this work has been carried on at 1.5 amp/cm².

RESULTS

Starting with a p-n junction diode whose surface has been lapped with 600 carborundum, Fig. 2 shows that about 25 μ (0.025 mm) of damaged material[1] must be removed before a low saturation current is obtained on the diode. The subsequent decrease in current as more material is removed is the result of reducing the cross-sectional area. (Original cross section was 0.63 x 1.27 mm.)

Fig. 3 shows the appearance of the original surface of the diode (frame 0) and the effect of successive 1-min applications of electroetching. Note that the extremities of the bar are not etched.

In the processing of n-p-n grown junction triodes, the introduction of this technique in place of chemical etching

[1] This figure is in agreement with the depth of damage due to various mechanical surfacing treatments on germanium reported by T. M. Buck and F. S. McKim at the Semiconductor Symposium of The Electrochemical Society in May 1955.

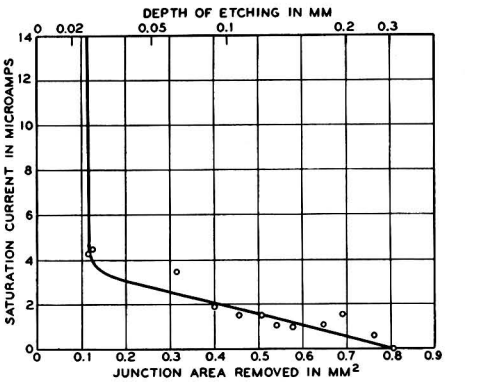

FIG. 2. Effect of electroetching on the saturation current of a p-n junction.

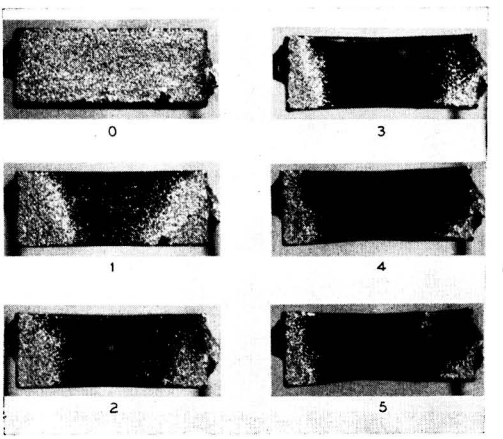

FIG. 3. P-n junction after successive 1-min electroetches.

has resulted in a considerable simplification of the fabrication. This includes the elimination of long-lifetime treatments[2] and their associated washes and masking operations and their subsequent removal with the appropriate organic solvents. This has resulted in an over-all savings of about 20% on the man hours required in the processing of such devices. In addition to the rather obvious economic advantage gained by cutting down the number of steps required, it has been found that a number of other advantages have accrued.

1. *Rate of etching can be controlled.* It is quite evident that the electroetching rate is under far better control than is realized in simple chemical etching. There is the further implication, however, that the process may be speeded up considerably. Although it is possible to perform the entire etching in a few seconds, from practical considerations, times of the order of one minute are usually employed.

2. *Contamination is minimized.* Since a continuously

[2] An anodic treatment in a suspension of hydrolyzed antimony trichloride.

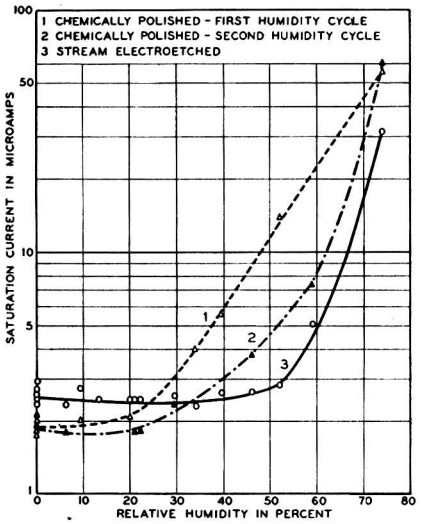

FIG. 4. Humidity stability of electroetched junctions. Curve 3 contains points from both the first and the second humidity cycle.

flowing system is used, contamination from previous etchings will be minimized. Further, since there is no masking, there will be no contamination by the masking material itself or by etchant which may be trapped or adsorbed by the masking.

3. *Etchant is inexpensive.* It is less than one-tenth the cost of chemical etchants usually employed. It should be pointed out that this cost differential will be even greater in large-scale production since it will then be necessary to neutralize the chemical etchants before disposing of them.

4. *Etchant is nonhazardous.* This appears as a pleasant change from the very hazardous chemical etches, the handling and disposal of which posed a considerable problem for very large-scale commercial usage.

5. *Etching can be done after the germanium has been mounted on its header.* When chemical etches were employed, it was customary to mask and etch at an early stage in the fabrication process since masking becomes more difficult and is more extensive as the device is further assembled. Now that the necessity for masking has been eliminated, the etching may be postponed to a later stage of fabrication, thus decreasing the chances for contamination and simplifying the precautions necessary during the early processing.

6. *A more stable surface is formed.* A number of recent tests have shown that a germanium surface which has been anodically etched in potassium hydroxide is more desirable than the chemically etched surface. For example, the electroetched grown junctions maintain their low reverse current even when exposed to a relative humidity of 50% (see Fig. 4). Under these same conditions, chemically etched junctions show over a 100% change in reverse current. Each point in Fig. 4 is the average of six junctions and the data were taken after at least 24 hr in the indicated humidity. Also, electroetched surfaces have low surface recombination rates, in fact, lower than has been reported for many of the other usual chemical etches (3, 4). And last, the spread in electrical characteristics has been noticeably less on electrolytically etched surfaces than on chemically etched surfaces.

Because of the very interesting properties displayed by these surfaces, they have been examined (5) by electron diffraction techniques. These studies have shown that some of the germanium dioxide which is formed during the electrolysis remains on the surface of the germanium as a thin film. It is believed that this oxide film is responsible for some of the unusual properties of electroetched germanium. In fact, the different reaction of the chemically etched surface after the first humidity cycle in Fig. 4 may be attributed to the slow building of an oxide film on the surface.

Microscopic examination of the electroetched surface shows various types of etch pits, including those found at lattice dislocation centers (6). Although a certain degree of control over the appearance of these pits may be achieved in the etching process, the exercising of this type of control has very little influence on the electrical characteristics of the etched device.

A technique has been developed for the electrolytic etching of germanium in a controlled stream of electrolyte. The three main advantages of the process as compared to chemical etching are: (*a*) the product has been improved, presumably by virtue of the oxide film formed during the etching; (*b*) handling and treatment operations are simplified by eliminating the masking and unmasking operations; and (*c*) the safety conditions have been improved by eliminating hazardous chemicals.

Manuscript received August 15, 1955. This paper was prepared for delivery before the Chicago Meeting, May 2 to 6, 1954.

Any discussion of this paper will appear in a Discussion Section to be published in the December 1956 JOURNAL.

REFERENCES

1. F. JIRSA, *Z. anorg. u. allgem. Chem.*, **268**, 84 (1952).
2. J. W. TILEY AND R. A. WILLIAMS. *Proc. I.R.E.*, **41**, 1706 (1953).
3. T. M. BUCK AND W. H. BRATTAIN, *This Journal*, **102**, 636 (1955).
4. J. P. MCKELVEY AND R. L. LONGINI. *J. Appl. Phys.*, **25**, 634 (1954).
5. Electron Diffraction Studies Performed at B.T.L. by Mrs. M. H. Read.
6. F. L. VOGEL, W. G. PFANN, H. E. COREY, AND E. E. THOMAS, *Phys. Rev.*, **90**, No. 3, 489 (1952).

Thermodynamics of the Oxidation of Chromium

J. N. RAMSEY,[1] D. CAPLAN, AND A. A. BURR

Department of Metallurgical Engineering, Rensselaer Polytechnic Institute, Troy, New York

ABSTRACT

By a microbalance technique in which oxidized chromium sheet is heated in prepared H_2-H_2O atmospheres the dissociation pressure of Cr_2O_3 is determined over the temperature range 598°–1154°C. From these data are calculated the free energy and enthalpy of formation of Cr_2O_3.

INTRODUCTION

Excellent oxidation resistance and strength at elevated temperatures make chromium an attractive base metal for heat-resistant alloys. Unfortunately, poor formability and extreme brittleness at room temperature have thus far hindered commercial development. Investigations now in progress at several laboratories and some recent publications (1–4) indicate that ductile chromium-base alloys can be produced provided that the impurity level is reduced to a sufficiently low value. Oxygen is known to embrittle the other body-centered cubic, high-melting metals, iron, molybdenum, and tungsten, and it is believed that it may also raise the ductile-to-brittle transition temperature of chromium. For this reason an investigation of the chromium-oxygen system was undertaken. A survey of the literature on the dissociation pressure of Cr_2O_3 revealed a considerable spread between the data of the various investigators. With the availability of high grade chromium sheet, experimental work was undertaken to check existing data. This paper describes the simple and direct experimental technique which was used.

The thermodynamics of the chromium-oxygen system may be arrived at either by determining experimentally the atmosphere which is in equilibrium with metal and oxide at various temperatures, or by calculating from tabulated entropy and heat capacity data (5, 6, 7) for oxygen, chromium, and chromium oxide along with the heat or free energy of formation of the oxide at one temperature. Results of such calculations are usually expressed by an equation having the form

$$\Delta F^\circ_T = \Delta Ho + aT \ln T + bT^2 + cT^{-1} + IT \qquad (I)$$

which expresses the standard state free energy change for the oxidation reaction as a function of temperature and constants related to entropy and heat content data. This free energy change is related to the equilibrium constant, K, by the expression

$$\Delta F^\circ_T = -RT \ln K \qquad (II)$$

Hence, for the reaction

$$2Cr + \tfrac{3}{2} O_2 = Cr_2O_3 \qquad (III)$$

$$\Delta F^\circ_T = -RT \ln \frac{1}{P^{\frac{3}{2}}_{O_2}} = RT \ln P^{\frac{3}{2}}_{O_2} \qquad (IV)$$

which by combination with equation (I) allows the calculation at any temperature of P_{O_2}, the equilibrium dissociation pressure of the oxide.

Such treatments have been described, notably by Maier (8), Thompson (9), Ellingham (10), Lustman (11), Richardson and Jeffes (12), Ward, Ray, and Herres (13), Smithells (14), Brewer (15), and Coughlin (16). The calculated curves of four of these investigators are drawn in on Fig. 1 and show a considerable variation. The most recent (16) is considered to embody the most accurate thermodynamic data, including a new determination of the heat of formation of Cr_2O_3 (17).

There have been several experimental determinations of the dissociation pressure of chromium oxide (18–23). Wartenberg and Aoyama (18) heated polished chromium at 600°–1400°C in a stream of hydrogen containing known small amounts of water vapor and estimated the equilibrium temperature for dissociation by the appearance and disappearance of temper colors on the specimen. Granat (20) passed dry hydrogen slowly through hot Cr_2O_3 at 1000°–1500°C and determined the H_2O content of the emerging gas. Grube and Flad (21, 22) passed hydrogen of known moisture content over Cr_2O_3 powder, part of which had previously been reduced to metal. Over the range 780°–1300°C equilibrium temperatures were obtained by detecting the temperature at which the powder

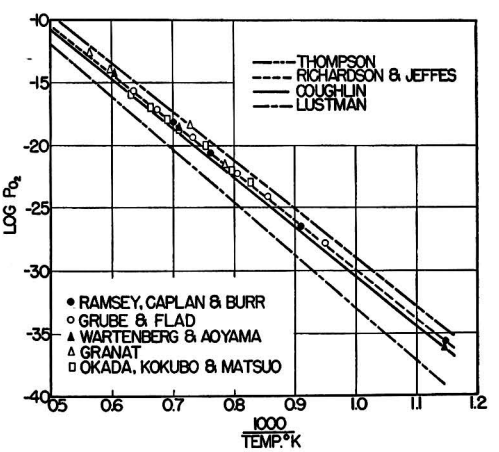

FIG. 1. Calculated and experimental data for the equilibrium dissociation pressure of Cr_2O_3.

[1] Present address: Massachusetts Institute of Technology, Cambridge, Mass.

neither gained nor lost weight while in a particular atmosphere. Okada, Kokubo, and Matsuo (23) used a similar constant weight technique to determine the equilibrium temperatures from 939° to 1310°C.

In the present work the equilibrium temperature is determined by detecting with a microbalance the point at which oxide-coated specimens begin to lose weight.

Experimental

The chromium used for the experiments was in the form of sheet which had been prepared by sheath rolling and finished by a pass or two in air at about 500°C. The following impurity contents were determined by semi-quantitative spectrographic analysis: Al 0.005, Mg 0.005, Ti 0.01, Zr < 0.001, Si 0.001, Fe 0.005, Ni 0.001, Mo < 0.001, Mn 0.001, Pb 0.005, Cu 0.005%. The specimen measured 0.012 x 0.6 x 1.2 in. and weighed approximately 1.0 g. Before each run it was heated in oxygen to form a surface layer of chromium oxide.

Fig. 2 is a schematic diagram of the apparatus used in the determination of the dissociation pressure. The oxidized sample of chromium sheet was attached to the beam of a quartz microbalance by a fine tungsten wire and hung in the vertical tube furnace. A plastic housing around the microbalance protected it from air currents. Changes in weight were detected by observing with a microscope sighted on a reference point on the tungsten suspension wire.

Hydrogen of a constant and known moisture content was prepared by passing cylinder hydrogen over platinized asbestos at 425°C to convert oxygen to water, adding an excess of water vapor with a humidifier, and condensing out the excess in a constant temperature cold trap consisting of 25 ft of copper tubing coiled in a thermoregulated bath of refrigerant. Any desired H_2-H_2O ratio could be obtained by suitable adjustment of the cold trap temperature. To avoid pick-up of moisture or oxygen only glass, copper, and porcelain was used in the gas train.

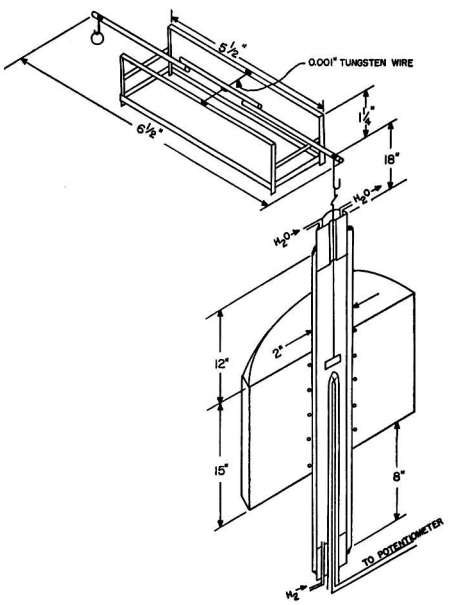

Fig. 2. Schematic diagram of microbalance and vertical tube furnace.

With the prepared atmosphere entering the vertical furnace tube at the bottom and the specimen hung just above the thermocouple used for measuring the temperature, the furnace was slowly heated and the temperature recorded at which the specimen first began to lose weight. Near the equilibrium temperature a heating rate of 2°C/min was used.

Results

The equilibrium temperatures for different settings of the cold trap temperature are shown in the first two columns of Table I. Using the following relationships, these data are converted to dissociation pressures or to standard free energies of formation: From the equation for the formation of water vapor

$$H_{2(g)} + \tfrac{1}{2}\, O_{2(g)} = H_2O_{(g)} \qquad (V)$$

one can write

$$2 \log K_{H_2O} = \frac{-2\Delta F^\circ_T}{4.576T}$$

From this relation, values of 2 log K_{H_2O} at the equilibrium dissociation temperatures are obtained by substituting the corresponding known values of ΔF°_T [e.g. reference (12)]. Since the P_{H_2} of the experiments is essentially one atmosphere, the term 2 log P_{H_2O}/P_{H_2} can be evaluated from the known vapor pressure of ice at the various cold trap temperatures (24). In this way the dissociation pressure is calculated and, through equation (IV), the standard state free energy change. Values so obtained are shown in the last two columns of Table I.

By combining these experimentally determined values of ΔF°_T with heat capacity and entropy data in the literature (5, 6), the standard heat of formation of Cr_2O_3 at the reference temperature 298°K can be calculated. One such procedure is that outlined by Darken and Gurry (25).

Thus for the reaction

$$\tfrac{2}{3}\, Cr + H_2O = \tfrac{1}{3}\, Cr_2O_3 + H_2 \qquad (VI)$$

values of the function $(F^\circ_T - H^\circ_{298})/T$ are calculated at even temperatures for the species Cr and Cr_2O_3 by expressing the function in the form $(H^\circ_T - H^\circ_{298})/T - (S_T - S_{298}) - S_{298}$. Values for these three terms are taken from Kelley's tables (5, 6). For the species H_2 and H_2O the function $(F^\circ_T - H^\circ_0)/T$ has already been tabulated (26). It is readily converted to the function above by the relationship $(F^\circ_T - H^\circ_{298})/T = (F^\circ_T - H^\circ_0)/T - (H^\circ_{298} - H^\circ_0)/T$.

By combining the $(F^\circ_T - H^\circ_{298})/T$ functions for the four reactants at even temperatures, values of $(\Delta F^\circ_T - \Delta H^\circ_{298})/T$ are obtained.[2] When this is done, interpolation to the

[2] These same values can be more simply obtained in another way since ΔF°_T data for H_2O and Cr_2O_3 are included in the tabulations of Coughlin (16). After subtracting ΔH°_{298} from the tabulated ΔF°_T values and dividing by T, combination of the resulting functions yields the $(\Delta F^\circ_T - \Delta H^\circ_{298})/T$ for the reaction.

TABLE I. *Experimental values for the oxidation of chromium to Cr_2O_3*

Cold trap temperature (°C)	Dissociation temperature (°C)	$\frac{P_{H_2O}}{P_{H_2}}$	P_{O_2} (atm)	ΔF° (kcal)
−74	598	1.38×10^{-6}	2.1×10^{-36}	−213.2
−49.5	826	4.41×10^{-5}	3.1×10^{-27}	−200.0
−28	1039	4.61×10^{-4}	2.4×10^{-21}	−185.7
−18	1154	1.23×10^{-3}	6.8×10^{-19}	−178.0

TABLE II. *Thermodynamics of the reaction* $\frac{2}{3}$ Cr + H_2O = $\frac{1}{3}$ Cr_2O_3 + H_2

Temp (°K)	$\frac{\Delta F^\circ_T - \Delta H^\circ_{298}}{T}$ (e.u.)	$K = \frac{P_{H_2}}{P_{H_2O}}$	$\frac{\Delta F^\circ_T}{T}$ (cal/deg)	ΔH°_{298} (cal)
871	9.71	7.25×10^5	−26.82	−31820
1099	9.20	2.27×10^4	−19.93	−32010
1312	8.82	2.17×10^3	−15.27	−31600
1427	8.64	8.13×10^2	−13.32	−31340

four experimental temperatures gives the values for $(\Delta F^\circ_T - \Delta H^\circ_{298})/T$ seen in the second column of Table II.

The equilibrium constant for reaction (VI), $K = P_{H_2}/P_{H_2O}$, which has been determined in the four experiments, permits the calculation of $\Delta F^\circ_T/T = -4.576 \log K$. This may now be combined with the values determined for the function $(\Delta F^\circ_T - \Delta H_{298})/T$ to give values for ΔH°_{298}. That is, $\Delta H_{298}/T = \Delta F^\circ_T/T - (\Delta F^\circ_T - \Delta H_{298})/T$. Table II shows the four values of ΔH_{298} obtained. The average value is $\Delta H_{298} = -31690$ cal.

Since the standard heat of formation at 298°K of $H_2O_{(g)}$ is −57,798 cal (16), addition of equations (V) and (VI) gives

$$\tfrac{2}{3}\ Cr + \tfrac{1}{2}\ O_2 = \tfrac{1}{3}\ Cr_2O_3 \qquad \Delta H^\circ_{298} = -89490 \text{ cal}$$

That is, the standard heat of formation of Cr_2O_3 at 298°K [equation (III)] is −268,500 cal.

Discussion

As can be seen from Fig. 1 the results of this research and of most of the prior work when plotted on the coordinates logarithm of the dissociation pressure and reciprocal of the absolute temperature lie nicely along a straight line nearly coincident with the calculated curve of Richardson and Jeffes (12). This curve is based on the equation

$$2Cr + \tfrac{3}{2}\ O_2 = Cr_2O_3;\ \Delta F^\circ_{298-1868} = -267{,}750 + 62.10T$$

which embodies the Roth and Wolf (27) determination of $\Delta H^\circ_{298} = -268.9$ kcal. It might have been expected that the theoretical curve of Coughlin (16) would most closely describe the experimentally determined values but, as the graph shows, values of the dissociation pressure read from the Coughlin curve would be slightly different from the experimental data and, from the Lustman or Thompson curve, more different still. The Coughlin curve, for the same reaction as above, is based on the equation

$$\Delta F^\circ_{298-1823} = -274{,}670 - 14.07T \log T + 2.01 \times 10^{-3} T^2 + 0.69 \times 10^5 T^{-1} + 105.65T$$

which incorporates a recent determination by Mah (17) of $\Delta H^\circ_{298} = -272.7$ kcal.

Coughlin (16) has combined this experimentally determined ΔH°_{298} with heat capacity and entropy data to calculate ΔF°_T and ΔH°_T. In the present investigation, an experimental determination of K and hence of ΔF°_T has been combined with the same heat capacity and entropy data to yield ΔH°_{298}. This value (−268.5 kcal) is slightly less negative than that given by Mah (−272.7 kcal). The difference probably lies within the combined experimental uncertainty of both values. A possible source of error in the present measurements is thermal separation in the H_2-H_2O atmosphere, although it is believed this has been minimized by arranging to have the uniform hot zone in the vertical tube furnace long relative to the length of the specimen. In this way a steady state should become established such that the gas composition around the specimen is that dictated by the cold trap temperature. The fact that the presently determined value for ΔH°_{298} checks the Roth and Wolf (27) value within 0.5 kcal probably does not lend support to either of these relative to the Mah value of −272.7 kcal.

Conclusions

1. The dissociation pressure of Cr_2O_3 is obtained as a function of temperature in the range 598°–1154°C from which is calculated the standard free energy change for the reaction

$$2Cr + \tfrac{3}{2}\ O_2 = Cr_2O_3$$

2. The average value for the standard state heat of formation at 298°K of Cr_2O_3 calculated from the above is $\Delta H_{298} = -268.5$ kcal.

3. Of several calculated equations in the literature for the free energy of formation of Cr_2O_3 as a function of temperature, the one which best fits the experimentally determined data both of the present research and of much of the prior work over the temperature range 600°–1500°C is that due to Richardson and Jeffes:

$$\Delta F^\circ_T = -267{,}750 + 62.10T$$

Acknowledgment

The authors wish to express their appreciation to Mr. R. W. Loofbourow of Utica Drop Forge and Tool Corporation for furnishing the spectrographic analysis, and to the United States Bureau of Mines, Albany, Oregon, for supplying the chromium sheet.

The work was done under Ordnance Contract No. DA-30-115-ORD-324. The authors are grateful to Watertown Arsenal and the Ordnance Corps for permission to publish.

Manuscript received March 31, 1955. This paper was prepared for delivery before the Cincinnati Meeting, May 1 to 5, 1955.

Any discussion of this paper will appear in a Discussion Section to be published in the December 1956 Journal.

References

1. A. H. Sully, E. A. Brandes, and K. W. Mitchell, *J. Inst. Metals*, **81**, 585 (1953).
2. H. L. Wain, F. Henderson, and S. T. M. Johnstone, *ibid.*, **83**, 133 (1954).

3. H. JOHANSEN AND G. ASAI, *This Journal*, **101**, 604 (1954).
4. H. B. GOODWIN, R. A. GILBERT, C. M. SCHWARTZ, AND C. T. GREENIDGE, *ibid.*, **100**, 152 (1953).
5. K. K. KELLEY, *Bur. Mines Bull. 476*, 241 pp (1949).
6. K. K. KELLEY, *Bur. Mines Bull. 477*, 147 pp (1950).
7. F. D. ROSSINI, D. D. WAGMAN, W. H. EVANS, S. LEVINE, AND I. JAFFE, *Natl. Bur. Standards Circ. 500* (1952).
8. C. G. MAIER, *Bur. Mines Bull. 436*, 109 pp (1942).
9. M. DEK. THOMPSON, "The Total and Free Energies of Formation of the Oxides of Thirty-Two Metals," Electrochem. Soc. 89 pp (1942).
10. H. J. T. ELLINGHAM, *J. Soc. Chem. Ind.*, **63**, 125 (1944).
11. B. LUSTMAN, *Metal Progr.*, **50**, 850 (Nov. 1946).
12. F. D. RICHARDSON AND J. H. E. JEFFES, *J. Iron Steel Inst.*, **160**, 261 (1948).
13. J. J. WARD, J. P. RAY, AND S. A. HERRES, Douglas Aircraft Co., Report R-108, 97 pp (1948).
14. C. J. SMITHELLS, "Metals Reference Book," Interscience Publishers, New York (1949).
15. L. BREWER, *Chem. Revs.*, **52**, 1 (1953).
16. J. P. COUGHLIN, *Bur. Mines Bull. 542*, 80 pp. (1954).
17. A. D. MAH, *J. Am. Chem. Soc.*, **76**, 3363 (1954).
18. H. v. WARTENBERG AND S. AOYAMA, *Z. Elektrochem.*, **33**, 144 (1927).
19. S. AOYAMA AND E. KANDA, *J. Chem. Soc. Japan*, **55**, 1174 (1934).
20. I. Y. GRANAT, *Metallurg*, **11**, No. 10, 34 (1936).
21. G. GRUBE AND M. FLAD, *Z. Elektrochem.*, **45**, 835 (1939).
22. G. GRUBE AND M. FLAD, *ibid.*, **48**, 377 (1942).
23. S. OKADA, S. KOKUBO, AND K. MATSUO, *J. Soc. Chem Ind. Japan*, **46**, 324 (1943).
24. International Critical Tables, Vol. III, p. 210, McGraw-Hill Book Co., New York (1928).
25. L. S. DARKEN AND R. W. GURRY, "Physical Chemistry of Metals," p. 231, McGraw-Hill Book Co., New York (1953).
26. National Bureau of Standards, Selected Values of Chemical Thermodynamic Properties. Series III.
27. W. A. ROTH AND W. WOLF, *Z. Elektrochem.*, **46**, 45 (1940)

Mathematical Studies on Galvanic Corrosion

V. Calculation of the Average Value of the Corrosion Current Parameter

J. T. WABER, JOHN MORRISSEY, AND JOHN RUTH

University of California, Los Alamos Scientific Laboratory, Los Alamos, New Mexico

ABSTRACT

Mathematical analysis for the mean current density has been completed for one general and two limiting ratios of electrode and corrodent dimensions with the same coplanar, juxtaposed arrangement of long, narrow electrodes as used previously. The resulting mathematical expressions were reduced to numerical evaluations, and many of these results have been graphically summarized in perspective illustrations.

The characteristic ratio ($\lambda/\mathfrak{L}$) was used to explain the behavior of all similar electrode systems and to emphasize that relative, not absolute, dimensions of the system establish its behavior. The theory and two experimental studies were in good agreement.

INTRODUCTION

Mixtures of phases are frequently present in commercial metals, and much of the gross corrosion behavior of such metals results from the action of local galvanic cells formed between constituents. Aside from the presence of impurity phases, certain commercial metals consist of two or more phases, and the percentage of the minor constituent in the matrix may approach 50%. Therefore, it is important to describe analytically the effect of increasing the percentage of one constituent on the average corrosion rate. In a two component phase diagram total corrosion should increase to a maximum with increase of the less noble phase, A, then decline as the fraction of B decreases so far that there are insufficient sites for cathodic reactions to occur without substantial polarization. Experience is in accord with this qualitative argument.

In many cases, interest does not lie in the detailed distribution of corrosion attack over the anodes, as described in previous papers (1–4), but in the average corrosion rate of one phase. For this reason attention was turned to the problem of calculating total and average values of the corrosion current parameter $C_a^*(x)$. This general problem can be investigated quantitatively assuming (*a*) the anodic and cathodic polarization parameters $\mathfrak{L}_a$ and $\mathfrak{L}_c$ are equal, and (*b*) the electrodes consist of long strips which are arranged alternately in a common plane. Avoidance of these limitations would introduce serious mathematical difficulties and would not contribute significantly more to an understanding of corrosion phenomena than does the present analysis.

The over-all behavior of the galvanic system can be characterized in terms of three parameters, each involving the ratio of lengths: a/c, $\mathfrak{L}/c$, and b/c (4). For purposes of describing commercial metals, a may be defined as the average radius of particles of the anodic phase, and c as half the average distance between centers of the anodic inclusions. However, the specific definitions of a and c which apply to the present analysis are: a is the half-width of the anodic strips, and c is half the distance between the repeated anodes. The quantity b is the thickness of the liquid electrolyte layer above the plane of the electrodes. In this paper both finite and infinite thicknesses are considered.

Mathematical Results

Boundary conditions.—The case of a finite thickness of the corrodent is physically equivalent to placing an insulator at the outer boundary of the liquid. This condition at the boundary can be expressed mathematically as

$$\left.\frac{\partial P^*}{\partial y}\right|_{y=b} = 0 \qquad [1]$$

An even, symmetrical, infinite, alternating array of electrodes juxtaposed and lying in a common plane is considered, as this arrangement is most pertinent to the practical case of local galvanic cells. At the center of the anode and cathode, the corrosion current must be continuous and have continuous derivatives. Thus, in terms of the geometrical relation of electrodes used before (1-4),

$$\left.\frac{\partial P^*}{\partial x}\right|_{x=0} = \left.\frac{\partial P^*}{\partial x}\right|_{x=c} = 0 \qquad [2]$$

The origin is taken at the center of one of the anodes. For polarized electrodes the following boundary condition (5) is used:

$$P^*(x, 0) - \mathfrak{L}\left.\frac{\partial P^*}{\partial y}\right|_{y=0} = E_a S_a(x) \qquad [3]$$

The definition of the anodic corrosion current parameter can be employed:

$$C_a^*(x) = \left(-\frac{2a}{E_a}\right)\left.\frac{\partial P^*}{\partial y}\right|_{y=0} \qquad (0 \le x < a) \quad [4]$$

This quantity is a dimensionless parameter since a and y are distances and E_a and P are voltages. Thus, equation [3] for the anodic side can be written:

$$P^*(x, 0) + \left(\frac{\mathfrak{L}E_a}{2a}\right) C_a^*(x) = E_a \qquad [5]$$

since the value for the step function $S_a(x)$ is unity in the anodic region.

Series solution of the problem.—A Fourier series which satisfies Laplace's equation and these several boundary conditions has been shown elsewhere (4) to be

$$P^*(x, y) = A_0^* + \sum_{n=1}^{\infty} A_n^* \cosh\left[\frac{n\pi}{c}(b - y)\right] \cos\left(\frac{n\pi x}{c}\right) \qquad [6]$$

where the coefficients are

$$A_0^* = E_a(a/c)$$

$$A_n^* = \frac{2E_a}{\pi n}\left[\frac{\sin\left(\frac{n\pi a}{c}\right)}{\cosh\left(\frac{n\pi b}{c}\right) + \left(\frac{n\pi\mathfrak{L}}{c}\right)\sinh\left(\frac{n\pi b}{c}\right)}\right] \qquad [7]$$

Derivation of mean parameter.—The mean value of the corrosion current parameter on the anode is obtained by integrating $C_a^*(x)$ over the interval

$$\overline{C_a^*} \equiv \frac{1}{a}\int_0^{a-0} C_a^*(x)\, dx \qquad [8]$$

Substituting $C_a^*(x)$ from either equation [4] or [5] gives the correct expression, but for practical reasons it is imperative to use [5]. The series obtained by differentiating P^* as in [4] depends on the denominator $[1 + (n\pi\mathfrak{L}/c) \tanh (n\pi b/c)]$ for convergence, whereas P^* is employed directly in [5] and the resulting series converges as $n[1 + (n\pi\mathfrak{L}/c) \tanh (n\pi b/c)]$, hence more rapidly. The integration step [8] raises the power of n in either denominator by one. Consequently, the series converges to a given accuracy with fewer terms if [5] is employed. Note that from equation [5]

$$C_a^*(x) = \frac{2a}{\mathfrak{L}}[1 - P^*(x, 0)/E_a] \qquad (0 \le x < a) \quad [9]$$

since $S_a(x)$ is unity in the anodic interval. By substitution, it is simple to show that

$$\overline{C_a^*} = \frac{2a}{\mathfrak{L}}\left(1 - \frac{a}{c}\right) - \frac{2c}{\mathfrak{L}\pi}\sum_{n=1}^{\infty} A_n^*\left(\frac{1}{n}\right) \cdot \cosh\left(\frac{n\pi b}{c}\right)\sin\left(\frac{n\pi a}{c}\right) \qquad [10]$$

The integration can be done termwise since the potential function has sufficient continuity to permit interchange of the order of summation and integration. Substitution from equation [7] leads to the series

$$\overline{C_a^*} = \frac{2a}{\mathfrak{L}}\left(1 - \frac{a}{c}\right) - \frac{4c}{\pi^2\mathfrak{L}}\sum_{n=1}^{\infty} \frac{\sin^2\left(\frac{n\pi a}{c}\right)}{n^2\left[1 + \left(\frac{n\pi\mathfrak{L}}{c}\right)\tanh\left(\frac{n\pi b}{c}\right)\right]} \qquad [11]$$

after dividing numerator and denominator of each term by the appropriate hyperbolic cosine.

An equivalent expression can be derived for an infinite liquid depth by replacing equations [6] and [7] with the appropriate Fourier series. The same expression can be obtained from [11] by noting that the hyperbolic tangent of an infinite argument is unity. Thus

$$\lim_{b\to\infty} \overline{C_a^*} = \frac{2a}{\mathfrak{L}}\left(1 - \frac{a}{c}\right) - \frac{4c}{\pi^2\mathfrak{L}}\sum_{n=1}^{\infty} \left[\frac{\sin\left(\frac{n\pi a}{c}\right)}{n}\right]^2 \left(1 + \frac{n\pi\mathfrak{L}}{c}\right)^{-1} \qquad [12]$$

Definition of the average parameter.—Expressions [11] and [12] are developed for the mean current distributed over the anode. In practice, this quantity is less useful than the average of the anodic current distributed over the entire electrode surface. That is, it is more common to employ the latter average when calculating polarization curves, etc. This is done since it is not always convenient to obtain independently the percentage of anodic phase.

Thus, Γ_a^* has been identified as the total or integrated corrosion current parameter,

$$\Gamma_a^* \equiv \int_0^{a-0} C_a^*(x)\, dx \qquad [13]$$

and the distinction between the mean and the average as Γ_a^*/a and Γ_a^*/c, respectively, has been made. It is clear then that

$$\frac{1}{c}\Gamma_a^* = \left(\frac{a}{c}\right)\overline{C_a^*} \qquad [14]$$

and the values of the more conventional and convenient average can be obtained easily from [11] and [12]. In the absence of external sources of current, $\Gamma_a^* = -\Gamma_c^*$, which is the total cathodic current.

Mean parameter for infinite cathode and infinite electrolyte.—When the electrodes are polarized, the coupling of an infinite cathode with a finite anode increases the current flowing, but the current remains finite. Because of the practical importance of this problem it seemed desirable to investigate it on its own merits. Further, previous results obtained by means of Fourier integrals (2) permit investigation of the limiting value of the mean corrosion current parameter as the anodic fraction (a/c) goes to zero. It should be emphasized that the ensuing derivation relates only to an infinite liquid layer thickness. A finite case is discussed below.

It was established elsewhere (2) that $C_a^*(x)$ for infinite c is

$$C_a^*(x) = \frac{2a}{\mathfrak{L}}\left\{\left[\frac{\pi}{2} - Si(\lambda)\right]\cos\lambda + Ci(\lambda)\sin\lambda + \left[\frac{\pi}{2} - Si(\lambda')\right]\cos\lambda' + Ci(\lambda')\sin\lambda'\right\} \qquad [15]$$

where the auxiliary dimensionless variables λ and λ' were defined as

$$\lambda = (a + x)/\mathfrak{L}$$
$$\lambda' = (a - x)/\mathfrak{L} \qquad [16]$$

and where x, a, and $\mathfrak{L}$ have the same meanings as employed before (1–4). The $Si(\lambda)$ and $Ci(\lambda)$ functions are the sine and cosine integrals.

From [13], [15], and [16],

$$\Gamma_a^* = \frac{2a}{\mathfrak{L}}\left\{\int_{a/\mathfrak{L}}^{2a/\mathfrak{L}}\left(\left[\frac{\pi}{2} - Si(\lambda)\cos\lambda + Ci(\lambda)\sin\lambda\right)d\lambda + \int_0^{a/\mathfrak{L}}\left(\left[\frac{\pi}{2} - Si(\lambda')\cos\lambda' + Ci(\lambda')\sin\lambda'\right)d\lambda'\right\}\right. \qquad [17]$$

Since λ' is the variable of integration (the dummy index) in the second definite integral, it may be replaced by the symbol λ.

$$\Gamma_a^* = \frac{2a}{\mathfrak{L}}\int_0^{2a/\mathfrak{L}}\left\{\left[\frac{\pi}{2} - Si(\lambda)\right]\cos\lambda + Ci(\lambda)\sin\lambda\right\}d\lambda \qquad [18]$$

This may be solved by integrating by parts. The sine and cosine integrals $Si(\lambda)$ and $Ci(\lambda)$ must be differentiated with respect to their upper limits. Recalling that

$$\frac{d}{da}\int_b^a f(x)\,dx = f(a) \qquad [19]$$

substitution of this expression into the results obtained by partially integrating [18] yields

$$\Gamma_a^* = a\sin\left(\frac{2a}{\mathfrak{L}}\right) - \frac{2a}{\pi}\{Si(\lambda)\sin\lambda + Ci(\lambda)\cos\lambda\}\Big|_0^{2a/\mathfrak{L}} + \frac{2a}{\pi}\int_0^{2a/\mathfrak{L}}\sin\lambda\left(\frac{\sin\lambda}{\lambda}\right)d\lambda - \frac{2a}{\pi}\int_0^{2a/\mathfrak{L}}(-\cos\lambda)\left(\frac{\cos\lambda}{\lambda}\right)d\lambda \qquad [20]$$

After combining the sine squared and cosine squared terms in the integrand, it can be shown that

$$\Gamma_a^* = a\sin\left(\frac{2a}{\mathfrak{L}}\right) + \frac{2a}{\pi}\{\ln\lambda - Si(\lambda)\sin\lambda - Ci(\lambda)\cos\lambda\}\Big|_0^{2a/\mathfrak{L}} \qquad [21]$$

This expression cannot be evaluated directly since both the logarithm and the cosine integral become infinite as λ approaches zero.

One of the definitions of the cosine integral is

$$Ci(\lambda) = \ln\lambda\gamma - \int_0^{\lambda}\frac{1 - \cos t}{t}\,dt \qquad [22]$$

where $\ln\gamma = 0.577216$. After substituting [22] into the previous equation, regrouping terms gives

$$\Gamma_a^* = a\sin\left(\frac{2a}{\mathfrak{L}}\right) + \frac{2a}{\pi}\left\{(1 - \cos\lambda)\ln\lambda - \ln\gamma\cos\lambda - Si(\lambda)\sin\lambda + (\cos\lambda)\int_0^{\lambda}\frac{1 - \cos t}{t}\,dt\right\}\Big|_0^{2a/\mathfrak{L}} \qquad [23]$$

By applying l'Hôpital's rule,

$$\lim_{\lambda\to 0}(1 - \cos\lambda)\ln\lambda = 0 \qquad [24]$$

Using the trigonometric identity

$$(1 - \cos\lambda) = 2\sin^2(\lambda/2) \qquad [25]$$

equation [23] reduces to

$$\Gamma_a^* = a\sin\left(\frac{2a}{\mathfrak{L}}\right) + \frac{2a}{\pi}\left\{2\sin^2\left(\frac{a}{\mathfrak{L}}\right)\ln\left(\frac{2a\gamma}{\mathfrak{L}}\right) - Si\left(\frac{2a}{\mathfrak{L}}\right)\sin\left(\frac{2a}{\mathfrak{L}}\right) + \cos\left(\frac{2a}{\mathfrak{L}}\right)\int_0^{2a/\mathfrak{L}}(1 - \cos t)\,d\ln t\right. \qquad [26]$$

after applying the limits of integration. Γ_a^*/a is a dimensionless quantity.

Mean parameter for infinite cathode but finite electrolyte.—The potential can be represented by the Fourier integral

$$P^*(x, y) = \int_0^{\infty} A^*(n)\cos(xhn)\cosh[(b - y)hn]\,dn \qquad [27]$$

where h is a quantity (to be chosen later) having the dimensions of reciprocal length needed to render the quantities in the arguments of the hyperbolic and circular cosine functions dimensionless. The quantity $A^*(n)$ must be chosen so that $P^*(x, y)$ converges to prescribed boundary conditions. Utilizing the boundary condition similar to [3],

$$P^*(x, 0) - \mathfrak{L}\left.\frac{\partial P^*}{\partial y}\right|_{y=0} = E_a S_a'(x) \qquad [28]$$

but with $S_a'(x)$ being the infinite step function defined earlier (2), it can be shown that

$$\int_0^\infty A^*(n)[\cosh(bhn) + (\mathfrak{L}hn)\sinh(bhn)]\cos(xhn)\,dn = E_a S_a'(x) \quad [29]$$

In order to obtain the coefficient $A^*(n)$ in this integral, both sides are multiplied by cos (xhm) and integrated with respect to x.

$$\int_0^\infty \cos(mhx)\left\{\int_0^\infty A^*(n)[\cosh(bhn) + (\mathfrak{L}hn)\sinh(bhn)]\cos(nhx)\,dn\right\}dx = \int_0^\infty E_a S_a'(x)\cos(mhx)\,dx \quad [30]$$

Substituting the value of $S_a'(x)$ into the right-hand side and rearranging the order of integration on the left,

$$\frac{1}{h}\int_0^\infty A^*(n)[\cosh(bhn) + (\mathfrak{L}hn)\sinh(bhn)]\cdot\left[\int_0^\infty \cos(mhx)\cos(nhx)\,d(hx)\right]dn = E_a\frac{\sin(mha)}{mh} \quad [31]$$

The inner integral on the left-hand side is equivalent to the Dirac function $\delta(n - m)$. Utilizing the properties of this function, the left-hand side reduces to

$$\frac{1}{h}\left(\frac{\pi}{2}\right)A^*(m)[\cosh(bhm) + (\mathfrak{L}hm)\sinh(bhm)] = \frac{E_a\sin(ahm)}{mh} \quad [32]$$

In this manner the coefficient $A^*(m)$ can be found and substituted into [27]. Thus the polarized potential function consistent with the imposed boundary conditions is

$$P^*(x, y) = \frac{2E_a}{\pi}\int_0^\infty \frac{\sin(ahn)\cosh[(b-y)hn]\cos(xhn)\,dn}{n[\cosh(bhn) + (\mathfrak{L}hn)\sinh(bhn)]} \quad [33]$$

Evaluation of this definite integral in terms of tabulated functions appears to be difficult. However, a simpler expression for the interfacial potential may be used (6),

$$P^*(x, 0) = \frac{2E_a}{\pi}\int_0^\infty \frac{\sin(ahn)\cos(xhn)\,dn}{n[1 + (\mathfrak{L}hn)\tanh(bhn)]} \quad [34]$$

This relation can be utilized to compute the anodic corrosion current parameter $C_a^*(x)$ from equation [5].

The mean value of the parameter $C_a^*(x)$ may then be computed. Thus the total anodic current is

$$\Gamma_a^* = \frac{2a}{\mathfrak{L}}\int_0^a\left[1 - \frac{P^*(x, 0)}{E_a}\right]dx \quad [35]$$

For convenience there can be substituted into [35] an even simpler expression for the interfacial potential,

$$P^*(x, 0) \equiv E_a\int_0^\infty P(n)\cos(xhn)\,dn \quad [36]$$

where the symbol $P(n)$ is the appropriate function of n, a, $\mathfrak{L}$, and b, but not of x, defined so that [34] and [36] are identical.

Then the mean value for anodic current parameter is

$$\frac{\Gamma_a^*}{a} = \frac{2}{\mathfrak{L}}\int_0^{a-0}\left[1 - \int_0^\infty P(n)\cos(xhn)\,dn\right]dx \quad [37]$$

Changing the order of integration,

$$\frac{\Gamma_a^*}{a} = \frac{2a}{\mathfrak{L}} - \frac{2}{\mathfrak{L}h}\int_0^\infty P(n)\left(\frac{\sin han}{n}\right)dn \quad [38]$$

or finally, after inserting the definition of $P(n)$,

$$\frac{\Gamma_a^*}{a} = \frac{2a}{\mathfrak{L}}\left\{1 - \frac{2}{ah\pi}\int_0^\infty \frac{\sin^2(ahn)\,dn}{n^2[1 + (\mathfrak{L}hn)\tanh(bhn)]}\right\} \quad [39]$$

Into this general expression, there is inserted the choice of h, $(2/\mathfrak{L})$, to bring equations [26] and [39] into more formal agreement.

Symmetry of the mean corrosion current.—The mean corrosion current parameter $\overline{C}_a^*$ is symmetrical about the value of $a/c = \frac{1}{2}$ when the polarization parameter $\mathfrak{L}$ is held constant. However, that point is considered again below.

For convenience, the three dimensionless ratios

$$\alpha = a/c; \quad \beta = c/\mathfrak{L}; \quad \eta = b/c \quad [40]$$

are introduced. On substitution into [11],

$$\frac{\Gamma_a^*}{a} = 2\alpha\beta(1 - \alpha) - \frac{4\beta}{\pi^2}\sum_{n=1}^\infty \frac{\sin^2(n\pi\alpha)}{n^2[1 + (n\pi\beta^{-1})\tanh(n\pi\eta)]} \quad [41]$$

To show that this parameter is symmetrical about $\frac{1}{2}$, it is assumed that

$$\alpha = \tfrac{1}{2} \pm \delta \quad [42]$$

where δ is some positive real number lying between zero and one half. On substitution,

$$\frac{\Gamma_a^*}{a} = \left(\frac{\beta}{2}\right) - 2\beta\delta^2 - \frac{4\beta}{\pi^2}\sum_{n=1}^\infty \frac{\sin^2 n\pi(\tfrac{1}{2} \pm \delta)}{n^2[1 + n\pi\beta^{-1}\tanh(n\pi\eta)]} \quad [43]$$

First, it is necessary to show that the numerator of the summand in [43] is symmetrical. After expressing the sine of a sum of two angles and squaring it,

$$\sin^2\left(\frac{n\pi}{2} \pm n\pi\delta\right) = \sin^2\left(\frac{n\pi}{2}\right)\cos^2(n\pi\delta) + \cos^2\left(\frac{n\pi}{2}\right)\sin^2(n\pi\delta) \pm 2\sin\left(\frac{n\pi}{2}\right)\cos\left(\frac{n\pi}{2}\right)\sin(n\pi\delta)\cos(n\pi\delta) \quad [44]$$

Note that

$$2\sin\left(\frac{n\pi}{2}\right)\cos\left(\frac{n\pi}{2}\right) = \sin(n\pi) = 0 \quad [45]$$

Thus, the numerator of the summand in equation [43] is independent of the choice of the sign accompanying δ, since [45] causes the cross product term on the right side of [44] to drop out, and only this term is affected by the choice. The term $\alpha(1 - \alpha)$ in [41] is symmetrical about ½. Therefore, the expression for either the mean or the average value of the corrosion current parameter is symmetrical about one half.

This statement is correct as long as β or η are independent of changes in α. Specifically, $\overline{C_a^*}$ is calculated in a later section subject to the condition that $a/\mathfrak{L}$ or $\alpha\beta$ is constant. In this case, Γ_a^*/a increases rapidly as α approaches zero. Graphical examples demonstrating the important difference between the two conditions were prepared.

The symmetrical behavior of the integrated anodic current parameter Γ_a^* is similar to that of Γ_a^*/c. It is clear that the parameter Γ_a^* can be related to total current flowing in a galvanic system by substituting the values of a, E_a, and the specific conductivity σ which are pertinent to the system.

Numerical Evaluation

Summation of the series.—Details of coding these problems for calculation on the MANIAC computer need not be presented here. Convergence of the series was so rapid that serious errors were not introduced by truncation of the series at $n = 100$.

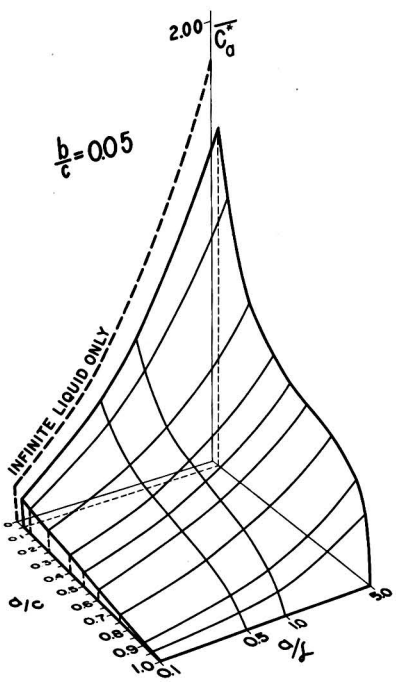

FIG. 1. Dependence of the mean value of the anodic current density parameter $\overline{C_a}^*$ on the characterizing ratio $(a/\mathfrak{L})$ and the anodic fraction (a/c). Computed for a relative thickness (b/c) of the electrolyte equal to 0.05.

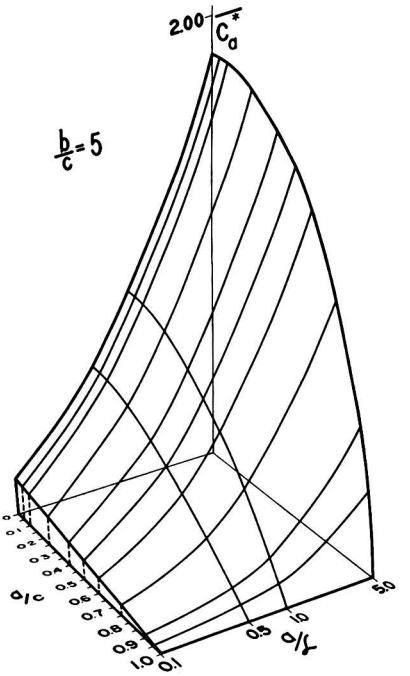

FIG. 2. Dependence of the mean value of the anodic current parameter $\overline{C_a}^*$ on the characterizing ratio $(a/\mathfrak{L})$ and the anodic fraction (a/c). Computed for a relative thickness of 5.

To facilitate computation of each term in the series, it was noted that the hyperbolic tangent did not differ significantly from one when its argument exceeded five. This substitution of unity eliminated the separate series evaluation of hyperbolic tangent for each term after the N_0-th which was dependent on b/c.

Values of the quantities chosen.—In the detailed evaluation, c was fixed at 10, as has been done in many of the calculations to date, and the dependence on (a/c) was investigated by letting a vary in the range 0–10. Five relative thicknesses of liquid layer, namely b/c = 0.005, 0.05, 0.5, 1.0, and 5.0, were employed. Two choices were available for using the polarization parameter. In most of the evaluations, constant values of the dimensionless ratio $(a/\mathfrak{L})$ were chosen rather than constant $\mathfrak{L}$ values. This choice, of course, affects the values of $\mathfrak{L}/c$ which appear in the denominator of equations [11] and [12]. This ratio was found from the product $(a/c)(\mathfrak{L}/a)$ without the intervening computation of $\mathfrak{L}$.

Values of the mean anodic current parameter.—Values of the mean anodic corrosion current parameter were computed for over 400 combinations (7) of the ratios $(a/\mathfrak{L})$, (a/c), and (b/c). In these calculations the polarization parameter was not fixed but was permitted to vary in such a way that the ratio $(a/\mathfrak{L})$ characterizing the behavior of the galvanic system was kept constant. Some of the values have been assembled into graphical summaries. Two perspective drawings made to scale are presented in Fig. 1 and 2. In the former, b/c was chosen as 1/20 and, in the latter,

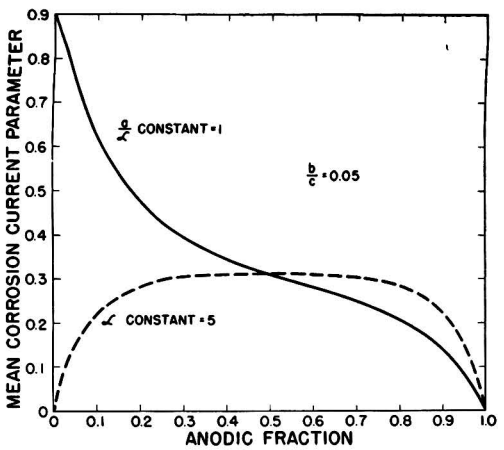

FIG. 3. Comparison of the mean anodic current density for constant $\mathfrak{L}$ and for constant $(a/\mathfrak{L})$ values. Curves computed for a relative thickness of 0.05.

as 5. It was shown (4) that the electrolyte layer is effectively "infinitely thick" whenever the relative thickness (b/c) exceeds unity, in all practical problems. Thus the two graphs pertain to a small finite and an "infinite" liquid layer thickness, respectively.

Note that in these perspective drawings the characterizing ratio $(a/\mathfrak{L})$ is plotted on a logarithmic scale with large values of $\mathfrak{L}$ in the front and with a increasing in relative size on the receding "picture planes." This choice of logarithmic scale permits combining a large amount of data into a form which can be easily assimilated and giving equal weight to very small and to very large $(a/\mathfrak{L})$ values.

In many practical problems, one might regard $\mathfrak{L}$ as essentially fixed and wish to know how the mean current density would vary with the (a/c) ratio. For this reason, additional values of the mean, namely (Γ_a^*/a), have been computed with $\mathfrak{L}$ constant and a varying in the (a/c) ratio. Fig. 3 compares the values of $\overline{C_a^*}$ obtained when $(a/\mathfrak{L})$ or $\mathfrak{L}$ are fixed. The dotted line is for the constant $\mathfrak{L}$ data. As would be expected, the curve for constant $\mathfrak{L}$ is symmetrical about the line $a/c = \frac{1}{2}$. In the case of the constant ratio curves, the increasing polarization parameter (as a/c is increased above $\frac{1}{2}$) reduces the corrosion current density over the entire anode and thus reduces Γ_a^*. However, when a/c is small, the $\mathfrak{L}$ values in the constant ratio curves are also small. The corrosion current density rises rapidly.

Average corrosion current parameter.—There is no important difference between the *average* value of the corrosion current parameter on the anode and on the cathode, since Γ_a^* is equal in magnitude to Γ_c^* but has the opposite sign and, in either case, c is the divisor. This is not true of the mean values; thus the distinction between the two quantities in this section.

Values of Γ_a^*/c were obtained from the mean values by equation [14]. A graphical summary of the important results is presented in Fig. 4 and 5. The same values of the three parameters were employed in these graphs as in

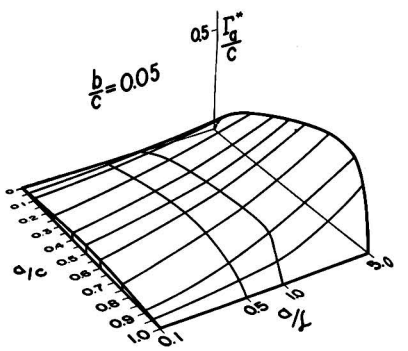

FIG. 4. Dependence of the average value of the current density parameter upon the ratios $(a/\mathfrak{L})$ and (a/c). Computed for a (b/c) value of 0.05. This illustration supplements Fig. 1.

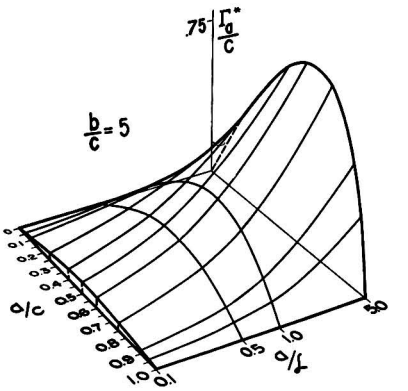

FIG. 5. Dependence of the average value of the current density parameter upon the ratios $(a/\mathfrak{L})$ and (a/c). Computed for a (b/c) value of 5. This illustration supplements Fig. 2.

Fig. 1 and 2, respectively. These four drawings are complementary.

Effect of relative thickness.—The previous illustrations have shown the effect of two limiting relative thicknesses of the corrodent layer. However, it seemed desirable to present in one or two graphs a summary of the effects to be expected with intermediate thicknesses.

Fig. 6 was constructed for a constant value of the characterizing ratio $(a/\mathfrak{L})$. Examination indicates that, when sections of the surface are taken at constant small (b/c) values, the curves are similar in shape to those presented in Fig. 1, and that, as the relative thickness is increased, there is a smooth transition toward a curve which is concave downward as the surface is in Fig. 2. Note that here, as in several other perspective drawings, the surface is not extended to intersect the plane corresponding to a zero anodic fraction. Such an extension could be made by computing the values from the integral derived above in connection with the second limiting case. When the anode is greater than about one-ninth the size of the cathode $(a/c > 1/10)$, the current is less for relatively shallow cor-

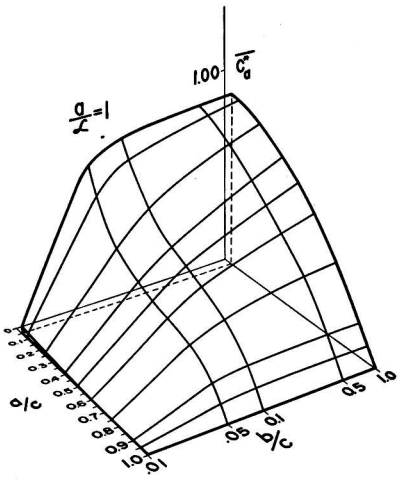

FIG. 6. Dependence of the mean current density on the relative thickness (b/c) and the anodic fraction (a/c). Computed for $a/\mathfrak{L} = 1$.

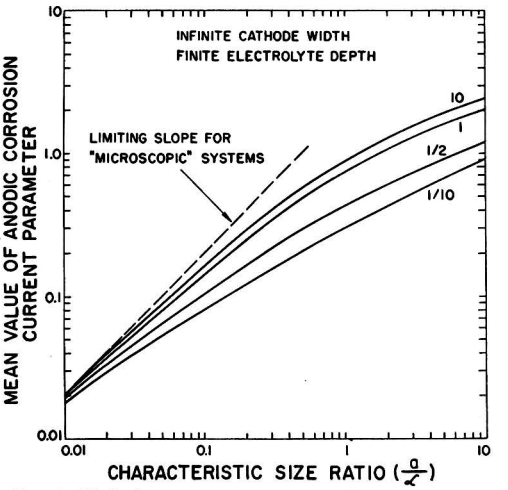

FIG. 7. Variation of the mean value of the anodic corrosion current parameter C_a^* with the characterizing ratio ($a/\mathfrak{L}$). Computed for (b/a) = 0.1, 0.5, 1, and 10 as a parameter.

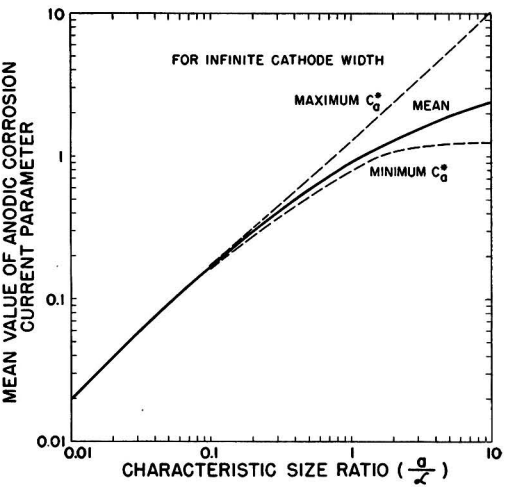

FIG. 8. The spread between the maximum, mean, and minimum values of $\bar{C}_a^*(x)$ for different fixed values of the characterizing ratio ($a/\mathfrak{L}$).

rodents than for deep ones. This apparently results from concentration of the corrosion current into the vicinity of the anode-cathode junction (4). This concentration is greater when (b/c) is smaller than (a/c). In Fig. 6, the mean value of the corrosion current parameter, $\bar{C}_a^*$, decreases very rapidly as (b/c) approaches 0.01 at which time the latter becomes significantly smaller than any of the (a/c) values employed. However, as (a/c) approaches zero, and (a/c) becomes smaller than the intermediate values of (b/c) which have been used to construct Fig. 6, the values of $\bar{C}_a^*$ rise rapidly.

When the value of $\mathfrak{L}$ is, relatively speaking, ten times as large as in Fig. 6, an upswing of the $\bar{C}_a^*$ values as (a/c) approaches zero also occurs for small (b/c) values. Similarly, a curve drawn for (b/c) = 1 is concave downward.

Further discussion in terms of small (a/c) is presented in the next section, where the numerical results pertinent to the two limiting cases are discussed.

Evaluation of the mean current parameter for the limiting cases.—Equation [26] was numerically evaluated by hand as the integral in it converges rapidly after the first ten terms. The sine and cosine terms had been evaluated previously for large arguments (2). Tabulated values of the sine and cosine integrals were used.

The reduction of the integral in [39] to tabulated functions did not appear to be simple. Therefore, numerical integration was used, since convergence should be rapid. The maximum error is less than 1% and decreases rapidly as ($a/\mathfrak{L}$) increases.

By far the more important limiting case is the second, which involves finite liquid depths, since it is more pertinent to the material already presented. The case of an infinite liquid depth can be regarded as a limit to the case under discussion. The finite liquid case is discussed in more detail for this reason.

A graphical summary of the mean values of $\bar{C}_a^*$ computed for various ($a/\mathfrak{L}$) and (b/a) values from equation [39] is presented in Fig. 7. The curve for (b/a) = 10 is indistinguishable from that drawn for (b/a) = ∞. However, when b is much smaller than a, say for (b/a) = 1/10, the current density is small. Thus, in this sense b is the critical dimension λ.

The limiting value of ($2a/\mathfrak{L}$) for $\bar{C}_a^*$ which results for small values of the characterizing ratio ($a/\mathfrak{L}$) was added as a tangent to this figure. It can be deduced from earlier equations (2). Inspection of Table I of (2) indicates that for small $a/\mathfrak{L}$ values, the maximum value of C_a^* is approximately $2a/\mathfrak{L}$.

Using equation [15], it can be shown that

$$\lim_{(a/\mathfrak{L})\to 0} \max C_a^* = \lim_{(a/\mathfrak{L})\to 0} C_a^*(0) = \frac{2a}{\pi\mathfrak{L}}\left\{\frac{\pi}{2}+\frac{\pi}{2}\right\} = \frac{2a}{\mathfrak{L}} \quad [46]$$

since all of the quantities within the brace can be approximated by either 1, λ, or λ'. Therefore, those which would be second order in $(a/\mathfrak{L})$ in the total expression can be neglected. Only the two terms containing $(\pi/2 \cdot \cos 0)$ remain. The manner in which the mean value $\overline{C}_a^*$ is bounded between the maximum and minimum values of $C_a^*(x)$ is indicated in Fig. 8, which has been plotted from Table I of (2) and the data computed from equation [26].

Comparison with Experimental Results

Jaenicke and Bonhoeffer (8) employed a galvanic assembly in which thin cathodic cylinders of platinum were bolted between two anodic cylinders of zinc. The platinum cylinders were varied in length to give different anode-cathode ratios. The assembly was immersed in acid solution contained in a shallow dish, and the quantity of zinc dissolved in a given time was used to compute the dissolution rate and thus the average cathodic current. The dissolution rate of the zinc, under the same conditions but while not coupled to the platinum, was subtracted from the latter rate to obtain the correct rate due to galvanic action. Their data are tabulated as mean cathodic current densities.

The quantity $\mathfrak{L}_c$ can be obtained from their data by the formula Wagner (5) used,

$$\mathfrak{L}_c = \sigma\beta/J_c \qquad [47]$$

where σ is the specific conductivity in $ohm^{-1}cm^{-1}$, β, the coefficient in Tafel's equation for hydrogen overvoltage, is 0.050, and J_c is current density in amp/cm^2. Employing the data given for J_c in their Table 4, the value of $\mathfrak{L}_c$ for $0.05N$ hydrochloric acid lies in the range 0.0225–0.069 cm, whereas the calculated values for $0.05N$ hydrochloric acid plus $1M$ potassium chloride range from 0.145 to 0.252 cm. The equivalent limiting values of $a/\mathfrak{L}$ are 133, 44, and 21, 12 respectively in the two media.

The average current density over the cathode, J_c, was computed from the mean anodic corrosion current parameter $\overline{C}_a^*$ by the expression

$$\overline{J}_c = \left(\frac{E_a}{2a}\right)\sigma\left(\frac{a}{c-a}\right)\overline{C_a^*} \qquad [48]$$

In this equation, the a in the numerator and denominator has not been cancelled to facilitate rapid recognition of the source of each factor. $\overline{C}_a^*$ was computed for $b = 2.5$ cm, for several values of the parameter $a/\mathfrak{L}$, (15, 30, 60, 120), and for each cathode breadth which Jaenicke and Bonhoeffer employed. The appropriate values of σ and E_a were estimated from their data. The resulting $\overline{J}_c$ data are tabulated in Fig. 9. The agreement is surprisingly good in the case of the more concentrated solution. However, the data for $0.05N$ hydrochloric acid are smaller by a factor of three or four than would have been expected from the low $\overline{J}_c$ values. In the more poorly conducting solution, the voltage difference between the two materials was higher, otherwise the current density would have been significantly smaller. Comparison of the two curves for $a/\mathfrak{L} = 30$ shows that the product $(E_a\sigma)$ appearing in [48] was approximately constant for the two solutions. Thus the data for hydrochloric acid are low for some reason.

Robertson and Uhlig (9) prepared alloy mixtures of magnesium and tin which contained the intermetallic compound Mg_2Sn. The composition of six alloys used was adjusted so that a different percentage of the compound would be mixed with either parent metal. Samples of these alloys were immersed in a $1N$ sodium chloride solution. The hydrogen that evolved during the corrosion was collected and served as a measure of the average corrosion rate. The authors did not study polarization characteristics of Mg_2Sn, magnesium, or tin present in their alloys, and the self-corrosion rates of magnesium and Mg_2Sn were not obtained separately. Thus, accurate values of $\mathfrak{L}_a$ and $\mathfrak{L}_c$ cannot be obtained. Equation [47] may be employed to estimate $\mathfrak{L}_c$ from the rate of hydrogen evolution shown in their Fig. 10. The rate for 70% free magnesium gives $\mathfrak{L}_c \simeq 0.8$ cm, which is consistent with values noted in other experimental studies (2–4). Robertson and Uhlig employed powdered samples, and the size of the particle ranged from 0.015 to 0.065 cm. Thus, if virtually the entire particle was free magnesium, the maximum value of $a/\mathfrak{L}$ was 0.04, since a is chosen as one half of the anode size. The average cathodic current at 30 and 80% compound was compared with data computed for a constant $a/\mathfrak{L} = 0.05$ and for $b/c = 0.1$. The experimental ratio is 1.49, whereas the theoretical ratio was 1.48. This suggests good agreement.

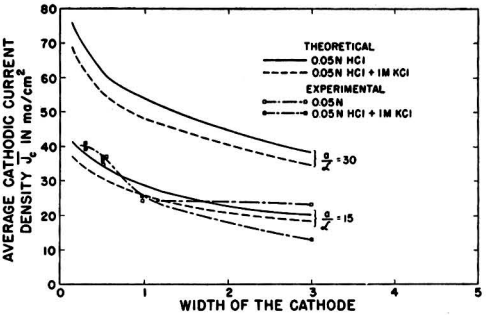

FIG. 9. Comparison between the computed and experimental values of $\bar{J}_c$, based on the data of Jaenicke and Bonhoeffer.

Discussion

When the characterizing ratio $(a/\mathfrak{L})$ is kept constant as in Fig. 1, and (a/c) approaches zero, then in the limit either $\mathfrak{L}$ must go to zero to maintain $(a/\mathfrak{L})$ constant or c must go to infinity. The former case has been discussed. The rapid increase in the average current near the origin of Fig. 1 is due to the forced, simultaneous decrease in $\mathfrak{L}$. Fig. 2 reveals that the same increase is, however, small when (b/c) is large.

A constant $(a/\mathfrak{L})$ section was made through the surfaces in Fig. 1 and 2, and these sections were combined in constructing Fig. 10. The two curves with the largest and smallest (b/c) values become equal when the anodic function (a/c) approaches either one of its limiting values, zero or unity, i.e., when either the anode or the cathode, respectively, becomes vanishingly small. However, near the middle range of (a/c), the mean corrosion current is less for shallow electrolyte "films" than deep liquid layers.

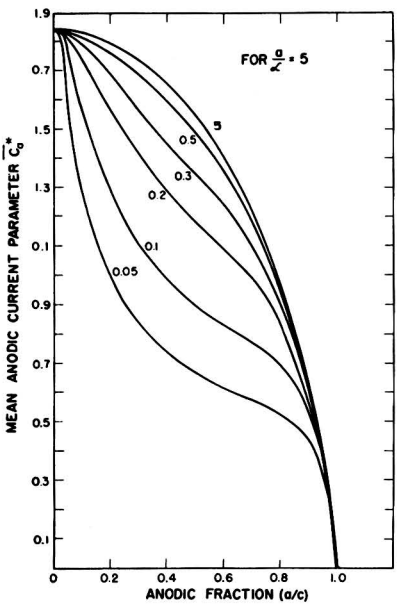

FIG. 10. Variation with the anodic fraction of the mean values of the anodic corrosion current parameter. Computed for $(b/c) = 0.05, 0.1, 0.2, 0.3, 0.5$, and 5. Curves for the smallest and largest relative thicknesses were obtained from Fig. 1 and 2, respectively.

Thus, one may conclude that the current is concentrated into the vicinity of the junction and limited in magnitude when the relative thickness (b/c) is small in comparison to unity. This behavior was convincingly displayed earlier (4).

As might be expected for larger values of (b/c), the significant departure from equality does not occur until the anodic fraction is substantially farther away from the limits, one or zero. That is, when (b/c) is large, the electrolyte appears to be "infinitely deep" for most electrode widths. It is important to look at the relative size of b and of the smaller electrode width, a or $(c - a)$. For clarity, four additional curves were added to Fig. 10; these were computed for $(b/c) = 0.1, 0.2, 0.3$, and 0.5.

Similar slopes of the family of curves near $\alpha = 0$ can be deduced qualitatively. When a becomes very small in comparison to some finite c, b will become larger than a as long as the relative thickness (b/c) is fixed. Earlier (4) it was concluded that the corroding liquid was essentially "infinitely deep," if its dimension were a few times larger than the anode dimension. This means that the various values of $\overline{C}_a^*$ become essentially equal to the single value obtained for infinite b when α is very small. However, this is based on the assumption that the sum of the anode and cathode widths c is finite.

The argument also applies when c is infinite. Then, of course, both α and η are zero. The ratio (b/a) may take on any value and still satisfy the condition that α and η are zero. For any given $(a/\mathfrak{L})$ value in Fig. 7, the values of $\overline{C}_a^*$ approach a limit, set by the infinite electrolyte depth, as b/a increases. That is, b is essentially "infinite," if it is several-fold larger than a. Thus one may arrive at the conclusion that the curves will asymptotically approach the limiting curve in Fig. 10 in the region of $\alpha = 0$, even though c is finite but very much larger than a.

The discussion of these two limiting cases has increased the understanding of the over-all behavior of similar electrochemical systems. When $\mathfrak{L}$ is large, the $\overline{C}_a^*$ values are small and are approximately equal, independent of the relative sizes of the dimensions a and b, i.e., when the galvanic system is behaving "microscopically." However, in certain instances, either a (or b) may be larger than $\mathfrak{L}$, and the other one, (b or a) may limit the local distribution of the current density. In such cases, the system will be "microscopic" if that dimension, say b, is much smaller than $\mathfrak{L}$.

When c is very large, the really significant ratio becomes (b/a), and the direct dependence upon c is eliminated. A variation of this statement is that either a or b may become the critical dimension λ, i.e., that dimension which most strongly affects the distribution of current density. For a fixed (b/c) ratio, a becomes λ as the anodic fraction α goes to zero, since b appears to be "infinite." The curves for $\alpha = 0$ in Fig. 1 and 2 can be derived from the limiting cases of finite and infinite electrolytes, respectively.

If (b/c) is large but c finite, then, as the anode becomes vanishingly small, the current approaches a uniform value over the anode, and the electrochemical systems appear to behave microscopically. A similar result is obtained when the cathode width $(c - a)$ becomes infinitely small in comparison with the size of the anode a. The limiting case just discussed of an infinite cathode and electrolyte also adequately describes this feature of the over-all behavior.

The second limiting case of a thin finite electrolyte layer pertains to Fig. 1 where it is assumed that in most cases the anode and cathode are larger than the liquid depth. The smallest value of the anodic fraction (a/c) employed in the calculation is 0.05 which is equal to the specific value of the relative thickness used for constructing that figure. That is, the smallest (a/b) used was unity.

When the anode is very tiny in comparison to b or c, because of a fixed (b/c) ratio, a is the critical dimension, and the liquid depth appears to be "infinite" despite the smallness of b, because the ratio (b/a) is large. A similar argument applies to vanishingly small cathodes as well.

When (b/a) is smaller than approximately one, the current will be concentrated into the vicinity of the anode-cathode junction, and the curve of the mean value of C_a^* as a function of α in Fig. 4 reflects this fact. That is, the $\overline{C}_a^*$ curve for small b/c lies below that for infinite relative thickness. When b/c is small, the significant ratio (b/a) can be greater than one for very small values of a/c. Analysis of the second limiting case shows that mean value of $\overline{C}_a^*$ rapidly approaches a certain maximum value as a becomes infinitely small and that this maximum value is that obtained for an infinite electrolyte in the other limiting case.

Qualitatively this result can be deduced by noting that for any b/c value greater than zero, there will be some values of a/c such that a/b will be smaller than one half. Thus, for any thin film of electrolyte, there will be some small size of either the anode or the cathode for which this

film will effectively be "infinitely deep." Thus, the equality of the $\overline{C}_a^*$ curves at $\alpha = 0$ or 1 in Fig. 11, independent of the (b/c) values, is explained, and the general behavior of any similar electrochemical system which is consistent with the basic premise of equal polarization parameters is elucidated.

Summary

On the basis of the detailed theoretical analysis it can be concluded that the mean current density over the anodes is a maximum when the anodic fraction $(a/c) = \frac{1}{2}$ and becomes zero as either the anode or cathode becomes vanishingly small, provided the polarization parameter $\mathfrak{P}$ is constant. This maximum value is dependent on the relative liquid depth. In the event that the characterizing ratio $(a/\mathfrak{P})$ is kept constant, the same mean current density increases to a large value which is independent of the relative electrolyte depth, as the anodic fraction approaches zero. These phenomena can be explained in terms of the characteristic ratio $(\lambda/\mathfrak{P})$. For a given anodic fraction, other than zero or unity, as the relative electrolyte thickness (b/c) is reduced, the mean current density decreases from some maximum value. The qualitative agreement between these theoretical deductions and two previously published experimental studies was discussed.

Acknowledgment

The authors are deeply indebted to Professor Carl Wagner who checked the integration of the Fourier series and who has offered considerable guidance and inspiration during the course of this work.

Calculations for Fig. 8 were performed by Max Goldstein and Clifford Moss. The authors are grateful to them for this important assistance. Miss Elizabeth Scott constructed the perspective illustrations for this report.

Manuscript received March 10, 1955. Work on this paper was done under the auspices of the Atomic Energy Commission.

Any discussion of this paper will appear in a Discussion Section to be published in the December 1956 Journal.

REFERENCES

1. J. T. Waber, *This Journal*, **101**, 271 (1954).
2. J. T. Waber and M. Rosenbluth, *ibid.*, **102**, 341 (1955).
3. J. T. Waber, *ibid.*, **102**, 420 (1955).
4. J. T. Waber and B. Fagan, *This Journal*, **103**, 64 (1956).
5. C. Wagner, *ibid.*, **98**, 116 (1951).
6. J. T. Waber and J. Morrissey, Unpublished work.
7. J. T. Waber and J. Morrissey, Unpublished work.
8. W. Jaenicke and K. F. Bonhoeffer, *Z. phy. Chem.*, **193**, 301 (1944).
9. W. D. Robertson and H. Uhlig, *Trans. Electrochem. Soc.*, **96**, 27 (1949).

FUTURE MEETINGS OF

The Electrochemical Society

San Francisco, April 29, 30, May 1, 2, and 3, 1956

Headquarters at the Mark-Hopkins Hotel

Sessions will be scheduled on

Corrosion (joint symposium with Theoretical),
Electric Insulation, Electronics (including Luminescence and Semiconductors),
Electrothermics and Metallurgy, Industrial Electrolytics,
and Theoretical Electrochemistry

★ ★ ★

Cleveland, September 30, October 1, 2, 3, and 4, 1956

Headquarters at the Statler Hotel

Sessions probably will be scheduled on

Batteries, Corrosion, Electrodeposition,
Electrothermics and Metallurgy, and Theoretical
Electrochemistry (joint with Electrodeposition)

★ ★ ★

Washington, D. C., May 12, 13, 14, 15, and 16, 1957

Headquarters at the Statler Hotel

★ ★ ★

Buffalo, October 6, 7, 8, 9, and 10, 1957

Headquarters at the Statler Hotel

★ ★ ★

New York, April 27, 28, 29, 30, and May 1, 1958

Headquarters at the Statler Hotel

★ ★ ★

Ottawa, September 28, 29, 30, October 1, and 2, 1958

Headquarters at the Chateau Laurier

★ ★ ★

Papers are now being solicited for the meeting to be held in Cleveland. Triplicate copies of each abstract (*not exceeding 75 words in length*) are due at the Secretary's office, 216 West 102nd Street, New York 25, N. Y., *not later than June 15, 1956* in order to be included in the program. *Please indicate on abstract for which Division's symposium the paper is to be scheduled.* Complete manuscripts should be sent in triplicate to the Managing Editor of the JOURNAL at the same address.

San Francisco Meeting Plans

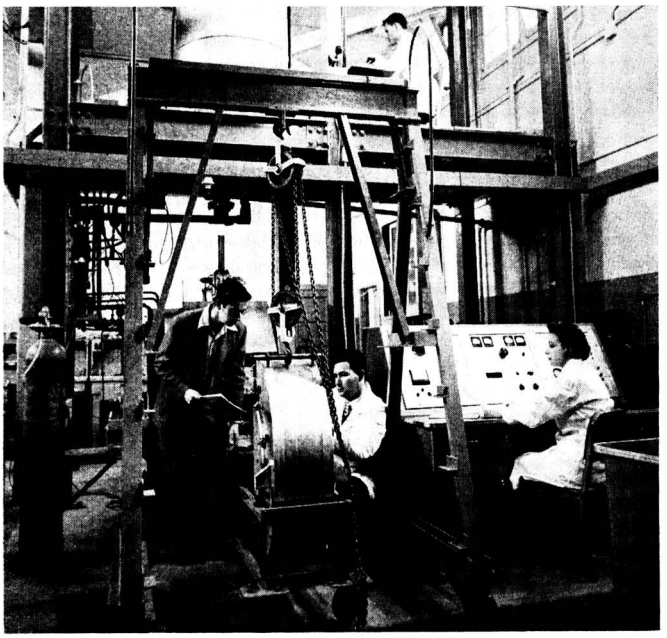

Stanford Research Institute's "proton bombarder," consisting mainly of a two million-volt generator, a 20-foot vacuum tube, and two large electromagnets. Weighing about five tons, it can detect one-millionth of one-millionth of a gram on a surface.

Plans for the San Francisco Meeting of the Society, April 29–May 3, are coming along nicely. The complete program, including general information, technical sessions, and abstracts, will appear in the March JOURNAL.

The Ladies' Program will include a tour of San Francisco, a "Tour of the Ships," a visit to the famous Rod McClellan Orchid and Gardenia Nursery and luncheon in Sausalito in Marin County across the Golden Gate from San Francisco.

Plant Trips

A plant trip is scheduled for the Radiation Laboratory at the University of California, Berkeley. This laboratory has played a prominent role in high energy nuclear physics, in developing numerous accelerators, and in discovering new elements and elementary particles.

Another trip is scheduled for the Stanford Research Institute which is the applied research center of the West and the second largest organization of its kind in the U. S. Founded in November 1946 by Stanford University with the encouragement of a number of prominent Western industrialists, the Institute has grown to a staff of 1200. Of this staff, two-thirds are technical and professional personnel comprising engineers, chemists, physicists, economists, and other specialists.

SRI, located in Menlo Park, Calif., is a nonprofit corporation affiliated with neighboring Stanford University. A confidential research and fact-finding service is provided to business, industry, and government agencies on a contract basis. Research programs are grouped under three main operating divisions: Engineering, Physical Sciences, and Economics.

The Institute's progress and expansion have depended upon income from research investigations conducted for industry and government and upon contributions. At the end of 1955, the annual rate of contract research was ten and one-half million dollars.

The Institute encourages the accumulation and dissemination of scientific and technical information through publication of scientific proceedings, articles, and papers. Numerous professional meetings and scientific symposia are sponsored by SRI each year. Also, in the public interest, research studies are conducted with Institute funds in many fields of technical and economic assistance: waste utilization, industrial air pollution, public health and agriculture, resources and area development.

The Institute's Electrochemical Laboratory carries out applied and basic studies related to low-temperature electrolysis, the electrochemistry of transition metals such as titanium, deposition of metals, and polarization phenomena.

News Notes in the Electrochemical Field

G.E. Water Treatment Laboratory

The General Electric Co. has put a new one and one-half million dollar laboratory into operation at the Hanford atomic plant to seek water treatment methods that will permit greater production of fissionable material. The goal is to find economical ways of chemically treating Columbia River water so that it can be used to cool Hanford atomic reactors operating at higher power than at present.

The new laboratory will be in operation 24 hours a day. It provides large-scale facilities for experiments in filtering and chemical treatment and for pumping water through simulated hydraulic systems and test channels in a nearby reactor. Equipment for corrosion and hydraulic studies is included. Also, indoor and outdoor fish troughs and ponds are available to expose aquatic life to various concentrations and types of reactor effluent.

Engineering Societies Directory

The Engineering Societies Directory, a complete list of all engineering societies in the United States, together with pertinent information about them, will be published by the Engineers Joint

Council tentatively as of June 1, 1956. The Directory will be a new publication, not a revision of the Engineering societies Yearbook, which was published in 1948, and which has been discontinued.

Questionnaires were mailed to all known societies about January 16 and should be returned to EJC by March 1. If a society did not receive such a questionnaire by that time, it should contact Engineers Joint Council, 29 W. 39th St., New York City.

The Directory will be the only complete listing of engineering societies at all levels and will be available at $3.50 per copy.

Olin Mathieson Trade Name Change

Olin Mathieson Chemical Corp. will sell its patterned metal used in heat and cold transfer under the trade name "Olin Roll-Bond." It formerly was sold under the name "Western Roll-Bond."

Olin Roll-Bond, a process which makes it possible to create any pattern of tubing—no matter how intricate—within a single homogeneous sheet of metal, was introduced by the corporation in October 1954. It may be used in every industry dealing with temperature control.

Corning Glass Works Expansion

Plans to enlarge its facilities for manufacturing glass electronic components in Bradford, Pa., have been announced for Corning Glass Works by John L. Hanigan, Vice-President and General Manager of the company's Electrical Products Division.

Enlargement of the Bradford plant, including the eventual installation of automatic resistor and capacitor production equipment, is part of the company's announced intention to manufacture and sell components to all parts of the electronics industry. A rapidly increasing demand, especially from radio and television set manufacturers, for Corning components necessitated the expansion.

Additional space has been obtained that will nearly double the present Corning plant area in Bradford. While necessary alterations to the newly acquired area are now being carried out, the expansion, which will include eventual consolidation of all the company's major electronic manufacturing operations, will be carried out gradually during 1956 to avoid disruption of delivery schedules. When the consolidation is complete, the full line of Corning components, including resistors and fixed capacitors, will be produced there.

G.E. European Office Established

General Electric Research Laboratory recently announced that it has established a European office and appointed Dr. George J. Szasz as its first scientific representative abroad. "The purpose of the new office," according to Dr. C. G. Suits, G.E. Vice-President and Director of Research, "is to strengthen scientific contacts between the General Electric Research Laboratory and basic research activities being conducted in Europe."

As a major part of his activities, Dr. Szasz will travel throughout Western Europe, attending scientific meetings and visiting laboratories which conduct fundamental research in scientific areas of interest to the General Electric Co. For the present, Dr. Szasz will maintain an office with the International General Electric Ltd., Crown House, Aldwych, London, W.C. 2, England.

The Research Laboratory's new European activities are part of an overall program of external scientific relations directed by Victor H. Fraenckel, laboratory consultant.

MCA Science Program

As part of its expanding activities in the field of education, the Manufacturing Chemists' Association has announced that it is embarking on a program designed to assist science teachers and students in the junior high schools, pilot testing in a few school systems in various sections of the country to begin in the early part of 1956. Once the program has been perfected it will be made available to MCA member companies for execution in their own plant communities.

The program was announced by Glen Perry, assistant director of public relations of E. I. du Pont de Nemours & Co., Inc., and chairman of MCA's Industry Education Program Committee. A rough blue-print for the next five years has been established, encompassing a range of activities from the elementary levels through the senior high schools. The pilot program for 1956, gauged for the junior high school alone, involves the preparation, use, and testing of materials such as a teacher's source and experiment book, a student experiment booklet, a wall chart, and a vocational guidance publication.

Vacuum Furnace Cross-Licensing Agreement

National Research Corp., Cambridge, Mass., has signed an agreement with Deutsche Gold- und Silber-Scheideanstalt A.G., Frankfurt am Main, Germany, ordinarily referred to as Degussa, for an exchange of information relating to high vacuum furnaces.

For a period of 15 years National Research Corp. has been the leading producer of industrial vacuum furnaces in the United States, and Vacuum Metals Corp., owned jointly with Crucible Steel Co. of America, is the country's first and largest producer of vacuum melted metals and alloys. NRC has designed and built many of the vacuum melting furnaces for the United States atomic energy program and for a number of industrial and research installations in the United States.

Degussa, one of Germany's principal inorganic chemical and metallurgical companies, also has substantial equipment manufacturing operations. Its Industrieofenbau, located at Wolfgang bei Hanau, near Frankfurt am Main, is the principal European manufacturer of vacuum furnaces. Degussa has specialized in the production of sintering furnaces for hard metals and carbides and in vacuum and controlled atmosphere heat-treating furnaces. Through the agreement, this know-how will be made available to NRC for the production of furnaces in the United States.

Air Pollution Abatement

Speaking at the 20th annual meeting of the Industrial Hygiene Foundation on November 17 in Pittsburgh, Pa., M. F. Crass, Jr., Secretary of the Manufacturing Chemists' Association, told his audience that the chemical industry spends at least forty million dollars annually on air pollution abatement efforts and that total industrial spending probably exceeds one hundred million dollars. Relatively new nonindustrial pollution sources, such as automobile exhausts, home heating plants, incinerators, and open burning in municipal garbage dumps, are adding to the problem. Added economic losses increase the cost of air pollution, he said, explaining that in cleaned-up Pittsburgh an average annual saving of some twenty-five million dollars is effected in laundry, housing maintenance, and dry cleaning alone. He summarized the activities of the MCA's

air pollution abatement committee by saying it consisted of four facets: continued supply of information to top-level industry executives on progress of air pollution abatement, encouragement of continued research and evaluation of existing data, continued dissemination of information to the general public, and assistance to local state and federal officials in connection with proposed legislation.

While urging an open mind on the changing air pollution situation, Mr. Crass stated the MCA was opposed to broad federal control, believing that jurisdiction should be kept at the local level. However, he stated that the MCA supported federal encouragement and sponsorship of research in the field. In connection with the national aspects of the problem, Mr. Crass reiterated an earlier proposal by the MCA that a national advisory committee on air pollution abatement, made up of government, industry, and public representatives, be appointed.

"Soviet Professional Manpower"

The Soviet Union is graduating almost twice as many technical specialists in certain fields as the United States. Between 1928 and 1954 the Soviet Union graduated about 682,000 professionals in the engineering field, as against 480,000 in the United States during roughly the same period; agricultural graduates in the Soviet Union totaled about 244,000, as against 133,000 in the United States; and Soviet graduates in medicine outnumbered those in the United States two to one, 320,000 against 148,000.

These and other findings are presented in a definitive study, "Soviet Professional Manpower," by Nicholas DeWitt, being published by the National Science Foundation in cooperation with the National Academy of Sciences–National Research Council. The book is the result of more than two years of research on the Soviet educational system and on the supply and distribution of its professional manpower.

In announcing its publication, Alan T. Waterman, Director of the National Science Foundation, and Detlev W. Bronk, President of the National Academy of Sciences–National Research Council, expressed the hope that the book would not only serve to focus nation-wide attention on the capabilities of other nations in science and technology but would also arouse interest, particularly at the local level, in the need for greater attention to our own problems in identifying and training persons with special aptitudes for careers in science and technology.

The book is for sale by the Superintendent of Documents at $1.25 a copy.

Report on Educational Problems

Three conditions must be met if private educational institutions are to accommodate the swelling college-age population, according to Dr. John T. Rettaliata, President of Illinois Institute of Technology, Chicago. The conditions listed in his 64-page annual report for the 1954–1955 school year, now being distributed, are: (*a*) private educational institutions must convince themselves they can acquire the means to expand their enrollments in order to accommodate the increasing number of students who will qualify for college admission; (*b*) public institutions should consider raising tuition charges so that students with adequate finances will pay a more appropriate share of the cost of their education and thus appreciate it more; (*c*) the friends, neighbors, and benefactors of private educational institutions must rally to give financial assistance to the colleges and universities, thus eliminating the need for the institutions to increase charges to students. Dr. Rettaliata warned that increased accommodations must be achieved without any sacrifice in the quality of the educational program.

The "tremendous need" for more college students capable of preparing for engineering and science careers was pointed out by Dr. Rettaliata, who said the reality of the shortage of technological and scientific personnel no longer is questioned. He contended that one of the factors adversely affecting the development of more scientists and engineers is that some students make career decisions too late. He attributed the increasing number of cases of this type to "the pronounced trend in the nation's high schools toward more general education."

Graham Crowley Moves

It has been announced by Dr. A. Kenneth Graham, President of Graham, Crowley and Associates, Inc., Jenkintown, Pa., that the company's general offices and Chicago research laboratory have moved into improved quarters at 5465 W. Division St., Chicago 51, Ill. Also, a new branch office has been opened at the site of the company's pilot plant, 2152 Portage St., Kalamazoo, Mich., in order to better serve industry in the Michigan area with respect to electroplating, industrial waste treatment, and engineering matters.

Ultrasonic Irradiation Studies

Changes in the internal characteristics of aluminum and other metals subjected to nuclear radiation can now be studied by ultrasonic methods, according to a recent announcement by the Vibro-Ceramics Corp., Metuchen, N. J.

Use of the company's ultrasonic attenuation analyzing equipment in making absorption measurements, before and after materials are exposed to irradiation, will supply vital data regarding the alteration of physical constants and electrical properties of the metals.

Vibro-Ceramics, an associate company of Gulton Industries, Inc., will continue to offer its BBC-2 Ultrasonic

JUNE 1956 DISCUSSION SECTION

A Discussion Section, covering papers published in the July–December 1955 JOURNALS, is scheduled for publication in the June 1956 issue. Any discussion which did not reach the Editor in time for inclusion in the December 1955 Discussion Section will be included in the June 1956 issue. Those who plan to contribute remarks for this Discussion Section should submit their comments or questions in triplicate to the Managing Editor of the JOURNAL, 216 W. 102nd St., New York 25, N. Y., *not later than March 1, 1956*. All discussions will be forwarded to the author, or authors, for reply before being printed in the JOURNAL.

Analyzer to industry in addition to conducting a complete service of ultrasonic irradiation studies for other commercial firms.

Nominations for 1956 Acheson Award

William Blum, Chairman of the Acheson Medal Award Committee, would like to receive suggestions for possible candidates for the next Acheson Medal Award, to be made in the fall of 1956.

The procedure to be followed by the membership, taken from the Rules Governing the Award of the Acheson Medal, is given below.

1. Nominations shall be accepted from the membership at large.

2. All nominations, whether made by a member of the Nominating Committee or by any other member of the Society, must be accompanied by a full record of qualifications of the nominee for the award. Such supporting documents from friends of the candidate or from his organization shall be in order.

3. The nominator must assume the responsibility for providing the Chairman of the Nominating Committee with nine copies of the supporting documents, one for each member.

Nominations must be sent to the Chairman not later than March 1 of the year in which the medal is awarded and nominations will be considered closed after that date.

All nominations of candidates for the medal shall be continued in force for a period of two consecutive awards of the medal. Any unsuccessful candidate may be renominated in the usual manner for any subsequent Medal award.

Correspondence should be addressed to William Blum, 2311 Connecticut Ave. N.W., Washington 8, D. C.

Silvercel Battery Falls 143.4 Miles Without Damage

Tests completed by the Naval Research Laboratory, Washington, D. C., have revealed that a new silver-zinc storage battery, used in the Viking 12 rocket, operated perfectly after falling to earth from a height of 143.4 miles, a distance beyond the earth's atmosphere.

Retrieved from the wreckage of the rocket in the desert at White Sands, N. Mex., the battery, known as the Yardney Silvercel and manufactured by Yardney Electric Corp. of New York City, was put under test by the Navy in Washington. It performed perfectly and at present is in use as a source of electrical energy for unrelated tests now in progress.

Fansteel Expansion

A tantalum-columbium production expansion program recently was authorized by the directors of the Fansteel Metallurgical Corp., North Chicago, Ill., work to begin immediately. The cost of the program is estimated at $1,000,000.

According to Dr. Frank H. Driggs, President, approximately $200,000 will be expended in new building construction and alterations to existing buildings. The remainder will be used for equipment, principally chemical processing equipment, electric furnace equipment, and electrical switchgear.

Registry of Rare Chemicals

The National Registry of Rare Chemicals, a sort of "bureau of missing chemicals," is conducted by Armour Research Foundation of Illinois Institute of Technology, Chicago, as a free service for scientists and others seeking compounds they cannot locate at regular supply houses. While not a storehouse of chemicals, the registry has catalogued on cards more than 30,000 rare chemicals. Since it began operation in 1942 it has assisted more than 20,000 persons. For further information write to: Program Development Office, Armour Research Foundation of Illinois Institute of Technology, 10 W. 35th St., Chicago 16, Ill.

Process for Super Cleaning Atmospheric Air

Wheelabrator Corp., Mishawaka, Ind., has announced Wheelabrator Ultra-filtration, a process developed by its engineers for super cleaning atmospheric air with industrial-type air filtration equipment. The process may be used in applications formerly employing disposable or viscous filters or low voltage electrostatic precipitators. The advantages of Wheelabrator Ultra-filtration lie in extremely high cleaning efficiency, moderate cost, and nearly complete freedom from maintenance expense.

Ultra-filtration employs conventional industrial Wheelabrator Dustube dust collectors of the tubular cloth filter type. Briefly, the process involves the charging of the filter bags with a filter aid which precoats the filtering surfaces and provides a highly efficient matrix upon which the fine particles of atmospheric dust and tarry matter are collected. One application of filter aid will last from two to three years under normal conditions. Since shaking the spent filter aid and accumulated dust from the filter bags comprises the only maintenance of the filter required, maintenance costs are limited to the infrequent cleaning and recharging of the collector.

(Continued on last page of Reader Service Page)

SECTION NEWS

Council of Local Sections

The Council of Local Sections announces the following Committees:

Nominating Committee

R. A. Woofter—Pittsburgh
C. A. Hampel—Chicago
M. F. Quaely—New York

Committee on Council Bylaws

L. O. Case—Detroit
R. A. Woofter—Pittsburgh
N. C. Cahoon—Cleveland

Transportation to San Francisco Meeting

F. A. Lowenheim—New York
F. W. Koerker—Midland

Guide for Programs for Local Sections

H. T. Francis—Chicago
N. C. Cahoon—Cleveland
M. B. Diggin—New York

Procedure for Formation of New Local Sections

F. W. Koerker—Midland
P. J. Ensio—Ontario-Quebec
J. C. White—Washington-Baltimore

Encouragement of High School Science

D. T. Ferrell, Jr.—Washington-Baltimore
S. H. Dreisbach—San Francisco
J. F. Hazel—Philadelphia

If you have suggestions or recommendations which might be of value to these committees, please write to the members of the proper committee or the officers of the Council.

F. W. KOERKER, *Chairman*
Council of Local Sections

New York Metropolitan Section

A regular meeting of the Metropolitan Section was held on November 16, 1955, with Dr. Harry P. Gregor as guest speaker. His subject was "Ion

Exchange Membranes." The attendance at the dinner was 39.

The meeting was called to order by Chairman Myron B. Diggin. The Treasurer did not have a report prepared. Mr. M. F. Quaely reported for the committee appointed to consider revision of the Bylaws. He reported that a petition requesting the change had been signed by 12 members, and that this petition was filed with the Secretary. The changes proposed in the Bylaws were read at the October 20, 1955 meeting and copies of the proposed revised Bylaws distributed to all members who wished to have a copy. The Chairman announced that the proposed revision would be brought up for vote at the next meeting. There was no new business.

KENNETH B. MCCAIN,
Secretary-Treasurer

Ontario-Quebec Section

The fall meeting of the Ontario-Quebec Section was held on November 18, 1955 at McGill University, Montreal, Canada. About 95 were in attendance.

Dr. H. H. Uhlig of the Department of Metallurgy, Massachusetts Institute of Technology, President of the Society, spoke on "Corrosion as an Electrochemical Process." He stated that the electrochemical theory of corrosion had its beginnings as early as 1801 through a publication of Wollaston, which was followed in 1830 by a discussion of de la Rive, and in 1903 by W. R. Whitney. The original theory was applied only to rusting and to acid attack of metals. Within the last few years, however, it has been recognized that other forms of corrosion are also electrochemical in nature, these being stress corrosion cracking, pitting, corrosion fatigue, intergranular corrosion and dezincification. As a result, considerable progress has been made toward an understanding of general corrosion reactions, and, in particular, it has been possible to predict that preventive measures like cathodic protection can be used effectively, with few exceptions, to stop any kind and all forms of corrosion damage.

The kinds of cells operating in corrosion processes are three in number. First, the dissimilar electrode cell accounts, for example, for the specific corrosion rate of magnesium or aluminum containing cathodic impurities, the behavior of galvanic couples, and the effect of variable cold work or differing grain size on the corrosion rate. In 1830 de la Rive presented data showing that the corrosion-accelerating effect of an added impurity to zinc immersed in acid depends on the nature of the impurity. Today we know that the important property determining rate is the hydrogen overvoltage characteristic of the impurity. This result is directly predictable from electrochemical theory.

A second type of cell is the concentration cell, the most important form of which is the differential aeration cell. The latter accounts for the fact that iron covered with mounds of moist rust tends to pit under the mounds, and it is also such cells that commonly initiate pits in stainless steels, aluminum, and other metals.

The third kind of cell is the differential temperature cell made up of electrodes or electrolytes at differing temperatures. These cells often operate in corrosion of heat exchangers, refrigerators, and boilers.

The mechanism of pitting in stainless steels immersed in sea water can be used to illustrate the application of electrochemistry to a specific corrosion process. When current flows, chloride ions transfer to local anodic areas on the metal surface acting as pit nuclei, and high current densities cathodically protect adjoining areas. Concentrated solutions of metal chlorides accumulate within the growing pit, these solutions having the property of destroying passivity and of setting up a cell between passive and active metal having a potential difference of about 0.5 v. The slow leaching out of corrosion products from a pit in the direction of gravity, destroying passivity in the process, explains why pits are often elongated. Pitting tendency can be inhibited by making the corrosive environment alkaline; hydroxyl ions are available which move more rapidly into the pit than do chloride ions and, hence, precipitate basic metal chlorides. The latter no longer have the property of destroying passivity and, hence, oxygen can diffuse into the pit and re-establish passivity. The fact that titanium does not corrode in sea water to form soluble chlorides, but basic chlorides instead, explains why titanium does not pit, even after many years' exposure.

Polarization curves can be used to supplement our knowledge of corrosion mechanisms and to explain the basic mechanism of cathodic protection. Polarization curves, in general, are useful as a means of measuring the degree of passivity, and can also be used to calculate the

very small corrosion rates of passive metals in passivating environments. Similarly, cathodic polarization data, in particular hydrogen overvoltage measurements, combined with corrosion potentials can be employed to calculate corrosion rates of metals in specific media.

In turn, the theory which applies here can be used to understand the origin of variations in measurements of the standard potential for iron obtained by various investigators in the past for so-called equilibrium potential measurements. The discrepancy of 0.031 v between the two most recently reported values for E^0 can be caused by the order of only 0.5 mg/dm²/day difference in the corrosion rate which is extremely small, and which can easily be accounted for by different sources of iron used for the potential measurements or by slight variations in electrolyte. Corrosion theory, therefore, has reached the stage where it is able to contribute to, as well as draw from, principles of physical chemistry.

Dr. W. C. Gardiner of the Olin Mathieson Chemical Corp. spoke on "Brine Impurities and Their Effect on the Operation of Caustic-Chlorine Cells." The mercury cell process for alkali-chlorine production was dealt with in particular. This process was described and illustrated with photographs of Mathieson E-8 cells. The particular conditions required by mercury cells were outlined. The various sources of salt and the impurities to be expected were mentioned. Various methods of handling brine in commercial plants were described and illustrated with flowsheets. It was mentioned that the effects of individual impurities had been studied by various investigators starting with Walker and Paterson of McGill University in 1903. Additional results obtained by Japanese, Swedish, Russian, and Austrian workers had been published during the past four years. Details of the Swedish results were discussed in detail. It was concluded that the most desirable brine for mercury cells would be nearly saturated with NaCl. It may be approximately saturated with $CaSO_4$ if the pH is maintained at about 3. Magnesium and iron should be below 5 mg and 10 mg per liter, respectively, and vanadium and chromium below 0.1 and 0.1 ppm, respectively.

During the general discussion of both papers which followed, representatives of six different industries using alkali-chlorine cells gave information regarding their cells and outlined some of the problems which they have encountered.

President Uhlig gave a brief talk on The Electrochemical Society, its aims, its accomplishments, and its problems.

R. R. Rogers,
Secretary-Treasurer

San Francisco Section

The regular meeting of the Section was held at the University of California Faculty Club on November 30, 1955. Dr. T. D. Parks, Director of Research, Clorox Chemical Co., delivered a talk entitled "Theory and Application of Amperometric Titrations."

After a brief outline of the history and development of polarography, Dr. Parks discussed some of the more recent uses of both polarographic and amperometric techniques in analytical determinations. The use of both the dropping mercury and the rotating platinum microelectrode was illustrated. The effect of temperature, "poisoning" materials, and the speed of rotation of the microelectrode were discussed.

After the talk, Dr. Parks answered specific questions relating to the analysis of materials commonly encountered in routine industrial analytical determinations, such as the quantitative evaluation of the concentration of lead, halide, phosphorus, molybdenum, and sulfate ions. The application of mixed solvents and the use of nonaqueous solvents in amperometric work was also discussed.

BERNARD PORTER

Washington-Baltimore Section

The 35th technical meeting of the Section was held on November 16, 1955 at Johns Hopkins University in Baltimore. The first speaker of the evening was Dr. John J. Chapman, Research Contract Director, Dielectrics Laboratory of the Johns Hopkins University, whose topic was "Dielectric Properties of Laminated Materials." Dr. Chapman described the variation of dielectric strength and loss factor of a number of laminated materials, over a range of frequency from 60 cycles/sec to 100 megacycles/sec. Data concerning the effects of temperature and moisture adsorption on the dielectric properties were also presented.

Dr. John M. Kopper, Research Scientist of the Radiation Laboratory, Johns Hopkins University, spoke on the subject "The Effect of Forming Current Frequency on the Abrasion and Corrosion Resistances of Protective Coatings on Magnesium." Dr. Kopper described the coatings formed in HAE electrolyte with alternating current frequencies from 9 to 2700 cycles per second. It was found that the abrasion resistance of the coatings rose to an asymptotic maximum at approximately 130 cycles per second, and that the corrosion resistance decreased with increasing frequency.

The third topic of the evening was "A Magnetic Model of Crystal Structure," presented by Dr. Robert B. Pond, Assistant Professor of Metallurgy, Mechanical Engineering Department, Johns Hopkins University. A unique model of the crystal structure of hexagonal close-packed and face-centered cubic metals was described. The individual atoms of the crystallographic array were represented as dipolar units. By using this model, an explanation of the mechanism of plastic deformation by slip was presented. A new dislocation form was described, and a short motion picture showed the working mechanical model.

JEANNE BURBANK, *Secretary*

ECS Membership Statistics

The following two tables give breakdown of membership as of January 1, 1956. The Secretary's Office feels that a regular accounting of membership will be very stimulating to membership committee activities. In Table I it should be noted that the totals appearing in the right-hand column are *not* the sums of the figures in that line since members belong to more than one Division and, also, because Sustaining Members are not assigned to Divisions. But the totals listed are the total membership in each Section. In Table I, Sustaining Members have been credited to the various Sections.

TABLE I. *ECS Membership by Sections and Divisions*

Section	Division												
	Battery	Corrosion	Electric Insulation	Electrodeposition	Electronics	Electro-Organic	Electrothermics & Met.	Industrial Electrolytics	Theoretical Electrochem.	No Division	Totals as of 1/1/56	Totals as of 1/1/55	Net Change
Chicago	9	33	2	44	14	8	10	14	20	13	105	102	+3
Cleveland	42	36	4	47	32	10	20	28	42	14	171	150	+21
Detroit	4	15	6	31	5	6	4	3	19	20	73	67	+6
India	7	1	2	10	2	5	3	9	8	3	23	23	0
Midland	5	12	0	3	1	2	6	15	8	4	38	36	+2
New York	63	98	19	126	70	26	45	55	74	76	427	374	+53
Niagara Falls	6	19	0	17	2	5	51	45	16	24	141	105	+36
Pacific Northwest	5	11	0	9	1	2	5	13	13	5	40	29	+11
Philadelphia	19	28	4	39	42	16	17	13	14	29	160	144	+16
Pittsburgh	3	29	3	22	11	5	21	13	27	11	85	69	+16
San Francisco	6	10	2	14	7	3	7	16	11	4	43	38	+5
Washington-Baltimore	30	37	9	31	18	3	11	13	27	7	108	104	+4
Quebec-Ontario	7	11	0	13	1	3	24	19	7	12	59	43	+16
U.S. Non-Section	72	140	29	157	88	54	92	93	140	101	622	581	+41
Foreign Non-Section	31	38	8	46	18	24	25	52	50	54	175	176	−1
Total as of Jan. 1, 1956	309	518	88	609	312	172	341	401	476	377	2270		
Total as of Jan. 1, 1955	281	516	81	590	276	169	309	374	460	306		2141	
Net Change	+28	+2	+7	+19	+36	+3	+32	+27	+16	+71			

NEW MEMBERS

In December 1955 the following were approved for membership in The Electrochemical Society by the Admissions Committee:

Active Members

JOHN H. ADAMS, Miami Lab., Eagle-Picher Co., Miami, Okla. (Electronics)

JOHN A. AYRES, General Electric Co.; Mail add: 1419 Wright Ave., Richland, Wash. (Corrosion)

A recent action of the Board of Directors of the Society requires that, commencing January 1, 1956, all prospective members include first year's dues with their applications for membership.

Also, please note that, if sponsors sign the application form itself, processing can be expedited considerably.

TABLE II. *ECS Membership by Grade*

	Total as of 1/1/56	Total as of 1/1/55	Net Change
Active	2013	1889	+124
Life	14	14	0
Emeritus	34	39	−5
Associate	49	63	−10
Student	53	31	+18
Honorary	5	5	0
Sustaining	102	100	2
Total	2270	2141	+129

RICARDO O. BACH, Central Research Labs., American Smelting & Refining Co., South Plainfield, N. J. (Electrodeposition)

WILLIAM G. BATT, The Biochemical Research Foundation of the Franklin Institute, Newark, Del. (Electrodeposition)

DANIEL BERMANE, Mass. Institute of Technology; Mail add: 4 Scott St., Cambridge, Mass. (Theoretical Electrochemistry)

JOHN J. DRANEY, Merck & Co.; Mail

add: 46 Van Buren Ave., Teaneck, N. J. (Electronics)

LIPMAN S. GERBER, Detroit Arsenal, U. S. Army Ordnance; Mail add: 2315 Calvert St., Detroit 6, Mich. (Battery)

JACK D. GUTTENPLAN, Central Engineering, Chrysler Corp., P.O. Box 1118, Detroit 31, Mich. (Battery, Corrosion, Electrodeposition)

WARREN W. HARRIS, Union Carbide Nuclear Co.; Mail add: 101 W. Damascus Rd., Oak Ridge, Tenn. (Corrosion)

JULIUS J. HARWOOD, Office of Naval Research; Mail add: 2511 Jennings Ct., Silver Spring, Md. (Corrosion)

FRANK W. HURD, Union Carbide Nuclear Co., Rm. 1701, 30 E. 42 St., New York, 17, N. Y. (Electrodeposition, Electrothermics and Metallurgy, Industrial Electrolytic)

WALTER J. KARASH, Duro-Test Corp., 2321 Hudson Blvd., North Bergen, N. J. (Electronics)

RINE KRUGER, Engineering Dept., Delco Battery Operations, Muncie, Ind. (Battery)

JAMES F. MACHOLL, Electric Storage Battery Co.; Mail add: 4618 Mackall Rd., South Euclid 21, Ohio (Battery)

JOHN D. METTLER JR., Electrometallurgical Co., 137-47th St., Niagara Falls, N. Y. (Electrodeposition, Electrothermics and Metallurgy, Industrial Electrolytic)

STANLEY J. NOESEN, General Electric Research Lab., Metals and Ceramics Bldg., Rm. 249, Schenectady, N. Y. (Electrothermics and Metallurgy)

HARRY G. OSWIN, Kaiser Aluminum & Chemical Corp.; Mail add: 818 W. 14 Ave., Spokane, Wash. (Corrosion)

FREDERICK J. PORT, Electric Storage Battery Co.; Mail add: 2335 Ardleigh Dr., Cleveland Heights, Ohio (Battery)

GEORGE W. PRATT, JR., Mass. Institute of Technology; Mail add: Glezen Lane, Wayland, Mass. (Electronics)

FRED M. REINHART, National Bureau of Standards, Rm. 105, N.W. Bldg., Washington 25, D. C. (Corrosion)

HAROLD R. SCHMIDT, General Engineering Lab., General Electric Co., 1 River Rd., Schenectady, N. Y. (Corrosion, Theoretical Electrochemistry)

ALBERT SHTASEL, Fansteel Metallurgical Corp., North Chicago, Ill. (Electronics, Theoretical Electrochemistry)

ROBERT C. SOMMER, Central Research Lab., American Smelting & Refining Co., South Plainfield, N. J. (Electrodeposition)

DAVID R. STERN, American Potash & Chemical Corp.; Mail add: 201 W. Washington Blvd., Whittier, Calif. (Electro-Organic, Industrial Electrolytic)

HENRY F. STOUT, Columbia-Geneva Steel Div.; Mail add: 1485 Grove Way, Concord, Calif. (Corrosion, Electrodeposition)

Associate Members

LEE ALDERUCCIO, Van der Horst Corp. of America, Olean, N. Y. (Electrodeposition)

FRED A. CAFASSO, New York University; Mail add: 405 Cary Ave., Staten Island 10, N. Y. (Theoretical Electrochemistry)

Student Associate Members

JAMES B. DONIHEE, University of Maryland; Mail add: 3414 Carpenter St., S.E., Washington, D. C. (Electrodeposition)

JULIUS KLERER, Graduate School of Arts & Sciences, New York University; Mail add: 880 Summit Ave., Jersey City 7, N. J. (Theoretical Electrochemistry)

Reinstatements to Active Membership

THOMAS C. BREITNER, American Smelting & Refining Co., South Plainfield, N. J. (Battery, Electrodeposition, Electro-Organic, Theoretical Electrochemistry)

FRANK P. ROMANOFF, Appollo Metal Works; Mail add: 6650 S. Oak Park Ave., Chicago, Ill. (Corrosion, Electrodeposition)

Deceased Members

HENRY PAIGE, New York, N. Y.

JOHN B. MERRILL, Towanda, Pa.

PERSONALS

WILBUR C. MYERS is at present employed as Senior Research Engineer in the Electronics Division of the National Cash Register Co., Hawthorne, Calif. He previously was located at Cleveland, Ohio.

JEROME KRUGER, physical chemist, has joined the Corrosion Section of the Metallurgy Division of the National Bureau of Standards, Washington, D. C. Dr. Kruger will direct a new Bureau project for studying the surface reactions of metal single crystals in selected environments. From 1952 to 1955, Dr. Kruger was engaged in research on corrosion inhibitive coatings at the Naval Research Laboratory in Washington.

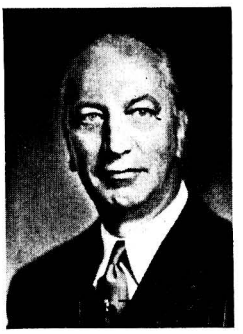

R. WOLCOTT HOOKER

R. WOLCOTT HOOKER, Vice-President of Hooker Electrochemical Co., Niagara Falls, N. Y., recently was elected President of the Synthetic Organic Chemical Manufacturers Association at the 34th annual meeting held in the Hotel Statler, New York City.

LOREN C. HURD

LOREN C. HURD has been appointed President and a Director of the Metals Disintegrating Co., Inc., Elizabeth, N. J., manufacturers of metal powders, metal pigments, metal abrasives, and pulverizing, air conveying, and dust collecting equipment.

GEORGE T. PAUL has accepted a position with the International Nickel Co., Inc., New York City, in the Corrosion Engineering Section, Development and Research Division. He had been with the American Cyanamid Co., Bound Brook, N. J.

(Continued on page 39C)

Society Prizes and Awards

The Edward Goodrich Acheson Medal and Prize

The Edward Goodrich Acheson Gold Medal and $1,000 Prize were founded by Dr. Acheson in August 1928.

The award is made once every two years (first award at the Fall Meeting, 1929) to the person who shall have made a distinguished "contribution to the advancement of any of the objects, purposes, or activities . . . of the Society. Such contribution may consist of but shall not be limited to (*a*) a discovery pertaining to electrochemistry, electrometallurgy, or electrothermics, (*b*) an invention of a plan, process or device, or research evidence by a paper embodying information, useful, valuable, or significant in the theory or practice of electrochemistry, electrometallurgy, or electrothermics, and/or (*c*) distinguished services rendered to the Society or its successor."

The award is made without distinction on account of sex, citizenship, race, or residence. See *Trans. Electrochem. Soc.*, **54**, 6 (1928).

The Palladium Medal

The Palladium Medal of The Electrochemical Society was founded in 1950. The source of funds for the establishment of the medal is the royalties derived from sales of the "Corrosion Handbook" which was sponsored and largely written by members active in the Corrosion Division of the Society. Dr. H. H. Uhlig served as Editor-in-Chief.

The award of the medal is to be made every two years to a scientist, in recognition of original and outstanding contributions to the knowledge of corrosion in one or more of the following fields: the theory of corrosion or corrosion control, electrode potentials, properties of electrolytes, electrode reactions, and the surface properties of metals. The jury for the selection of the medalist is appointed by the Board of Directors of the Society and consists of three members, including one member from the Corrosion Division and one from the Theoretical Division, both of whom are active in their respective fields. See *J. Electrochem. Soc.*, **98**, 95*C* (1951).

The Joseph W. Richards Memorial Lectureship

Dr. Joseph William Richards was one of the founders of The Electrochemical Society, and its first President. He was Secretary and Editor of the Society's TRANSACTIONS from 1904 to 1921. His very active and untiring interest in the Society and in the science and art of electrochemistry reflected itself in the rapid growth of the Society and of the electrochemical industry throughout the world. From the very start, Dr. Richards fostered the international spirit.

The Joseph W. Richards Memorial Lectureship was established in 1929 by a group of friends and admirers of Dr. Richards. The interest of the fund is used to meet the expenses incurred by inviting and entertaining distinguished scientists. See *Trans. Electrochem. Soc.*, **57**, 30 (1930).

The Electrochemical Society Prize to Young Authors

An annual prize of one hundred dollars was established by the Board of Directors in July 1928. The prize is awarded to the author of the best paper printed in the yearly volume of the JOURNAL of the Society. The judges to pass upon the merits of the paper are the Chairman of the Publications Committee, the Secretary of the Society, and three members of the Society, and two alternates, selected by the Chairman of the Publications Committee, the Committee being at liberty to invite the opinion of members not on the Committee.

The prize is open to students and graduates under thirty-one years of age of any technical school, college, or university, no matter where located. See *Trans. Electrochem. Soc.*, **55**, 22 (1929); **92**, viii (1947).

Francis Mills Turner Award, Sponsored by the Reinhold Publishing Corporation

For several years, Francis Mills Turner personally offered an annual prize consisting of $50.00 worth of scientific and technical books published

Honorary Members of the Society

CHARLES F. CHANDLER,* New York, N. Y.	Volume 35 (1919)
EDGAR F. SMITH,* Philadelphia, Pa.	Volume 35 (1919)
CARL HERING,* Philadelphia, Pa.	Volume 41 (1922)
EDWARD G. ACHESON,* Niagara Falls, N. Y.	Volume 43 (1923)
WILDER D. BANCROFT,* Ithaca, N. Y.	Volume 47 (1925)
EDWARD WESTON,* Montclair, N. J.	Volume 50 (1926)
THOMAS A. EDISON,* Orange, N. J.	Volume 54 (1928)
W. LASH MILLER,* Toronto, Canada	Volume 55 (1929)
EDWARD DEAN ADAMS,* New York, N. Y.	Volume 57 (1930)
CHARLES F. BURGESS,* Chicago, Ill.	Volume 62 (1932)
FREDERICK MARK BECKET,* New York, N. Y.	Volume 66 (1934)
L. H. BAEKELAND,* New York, N. Y.	Volume 69 (1936)
ROBERT A. WITHERSPOON,* Montreal, Canada	Volume 78 (1940)
ARCHER E. WHEELER, New York, N. Y.	Volume 80 (1941)
W. R. WHITNEY, Schenectady, N. Y.	Volume 85 (1944)
PAUL J. KRUESI, Chattanooga, Tenn.	Volume 85 (1944)
COLIN G. FINK,* New York, N. Y.	Volume 89 (1946)
JOHN W. MARDEN, Chester, N. J.	Volume 91 (1947)
WILLIAM BLUM, Washington, D. C.	Volume 100 (1953)

* Deceased

by the Reinhold Publishing Corporation. At the time of his demise, the Reinhold Publishing Corporation established the "Francis Mills Turner Memorial Award, Sponsored by the Reinhold Publishing Corporation," consisting of $100.00 worth of scientific and technical books to be given each year to an author under 31 years of age. This revision was gratefully accepted by the Board of Directors at the Society convention held in Philadelphia, May 4 to 8, 1952. See *J. Electrochem. Soc.*, **99**, 162C (1952).

Consolidated Fellowship Fund

Due to the deterioration of the Weston Fellowship funds, the Board of Directors on October 26, 1952 established a Consolidated Fellowship Fund from the accumulated earnings of the Weston Fellowship Fund, the entire Roeber Research Fund, the excess earnings of the Acheson Fund, and the $1000 returned by John W. Marden (Acheson Award) at the Montreal Meeting. This fund will be accumulated until such time as the Society has available sufficient yearly income from this source to justify offering a fellowship, at which time the Society again will be in a position to sponsor graduate studies in electrochemistry.

Former recipients of the Acheson Medal and Weston Fellowship are listed below.

Winners of Society Prizes and Awards

Acheson Medalists

EDWARD G. ACHESON* — Artificial Graphite and Carborundum—**56,** 7 (1929).

EDWIN F. NORTHRUP*—Induction Furnaces—**60,** 8 (1931).

COLIN G. FINK*—Electrochemistry—**64,** 2 (1933).

FRANK J. TONE*—Electrothermics—**68,** 2, 8 (1935).

FREDERICK M. BECKET*—Electrothermics—**72,** 3 (1937).

FRANCIS C. FRARY—Electrometallurgy—**76,** 4 (1939).

CHARLES F. BURGESS*—Electrochemistry—**82,** 3 (1942).

WILLIAM BLUM — Electrodeposition — **86,** 4 (1944).

H. JERMAIN CREIGHTON—Electro-Organic Chemistry—**90,** 5 (1946).

DUNCAN A. MACINNES—Electrochemistry—**94,** 4P (1948).

GEORGE W. VINAL — Batteries — **97,** 231C (1950); **98,** 11C (1951).

JOHN W. MARDEN—Electronics—**100,** 37C (1953).

GEORGE W. HEISE—Batteries—**101,** 291C (1954).

Weston Fellowship Holders

EDWARD B. SANIGAR*—"The Titration of Potassium Cyanide and of Free Cyanide in Silver-Plating Solutions by Means of Silver Nitrate"—**58,** 435 (1930); "Electrodeposition of Silver from Sulfate, Nitrate, Fluoborate and Fluoride Solutions"—**59,** 307 (1931).

KARL SOLLNER—"An Experimental Study of Negative Osmosis. Part I"; "Experimental Verification of a New Theory Concerning the Mechanism of Anomalous Osmosis. Part II"—**61,** 477, 487 (1932).

MARLIN E. FOGLE—"A Study of Cuprous Oxide Solid Photoelectric Cells"—**66,** 271 (1934).

ROBERT D. BLUE—"Electrodeposition of Aluminum from Non-Aqueous Solutions"—**65,** 339 (1934).

PIERRE A. JACQUET—"Effect of Colloids on Electrodeposition"—**65,** 21 (1934).

MYRON A. COLER—"Electrolytic Processes in the Magnetic Field"—**72,** 247 (1937).

HENRY B. LINFORD—"The Effect of the Speed of Rotation on the Electrode Potentials of Copper and Zinc"—**72,** 461 (1937).

GARTH L. PUTNAM—**71,** 26 (1937).

VITTORIO DE NORA—**73,** 39 (1938).

WALDEMAR P. RUEMMLER—**75,** 52 (1939); **77,** 50 (1940).

RODNEY E. BLACK—**79,** 44 (1941).

WILLIAM E. ROAKE—**81,** 46 (1942).

ROBERT D. MISCH—**93,** 14P (1948).

MASSOUD T. SIMNAD—**94,** 3N (1948)†; **97,** 161C (1950).

Joseph W. Richards Memorial Lecturers

JOHN A. MATHEWS,* Vice-President and Director of Research, Crucible Steel Company, New York, N. Y. "The Electric Furnace and the Alloy Age," **61,** 143 (1932).

R. S. HUTTON, Goldsmiths' Professor of Metallurgy, University of Cambridge, England. "Faraday and His Electrochemical Researches," **64,** 13 (1933).

W. S. LANDIS,* Vice-President and Director, American Cyanamid Company, New York, N. Y. "Joseph W. Richards, The Teacher—The Industry," **66,** 6 (1934).

KARL K. DARROW, Physicist, Bell Telephone Laboratories, New York, N. Y. "Electricity in Gases," **69,** 67 (1936).

CHARLES H. HERTY,* Director, Herty Foundation Laboratory, Savannah, Ga. "The Utilization of Southern Pine," **73,** 50 (1938).

BRADLEY STOUGHTON, Dean of Engineering, Lehigh University, Bethlehem, Pa. "Modern Marvels of Electrometallurgy," **76,** 29 (1939).

VLADIMIR K. ZWORYKIN, Associate Director of RCA Research Laboratories, Camden, N. J. "The Electron Microscope," **80,** 14 (1941).

B. D. SAKLATWALLA,* Metallurgical Consultant, Pittsburgh, Pa. "Thermal Reactions in Ferro-Alloy Metallurgy, the Basis of Alloy Steel Development," **84,** 13 (1943).

STEWART J. LLOYD, Professor of Chemical Engineering, University of Alabama, University, Ala. "Freedom in Science," **89,** 9 (1946).

OLIVER W. STOREY, Consultant, Burgess Battery Company Chicago, Ill. "Research in Industry—Is Government Antagonistic to It?" **96,** 3P (1949); **97,** 9C (1950).

J. O'M. BOCKRIS, Lecturer, Department of Inorganic and Physical Chemistry, Imperial College of Science and Technology, London University, London, England. "Overpotential," **98,** 153C (1951).

Palladium Medalists

CARL WAGNER, Department of Metallurgy, Massachusetts Institute of Technology, Cambridge, Mass. "The Electrochemistry of Ionic Crystals," **99,** 346C (1952).

NATHANIEL HOWELL FURMAN, Chairman, Department of Chemistry, Princeton University, Princeton, N. J. "Coulometry—Related Phenomena

* Deceased.

† *J. Electrochem. Soc.*

* Deceased.

of Electrolysis and Current-Sweep Polarography," **101,** 19C (1954).

ULICK RICHARDSON EVANS, Cambridge, England. "Electrochemical Corrosion in Nearly Neutral Liquids," **103,** 73 (1956).

Winners of Young Authors' Prize

WILLIAM C. GARDINER—"Hydrolysis of Mercurous Sulfate by Cadmium Sulfate Solution in the Weston Normal Cell"; "Oxidation of the Depolarizer in Preparing Standard Cells"; "Crystalline Mercurous Sulfate and the Weston Normal Cell"—**56,** 111 (1929).

DWIGHT K. ALPERN—"Engineering Development of Photovoltaic Cells"—**58,** 275 (1930).

FRANK L. JONES—"Electrodeposition of Tungsten from Aqueous Solutions"—**59,** 461 (1931).

F. W. GODSEY, JR.—"Alternating Current Capacities of Electrolytic Condensers"; and "Potential Gradients in Anodic Films"—**61,** 515, 549 (1932).

B. L. BAILEY—"Hardness Values for Electrochemical Products"—**63,** 369 (1933).

JOSEPH R. HEARD, JR.—"Electro-Organic Oxidations in Concentrated Aqueous Organic Salt Solutions"—**65,** 301 (1934).

UPTON B. THOMAS, JR.—"Electrochemical Behavior of Lead, Lead-Antimony and Lead-Calcium Alloys in Storage Cells"—**68,** 293 (1935).

W. A. JOHNSON—"Studies of Overvoltage: Effect of Fusion of the Cathode and Effect of Temperature on Gas Polarization"—**70,** 259 (1936).

R. SPENCER SOANES—"Potential Distribution in High Current Carbon Arcs in Air"—**72,** 281 (1937).

N. B. NICHOLS—"The Cathode Ray Oscillograph Applied to the Dropping Mercury Electrode"—**73,** 193 (1938).

G. A. MOORE—"Comportment of Palladium-Hydrogen System toward Alternating Electric Current"—**75,** 237 (1939).

J. S. MACKAY—"Photoelectric Cells Sensitive to Long Wave Length Radiation: The Bismuth Sulfide Cell"—**77,** 299 (1940).

EDWARD ADLER—"Photovoltaic Effect"; "Semi-Conductor Photocells and Rectifiers"—**79,** 367, 377 (1941).

SIDNEY SPEIL—"Electrophoretic Dewatering of Clay"—**81,** 119 (1942).

WALTER G. BERL—"A Reversible Oxygen Electrode"—**83,** 253 (1943).

JOHN P. COYLE—"The Extraction of Indium from Complex Lead-Tin Alloys"—**85,** 223 (1944).

AUSTIN E. HARDY—"The Photoconductivity of Zinc-Cadmium Sulfide as Measured with the Cathode-Ray Oscillograph"—**87,** 355 (1945).

NORMAN A. NIELSEN—"Passivation of Stainless Steels"—**89,** 167 (1946).

HENRY LEIDHEISER, JR.—"The Influence of Crystal Face on the Electrochemical Properties of a Single Crystal of Copper"—**91,** 95 (1947).

MICHAEL A. STREICHER—"The Dissolution of Aluminum in Sodium Hydroxide Solutions"—**93,** 285 (1948).

J. C. GRIESS, JR.—"The Electrodeposition Behavior of Traces of Silver"—**95,** 33 (1949).

GEORGE W. MURPHY—"The Separation of Simple Electrolytes in Solution by an Electro-Gravitational Method"—**97,** 405 (1950).

JOHN T. BYRNE—"Critical Interpretation of Electrodeposition Studies Involving Traces of Elements"—**98,** 457 (1951).

W. E. KUHN—"Production of Titanium Ingots by Melting Sponge Metal in Small Inert-Atmosphere Arc Furnaces"; "Development of Graphite Electrodes and Study of Heat Losses with Different Electrodes in the Single Electrode Inert-Atmosphere Arc Furnace"—**99,** 89, 97 (1952).

J. HALPERN—"Kinetics of the Dissolution of Copper in Aqueous Ammonia"—**100,** 421 (1953).

M. J. PRYOR—"The Protective Action of Pigments on Steel"—**101,** 141 (1954).

Winners of Turner Book Prize

SIDNEY SPEIL—"Electrophoretic Dewatering of Clay"—**81,** 119 (1942).

WALTER G. BERL—"A Reversible Oxygen Electrode"—**83,** 253 (1943).

JOHN P. COYLE—"The Extraction of Indium from Complex Lead-Tin Alloys"—**85,** 223 (1944).

JAMES T. WABER—"Stress Corrosion Cracking of Mild Steel"—**87,** 209 (1945).

BURKE CARTWRIGHT—"Electrolysis of Manganese into a Metal Cathode from Suspensions of Manganese Oxide and Carbon in Molten Manganous Chloride"—**89,** 373 (1946).

AUSTIN E. HARDY—"A Combination Phosphorometer and Spectroradiometer for Luminescent Materials"—**91,** 221 (1947).

MICHAEL A. STREICHER—"The Dissolution of Aluminum in Sodium Hydroxide Solutions"—**93,** 285 (1948).

RALPH F. HOECKELMAN—"Salt-Bath Chromizing"—**96,** 262 (1949).

PAUL DELAHAY—Parts I and II of the paper "A Polarographic Method for the Indirect Determination of Polarization Curves for Oxygen Reduction on Various Metals"—**97,** 198, 205 (1950).

KURT H. STERN AND CHARLES C. TEMPLETON—"The Electrical Conductance of Solutions of Cobalt (II) Nitrate Hexahydrate in Acetophenone at 25°C"—**97,** 443 (1951).

P. T. GILBERT—"The Nature of Zinc Corrosion Products"—**99,** 16 (1952).

ROBERT B. HOLDEN—"The Hot-Wire Process for Zirconium" (co-author, Bernard Kopelman)—**100,** 120 (1953).

D. A. VERMILYEA—"Formation of Anodic Oxide Films on Cathodes"—**101,** 389 (1954).

Personals

(Continued from page 36C)

JAMES T. MCKENZIE of the American Cast Iron Pipe Co., Birmingham, Ala., is the recipient of the 1955 Southern Chemist Award of the American Chemical Society. The medal was presented for the Memphis Section of the ACS by S. F. Clark, University of Mississippi, at the Southeastern Regional Meeting of ACS local sections in Columbia, S. C., in recognition of Dr. MacKenzie's work in metallurgical chemistry.

ROBERT B. MACMULLIN has received the Professional Achievement Award of the New York section of the American Institute of Chemical Engineers. He is with R. B. MacMullin Associates.

P. S. NARAYANA has been elected to the Managing Committee of the Institute of Management, Bangalore.

EDWARD HILLNER, formerly a student and Teaching Fellow at New York University, New York City, recently was inducted into the U. S. Army. He is at the Rocky Mt. Arsenal, Denver, Colo.

NORMAN P. SWEENY, recently separated from active duty in the U. S. Army, is now at the graduate school, Indiana University, Bloomington, Ind.

Nonmember Journal Prices

As of January 1, 1956, nonmember subscription rates to the JOURNAL are $18.00 instead of the $15.00 previously charged, and single copies of the JOURNAL to nonmembers are $1.75 instead of $1.50.

S. KRISHNAMURTHY has left Bangalore to join the Indian Standards Institution, New Delhi, as Assistant Director (Chemicals).

B. K. RAM PRASAD has been appointed Director of the Central Electrochemical Research Institute, Karaikudi.

ROBERT GERBERICH is at the University of Rochester, Rochester, N. Y., where he has an assistantship while studying for his master's degree. He was formerly a student at the College of Wooster, Wooster, Ohio.

ELLIS H. GATES has moved from Salt Lake City, Utah, to Canon City, Colo. He recently accepted a position as Metallurgical Engineer with the Metallics Recovery Corp. in Florence, Colo.

HARRY C. GATOS has resigned from his position with the E. I. du Pont de Nemours & Co., Inc., Wilmington, Del., to join the Lincoln Laboratory, Massachusetts Institute of Technology, Lexington, Mass.

RICHARD P. HUNNICUTT, formerly with the General Motors Corp., Mich., is now employed by the Aerojet-General Corp., Calif., as a metallurgist.

ALLAN E. CHESTER

Dr. Allan E. Chester, Vice-President of the Promat Division, Poor and Co., died on November 20, 1955 en route to Honolulu. He was 54 years old.

He received his Bachelor of Science degree at Kenyon College, Gambier, Ohio, and a Doctor of Science degree from California Institute of Technology, Pasadena, Calif. An outstanding research chemist, Dr. Chester held many patents in the fields of electrochemistry and vitreous enameling. He came to Poor and Co. from Ferro Corp. in 1938, and, as Research Director, formed the Promat Division. He was made Vice-President in 1952.

Besides The Electrochemical Society, which he joined in 1943, Dr. Chester was active and held offices in a number of technical societies, among them, The American Electroplaters' Society, the American Society for Testing Materials, the Ceramic Society, the National Association of Chrome Furniture Manufacturers, the Faraday Society, and The American Association for the Advancement of Science.

Dr. Chester is survived by his wife, Alice, Highland Park, Ill.; a daughter, Sister Vera C.S.J., Jamestown, N. D.; and two step-sons, John H. Bins, Lake Bluff, Ill., and Thomas W. Bins, Lake Forest, Ill.

EMPLOYMENT SITUATIONS

Please address replies to box shown, c/o The Electrochemical Society, Inc., 216 W. 102nd St., New York 25, N. Y.

Positions Available

PATENT OFFICE EXAMINERS. Engineers and scientists are needed immediately as Patent Examiners by the U. S. Patent Office, Washington, D. C. Patent Examiners pass upon applications for patents in a wide range of technical fields. The job keeps them in close touch with the latest developments in these fields. Salaries start at $4,345 per year and it is possible to reach $7,570 in 5½ years. Vacations and sick leave and pension benefits are liberal. The positions call for a college degree in engineering or applied science or a college degree with a major in chemistry or physics or with certain combined credits in these fields. There is no examination. For further information, address the Commissioner of Patents, Washington 25, D. C.

DRY CELL ENGINEER VICE-PRES. POSITION OPEN

DRY CELL CORP. IN MEXICO CITY WANTS ENGINEER (Chemist or Physicist) who has heavy experience in Production and Laboratory work in the manufacture of Dry Cells. MUST assume responsibility for production. HI-SALARY plus SHARE IN PROFITS, low taxes, excellent climate, and low living costs.

Send complete resumé and interview will be arranged. All replies will be held in strict confidence.

APARTADO POSTAL No. 7355
MEXICO 1, D. F.

ENGINEERS, ELECTRONIC SCIENTISTS, METALLURGISTS, PHYSICISTS, PHYSIOLOGISTS, PSYCHOLOGISTS, TECHNOLOGISTS. The Naval Air Material Center, located at the Naval Base, Philadelphia, Pa., has vacancies in the above engineering and scientific positions which must be filled. The Center is engaged in an extensive program of aeronautical research, development, experimentation, and test operations for the advancement of Naval Aviation. Engineering vacancies exist in the following options: Electrical, Electronics, General, Industrial, Mechanical, Structural, and Aeronautical (various suboptions). Starting salaries range from $3670 to $8990 per annum. Application for Federal Employment, Standard Form 57, should be filed with the Industrial Relations Dept., Naval Air Material Center, Naval Base, Philadelphia 12, Pa. Applications may be obtained from the above address or information as to where they are available may be obtained from any first or second class post office.

Positions Wanted

CHEMIST, 36, 11 years' experience, including batteries, electroplating, general physical and chemical commerical testing, seeks New Jersey, Philadelphia, New York City position. *Reply to Box 357.*

CHEMICAL ENGINEER, 40, B.S. degree, 14 years' experience, including materials engineering and research, electrodeposition processes, product engineering and development work involving capacitors. *Reply to Box 358.*

ADVERTISERS' INDEX

Journal of the Electrochemical Society

Literature and New Products

LITERATURE FROM INDUSTRY

SULFAMATE NICKEL PLATING. New 16-page technical bulletin describing a versatile nickel plating process is offered. Called Sulfamate Nickel Plating, the patented process can produce nickel deposits with considerable variations of stress, hardness, tensile strength, elongation, ductility, and electrical resistivity properties. It is applicable to a wide variety of engineering and functional uses. Hanson-Van Winkle-Munning Co. P-375

NICKEL-PLATED STEEL. A 12-page manual on CF&I Bart Lectro-Clad nickel-plated steel is available. It presents a technical description of CF&I Lectro-Clad nickel-plated products covering manufacturing techniques and fabrication procedures, including forming, welding, cleaning, handling, and testing methods. The Colorado Fuel & Iron Corp. P-376

ACE GLASS CATALOGUE SUPPLEMENT. Supplement No. 1 to Ace General Catalogue 50, featuring outstanding items added to the Ace line, is now ready for general distribution free of charge. Although Ace is noted primarily as a manufacturer of laboratory glassware, this supplement contains principally laboratory items other than glassware. Probably the most noteworthy of these are the Pushomatic quick couplings and the PSC air control equipment, both of which are handled exclusively by Ace. Ace Glass Inc. P-377

COLORS FOR ANODIZED ALUMINUM. Colors for anodized aluminum that resist fading from sunlight and outdoor exposure are shown in a recently published brochure. It describes the anodizing, dyeing, and sealing procedures necessary to obtain maximum light fastness and is offered as a service to metal finishing and related industries. Copies are available by request on company stationery. Sandoz Chemical Works. P-378

G-E CONTROL TRANSFORMERS. A new 32-page catalogue, designated GED-2767, describes the complete line of G-E control transformers. It contains ratings, dimensions, product features, and model numbers. Also included are list prices, weights, and wiring diagrams. A special section shows panel and machine tool voltage regulation curves for use in selecting the proper transformer for given applications. General Electric Co. P-379

"OUR SMALLEST SERVANTS." The first popular book on fermentation chemistry has been published. The 32-page book is illustrated in color with prints, photographs, drawings, and diagrams. It is being made available in the U. S. and abroad to public libraries, school and college libraries, students and teachers, writers and editors, and other groups interested in this aspect of scientific research and production. Chas. Pfizer & Co., Inc. P-380

"WHAT'S NEW FOR THE LABORATORY," 25th ed., features many new items including two Corning serological pipettes; "Blue M" Relative Humidity Apparatus; Freeze-Drying Equipment; Temperature Indicating Controller with Thermistor Sensing Probe; Fluorocarbon Lubricant for metal, glass, plastic, or ceramic parts; High Vacuum Pump; Pre-Cleaned Slides. Scientific Glass Apparatus Co. Inc. P-381

POLYVINYL CHLORIDE PIPE AND FITTINGS. Brochure covers polyvinyl chloride pipe and fittings. Valves of this material are also available. Complete facilities are available for the fabrication of any special items that might be needed. Albert Pipe Supply Co. Inc. P-382

NEW PRODUCTS

D-C AMPLIFIER. A new d-c amplifier, designated the Model 303 d-c Indicating Amplifier, has an input impedance of over one million megohms, a maximum gain of 160,000, and a frequency response of d.c.—100 kc. Other features include an accurate meter with ranges of 2 to 2000 mv full scale, a power amplifier for driving all common direct-writing recorders, a differential input, and a zero drift of

(*Continued on next page*)

It's for You

Send in this postage paid card for further information on the

"LITERATURE FROM INDUSTRY" and "NEW PRODUCTS"

listed briefly on the accompanying pages.

Please send manufacturers data on items in February issue indicated by numbers circled:

P-375	P-376	P-377	P-378	P-379	N-242	N-243	N-244	N-245	N-246
P-380	P-381	P-382	P-383	P-384	N-247	N-248	N-249	N-250	N-251
P-385	P-386	P-387	P-388	P-389	N-252	N-253	N-254	N-255	N-256
P-390	P-391	P-392	P-393	P-394	N-257	N-258	N-259	N-260	N-261
P-395	P-396	P-397	P-398	P-399	N-262	N-263	N-264	N-265	N-266

I'd like to have information about products advertised:

By _____
By _____
By _____

Name _____

Address _____

City _____ State _____

Title _____

less than 2 mv/hr on any range or gain setting. Keithley Instruments, Inc. N-242

SUN BATTERY CELLS. A new series of selenium Sun Battery Cells is available. The low cost and high self-generated output of these cells make them ideal components for transistor power supplies, control applications, photometric equipment, as well as experimental uses. Now in production in a wide range of sizes and power ratings. International Rectifier Corp. N-243

"VOLTAGE SENSING" RECTIFIERS. Rapid Electric Co. has developed "Voltage Sensing" in conjunction with their selenium and germanium rectifiers. These rectifier units automatically increase the output voltage as the load or current demand is increased. Developed for automatic plating operation, its use can be extended to other electrolytic applications where a greater degree of constant current density is required. Rapid Electric Co. N-244

AUTOMATIC PROGRAMMING EQUIPMENT. Any sequence of plating operations can be made completely automatic through the use of Rapid Electric automatic programming equipment. Either selenium or germanium power units can be combined with program timing equipment for automatic operation of any series of plating steps. Simple application to any existing installation plus elimination of supervision and manual control are additional features. Rapid Electric Co. N-245

MODEL A HOFFMAN CONTROL. Separate, automatic plating-cycle control, in production barrel plating plants, for each tank, is achieved with a new control unit. A control box having two signal lights and an automatic cut-off time switch make up the new system. It is more compact, lighter in weight, and lower in cost than previous models. Hoffman Control Co. N-246

PAPER ELECTROPHORESIS APPARATUS. Improvements over early work in terms of flexibility and efficiency have been engineered into the new Spinco Continuous-Flow Paper Electrophoresis apparatus. New methods of electrolyte feed and wide-range controls permit the instrument to give maximum throughput under any required degree of resolution. At the same time, design efficiency has been raised so that resolutions formerly requiring as much as 1500-volt operation are made at ⅓ this value. Spinco Div., Beckman Instruments, Inc. N-247

NEOPRENE CASING FOR ELECTRONIC COMPONENTS. New concept in the design of component seals combines the advantages of metal cans and resin embedment in a tough, yet flexible, casing. The new seal is a neoprene case molded in two pieces and lined with a shell of phenolic resin for reinforcement. It makes for assembly ease, can be production-tested for seal effectiveness. First cost is lower than metal cans or embedments, rejects are reduced. Case can be completely filled, thus eliminating air voids. E. I. du Pont de Nemours & Co. N-248

PROTOMĀKA. A unit for making production prototypes of printed electronic circuits has been announced. Called the PROTOMĀKA, the unit measures only 60 in. long × 50 in. wide × 45½ in. high, but is capable of producing an average printed circuit in only 30 to 40 min. Circuits up to 12 in. × 16 in. in size can be manufactured. This is the first time that the printed circuit process has been designed into a single compact unit. Printed Electronics Corp. N-249

News Items

(Continued from page 32C)

Fluidized Coating Process

Announcement of a revolutionary new process for providing corrosion-resistant coatings of polyethylenes, polyfluorocarbons, nylon, and other plastics on metallic and dissimilar plastic molded targets has been made by the American Agile Corp., Maple Heights (Cleveland), Ohio.

Prior to this, certain targets could be coated with polyethylene, to provide corrosion-resistant surfaces, by using special spraying equipment. However, many additional targets could not be sprayed because of their small size and/or irregular shapes.

The new process, known as the fluidized-coating process, was displayed for the first time at the 25th National Chemical Show, December 5–9, 1955, in Philadelphia. It involves the use of a Powder Fluidizer, a compact unit consisting of a specially designed gas distribution system which maintains the plastic powder in a turbulent dense fluid state. The appearance of the fluidized bed closely resembles that of a boiling liquid.

Also available is a line of specially blended polyethylene coating powders, developed by American Agile, which can also be used with a spraying unit where this process may be utilized.

The fluidized-coating process provides a uniform coating up to 3/16 in. thick. The target to be coated is first preheated to predetermined temperature, then immersed in the fluidized coating powder for from 10 to 15 sec. It is then replaced in the oven, and allowed to cure for a short period.

The process, at present, is available for use only in laboratories. Within the next few months however, as larger coating units are built, applications to industry in general will be possible.

Sustaining Members of The Electrochemical Society

Air Reduction Company, Inc., New York, N. Y.

Ajax Electro Metallurgical Corporation, Philadelphia, Pa.

Alloy Steel Products Company, Inc., Linden, N. J.

Aluminum Company of America, New Kensington. Pa.

Aluminum Company of Canada, Ltd., Montreal, Canada

American Machine & Foundry Co., Raleigh, N. C.

American Platinum Works, Newark, N. J. (2 memberships)

American Potash & Chemical Corp., Los Angeles, Calif.

American Zinc, Lead and Smelting Company, St. Louis, Mo.

Auto City Plating Company Foundation, Detroit, Mich.

Bart Manufacturing Company, Bellville, N. J.

Becco Chemical Div., Food Machinery & Chemical Corp., Buffalo, N. Y.

Bell Telephone Laboratories, Inc., New York, N. Y.

Bethlehem Steel Company, Bethlehem, Pa. (2 memberships)

Burgess Battery Company, Freeport, Ill. (4 memberships)

Canadian Industries (1954) Limited, Montreal, Canada

Carborundum Company, Niagara Falls, N.Y.

Chrysler Corporation, Detroit, Mich.

Columbia-Southern Chemical Corporation, Pittsburgh, Pa.

Consolidated Mining and Smelting Company of Canada, Ltd., Trail, B. C. (2 memberships)

Corning Glass Works, Corning, N. Y.

Crane Company, Chicago, Ill.

Diamond Alkali Company, Cleveland, Ohio (2 memberships)

Dow Chemical Company, Midland, Mich.

Wilbur B. Driver Company, Newark, N. J.

E. I. du Pont de Nemours & Company, Inc., Wilmington, Del.

Eagle-Picher Company, Joplin, Mo.

Eaton Manufacturing Company, Stamping Div., Cleveland, Ohio

Electric Auto-Lite Company, Toledo, Ohio

Electric Storage Battery Company, Philadelphia, Pa.

Electro Metallurgical Company, Division of Union Carbide & Carbon Co., New York, N. Y.

The Eppley Laboratory, Newport, R. I.

Ford Motor Company, Dearborn, Mich.

General Chemical Division, Allied Chemical & Dye Corporation, New York, N. Y.

General Electric Company, Schenectady, N. Y.

General Motors Corporation, Research Laboratories Division, Detroit, Mich.

Gould-National Batteries, Inc., Depew, N. Y.

Graham, Crowley & Associates, Inc., Chicago, Ill.

Great Lakes Carbon Corporation, Niagara Falls, N. Y.

Hanson - Van Winkle - Munning Company, Matawan, N. J. (2 memberships)

Harshaw Chemical Company, Cleveland, Ohio (2 memberships)

Hooker Electrochemical Company, Niagara Falls, N. Y. (3 memberships)

Houdaille-Hershey Corporation, Detroit, Mich.

International Graphite & Electrode Div., Speer Carbon Company, St. Marys, Pa. (2 memberships)

International Nickel Company, Inc., New York, N. Y. (2 memberships)

Kaiser Aluminum & Chemical Corporation, Division of Metallurgical Research, Spokane, Wash.

Mathieson Chemical Corporation, Niagara Falls, N. Y. (4 memberships)

McGean Chemical Company, Cleveland, Ohio

Merck & Company, Inc., Rahway, N. J.

Metal & Thermit Corporation, New York, N. Y.

Monsanto Chemical Company, St. Louis, Mo.

National Carbon Division, Union Carbide and Carbon Corporation, New York, N. Y. (2 memberships)

National Cash Register Company, Dayton, Ohio

National Lead Company, Doehler-Jarvis Div., Grand Rapids, Mich.

National Research Corporation, Cambridge, Mass.

Niagara Alkali Company, Niagara Falls, N. Y.

Norton Company, Worcester, Mass.

Pennsylvania Salt Manufacturing Company, Philadelphia, Pa.

Philco Corporation, Lansdale, Pa.

Philips Laboratories, Inc., Irvington-on-Hudson, N. Y.

Potash Company of America, Carlsbad, N. Mex.

Promat Division, Poor & Company, Waukegan, Ill.

Ray-O-Vac Company, Madison, Wis.

RCA Victor Division, Radio Corporation of America, Harrison, N. J.

Solvay Process Division, Allied Chemical & Dye Corporation, Syracuse, N. Y. (3 memberships)

Stackpole Carbon Company, St. Marys, Pa.

Standard Steel Spring Division of the Rockwell Spring and Axle Company, Coraopolis, Pa.

Stauffer Chemical Company, San Francisco, Calif.

Sylvania Electric Products Inc., Bayside, N. Y. (2 memberships)

Sarkes Tarzian, Inc., Bloomington, Ind.

Tennessee Products & Chemical Corporation, Nashville, Tenn.

Udylite Corporation, Detroit, Mich. (2 memberships)

United Chromium, Inc., New York, N. Y.

Vanadium Corporation of America, New York, N. Y.

Victor Chemical Works, Mt. Pleasant, Tenn.

Wagner Brothers, Inc., Detroit, Mich.

Western Electric Company, Inc., Chicago, Ill.

Western Electrochemical Company, Henderson, Nev.

Westinghouse Electric Corporation, E. Pittsburgh, Pa.

Wyandotte Chemicals Corporation, Wyandotte, Mich.

Yardney Electric Corporation, New York, N. Y.

STRIPPING ENAMEL . . .

SAVING TIME

Enthonics* AT WORK

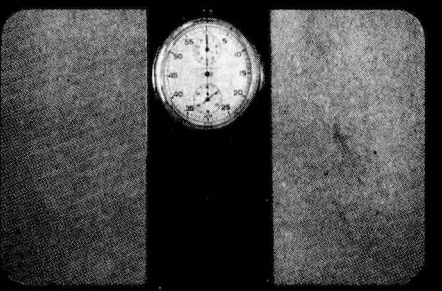

IMMERSED . . . THE WATCH STARTS!

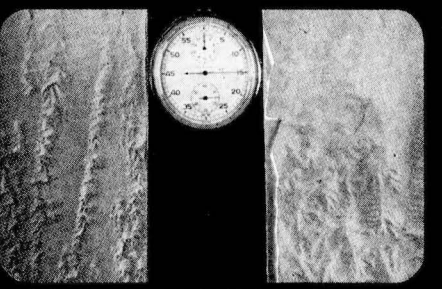

15 SECONDS . . . WRINKLING TAKES PLACE!

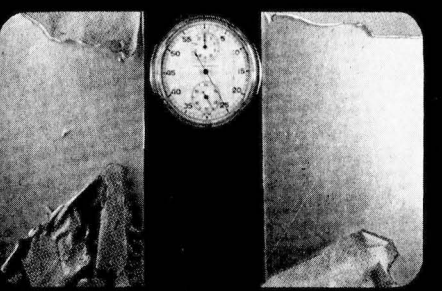

25 SECONDS . . . STRIPPING COMPLETED!

25 seconds from immersion to completed stripping!

That's the fast, dramatic story of ENTHONE Enamel Stripper S-18 in action — another example of *Enthonics at work.**

Enthone Enamel Stripper S-18 is the modern organic stripper developed for removing the newest organic finishes such as Epon or Epoxy coatings and many synthetic enamels from copper, copper alloys, steel and aluminum.

For the right strippers to solve your organic stripping problems fill out a questionnaire we'll send at your request; return it with typical samples of your work. Enthonics will find the answer . . . without obligation!

And ask for your copy of the "Enthone Check List" of literature covering more than 60 products and processes developed for modern electroplating and metal finishing.

* *The Scientific Solution of Metal Finishing Problems*

ENTHONE INCORPORATED

METAL FINISHING PROCESSES

442 ELM STREET, NEW HAVEN 11, CONNECTICUT

ELECTROPLATING CHEMICALS

STOCK POINTS: Seattle, San Francisco, Los Angeles, Chicago, Detroit, Dayton, Cleveland, Binghamton, New Haven